Check for updates

Advanced Materials Technologies

ADVANCED MATERIALS TECHNOLOGIES
www.advmattechnol.com

REVIEW

Underwater Bionic Tactile Sensing: Biological Perception Mechanisms, Technological Progress, and Future Challenges

Xinyue Zhou[1] | Yuanzheng Li[1] | Jianhua Liu[1] | Xingfu Wan[1] | Gengchen Xu[1] | Aiqiang Yu[1] | Zongchen Su[1] | Bowen Dong[1] | Kecheng Zhang[1] | Fanqing Hu[1] | Yuchen Li[1] | Xinlei Liu[1] | Peng Xu[2] | Siyuan Wang[1] | Minyi Xu[1]

[1]Dalian Key Lab of Marine Micro/Nano Energy and Self-Powered Systems, Marine Engineering College, Dalian Maritime University, Dalian, China | [2]Intelligent Biomimetic Design Lab, Peking University, Beijing, China

Correspondence: Peng Xu (pengxu@pku.edu.cn) | Siyuan Wang (wsydlmu@dlmu.edu.cn) | Minyi Xu (xuminyi@dlmu.edu.cn)

Received: 9 November 2025 | **Revised:** 7 January 2026 | **Accepted:** 8 January 2026

Keywords: bionic lateral lines sensors | bionic seal whiskers sensors | bionic tentacles sensors | marine organisms | tactile sensing mechanisms | underwater detection | underwater operation

ABSTRACT

Marine organisms are known to rely on highly sensitive tactile organs to accurately perceive external disturbances, particularly in low-light or completely dark underwater environments. These tactile perceptual mechanisms serve as ideal biological prototypes for the development of advanced underwater sensing devices. This manuscript provides a comprehensive review of the perceptual mechanisms of marine organisms and their technological translations. The intricate sensory systems of three representative species are examined: the lateral line system of fish, featuring both superficial and canal neuromasts for precise fluid dynamic detection; the undulating morphology of seal whiskers, specialized for hydrodynamic trail tracking; and the highly flexible tentacles of certain marine organisms, capable of detecting underwater pressure and deformation with exceptional sensitivity. Inspired by these biological mechanisms, biomimetic tactile sensors have been developed based on triboelectric, piezoelectric, piezoresistive, capacitive, magnetic, and optical fiber principles. Their broad application potential has been highlighted in tasks such as underwater flow velocity monitoring, vortex detection, and underwater object manipulation. Finally, current challenges, including environmental interference and limited durability, are discussed, along with future directions such as multimodal sensing integration and AI-assisted data processing, providing valuable insights for advancing next-generation underwater tactile sensing technologies.

1 | Introduction

The oceans, as the Earth's largest reservoir of resources and the core of its ecosystem, store strategic energy resources such as seabed minerals, crude oil, and natural gas [1]. They offer irreplaceable strategic value for energy security, climate regulation, and ecological stability [2–5]. The realization of these benefits fundamentally relies on a precise understanding of the marine environment. However, marine physical parameters and chemical properties exhibit pronounced spatial heterogeneity and temporal dynamics [6], posing multiple challenges to the environmental adaptability of underwater sensing devices and the precision control of engineering operations. For example, deep-sea high pressure can induce structural deformation in equipment [7]; seawater ion corrosion shortens sensor lifespan [8]; and dynamic currents increase uncertainty in target detection

© 2026 Wiley-VCH GmbH

[9]. Underwater sensing devices with high sensitivity, long-term stability, and environmental robustness have become a central focus in ocean science and engineering [10, 11]. Existing sensors can acquire and analyze environmental parameters [12], but they still suffer from significant limitations under complex marine conditions. For example, Synchronous processing of multidirectional flow signals remains vulnerable to interference; algorithmic complexity and energy consumption are hard to balance in autonomous navigation [13–16]; and inadequate material corrosion resistance leads to degraded sensing accuracy during long-term monitoring [17].

The tactile perceptual mechanisms refined through marine evolution have become a viable pathway to address the technical bottlenecks outlined above. The sensory systems of marine organisms are products of natural selection, which require precise environmental sensing to execute essential behaviors such as foraging, predator avoidance, and migration [18, 19]. This "survival-optimized" tactile sensing organ can maintain long-term, high-precision perception in complex marine environments [20, 21]. Moreover, these evolutionarily honed sensory features provide ideal biological prototypes and design inspiration for underwater biomimetic tactile sensors. By emulating the tactile systems of marine life and extracting their evolutionary advantages, engineers can translate these insights into practical devices [22–24]. For example, Fish lateral lines offer exceptional detection of weak flows and vortices [25]; coral tentacles perceive local flow direction and velocity changes [26]; octopus arms combine remarkable flexibility with high tactile sensitivity for precise perception and manipulation in turbulent flows [27]; sea otter palm skin delivers highly sensitive, adaptive sensing of underwater pressure, vibration, and deformation [28]; and seal whiskers can detect flow changes during self-motion and track wake signatures [29]. These tactile perceptual mechanisms provide ideal biological prototypes for a next-generation underwater sensing device.

Based on the evolutionary advantages of marine organisms' innate tactile systems, flexible materials such as conductive polymers [30] and liquid metals [31] are utilized to overcome the limitations of silicon-based sensors with corrosion-prone, brittle, and low-sensitivity in seawater [32]. Particularly, conductive polymers resist chloride-ion corrosion; liquid metals withstand high-pressure deformation; carbon nanotubes provide both compressive strength and high sensitivity; and ion gels stably respond to impact vibrations. In the aspect of structural fabrication, the tactile sensors employ 3D-printing techniques to replicate biological sensing architectures, thereby coupling materials with structure while simplifying manufacturing and conforming to curved substrates for efficient flow-field capture. To further improve detection accuracy and spatial resolution, flexible sensing units have been integrated into arrays [33], enabling distributed real-time monitoring and fusion of multimodal signals (pressure, shear, vibration, temperature) through multi-point collaborative sensing [34]. This arrayed approach disperses the risk of individual unit failure and enhances system robustness and reliability in complex marine environments [35].

Underwater biomimetic tactile sensors exhibit substantial promise in marine engineering applications. On autonomous underwater vehicles and submersible robots, biomimetic tactile arrays can capture flow disturbances and contact-force signals in real time to support intelligent obstacle avoidance and precise grasping, markedly improving operational safety and mission efficiency [36, 37]. For subsea pipeline and structural health monitoring, flexible tactile patches exhibit extreme sensitivity to minute pressure fluctuations and vibrations, enabling early warning of leaks, cracks, and biofouling [38, 39]. Moreover, in underwater archaeology and salvage operations, tactile feedback effectively compensates for visual blind spots, guiding robotic arms to perform delicate tasks in turbid environments [40, 41]. With ongoing advances in multimodal information fusion and artificial intelligence algorithms, underwater biomimetic tactile systems are poised to achieve breakthroughs in deep-sea exploration, marine resource development, and environmental monitoring.

As illustrated in Figure 1, this paper systematically analyzes the development of underwater bionic tactile sensing. We begin by introducing the tactile mechanisms of representative aquatic organisms—fish lateral lines, marine organism tentacles, and seal whiskers. The sensory structures and signal processing strategies that have evolved over millennia serve as the primary inspiration for biomimetic design. Building on this foundation, we review recent advances in triboelectric, piezoelectric, and piezoresistive tactile sensors and outline their operating principles and fabrication processes. The selection of each technical pathway and manufacturing technique is precisely matched to the performance requirements dictated by the corresponding biological mechanism. We then explore the application potential and technical challenges of these sensors in underwater flow-field sensing and operational scenarios. Finally, by comparing different biological prototypes and technological approaches, we analyze emerging trends toward high-performance, multifunctional, intelligent underwater sensing platforms.

2 | Biological Prototypes and Biomimetic Mechanisms

This chapter focuses on several representative underwater tactile systems—namely the fish lateral lines, marine organism tentacles, and seal whiskers—to examine in depth how these evolutionarily honed sensory organs leverage their unique structural designs and functional mechanisms to achieve high-sensitivity capture and multimodal integration of multidimensional cues (flow, pressure, vibration, chemical signals, etc.) within dynamic flow environments.

2.1 | Fish Lateral Line System

Fish are able to accurately probe and perceive their surrounding fluid field even in dimly lit or turbid waters to perform essential behaviors such as foraging [54], obstacle avoidance, navigation, and schooling. This capability derives from the fish lateral line system, a highly sensitive hydrodynamic sensor that responds to flow along the body surface [55]. As shown in Figure 2a, the lateral line is distributed along the fish body and comprises thousands of neuromasts serving as the sensing units. It can transduce mechanical stimuli, flow velocity, and pressure gradient into

2365709x, 0, Downloaded from https://advanced.onlinelibrary.wiley.com/doi/10.1002/admt.202502446 by Tongji University, Wiley Online Library on [05/02/2026]. See the Terms and Conditions (https://onlinelibrary.wiley.com/terms-and-conditions) on Wiley Online Library for rules of use; OA articles are governed by the applicable Creative Commons License

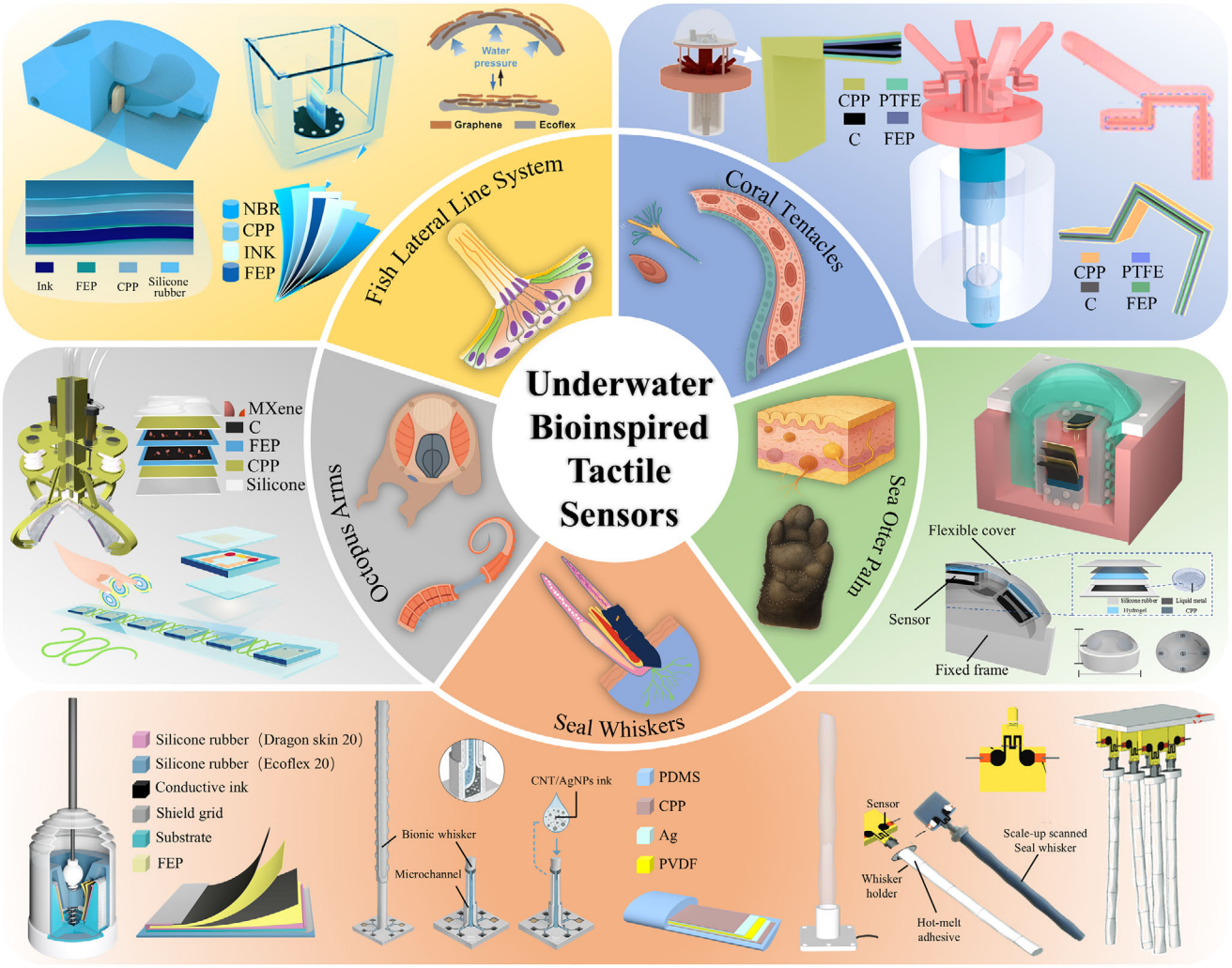

FIGURE 1 | Types and structures of underwater bionic tactile sensors. Reproduced with permission [29]. Copyright 2022, Wiley-VCH GmbH. Reproduced with permission [42]. Copyright 2023, Wiley-VCH GmbH. Reproduced with permission [43]. Copyright 2025, Wiley-VCH GmbH. Reproduced with permission [44]. Copyright 2022, SpringerOpen. Reproduced with permission [45, 46]. Copyright 2025, Elsevier. Reproduced with permission [47]. Copyright 2025, Nano Energy. Reproduced with permission [48]. Copyright 2025, Wiley-VCH GmbH. Reproduced with permission [49]. Copyright 2022, Springer Nature. Reproduced with permission [50]. Copyright 2024, Springer Nature. Reproduced with permission [51]. Copyright 2024, Wiley-VCH GmbH. Reproduced with permission [52]. Copyright 2022, Mary Ann Liebert, Inc. Reproduced with permission [53]. Copyright 2023, Elsevier.

neural signals for navigation, locate prey, and coordinate group movements in low-visibility environments [56, 57].

Neuromasts are classified into superficial neuromasts (SNs) and canal neuromasts (CNs) [58]. SNs lie on the fish's skin surface, whereas CNs reside within subepidermal lateral-line canals in Figure 2b(I),(II). Superficial neuromasts, with small diameters and tall bundles of stereocilia, function as micro-displacement sensors that detect flow velocity and vertical flow direction. When external currents move relative to the fish's body, SNs deflect under shear forces and generate neural signals transmitted to the central nervous system [59]. In contrast, canal neuromasts are housed in mucus-filled canals with larger diameters and greater hair-cell density. They are more sensitive to high-frequency disturbances [59]. The velocity differences between canal inlets induce internal flow, deflect CNs, and trigger neural responses.

Neuromasts, as the basic sensing units of the fish lateral-line system, are shown in Figure 2c. Their primary components include hair cells, supporting cells, and mantle cells [60, 61]. Hair cells, located within the neuromast, serve as the key structures for converting mechanical stimuli into neural signals [59]. Their apical stereociliary bundles (composed of kinocilia and multiple stereocilia) are highly sensitive to fluid-induced deflection. When water flow bends the neuromast's cupula, these bundles deform under hydrodynamic forces. This leads to opening ion channels at the hair-cell apex, which induces membrane-potential changes, and relays signals to the central nervous system via synaptic transmission in Figure 2d [62]. Supporting cells, situated between hair cells and mantle cells, maintain neuromast structural integrity and regulate ionic homeostasis. Encasing the neuromast is a bi-layered gelatinous cupula [63] that forms a cap over clustered stereocilia [64]. This cupula deflects in response to flow disturbances, enabling precise flow-field detection.

2365709x, 0, Downloaded from https://advanced.onlinelibrary.wiley.com/doi/10.1002/admt.202502446 by Tongji University, Wiley Online Library on [05/02/2026]. See the Terms and Conditions (https://onlinelibrary.wiley.com/terms-and-conditions) on Wiley Online Library for rules of use; OA articles are governed by the applicable Creative Commons License

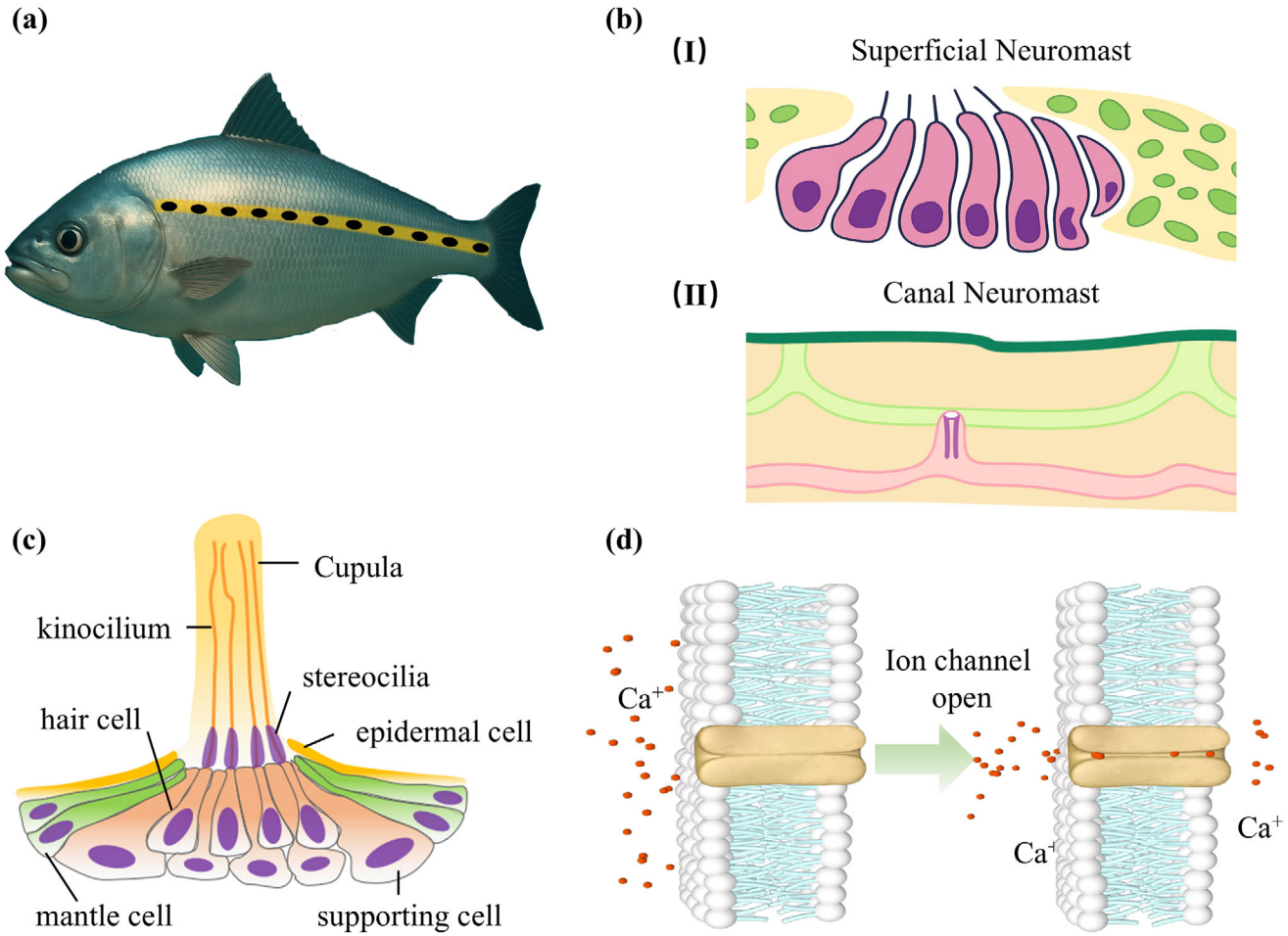

FIGURE 2 | Structure and Sensing Mechanism of the Fish Lateral Line System. (a) Distribution of the lateral line along both sides of the fish. (b) Locations and structural features of Superficial Neuromasts. (I) and Canal Neuromasts. (II). (c) Core structural components of a neuromast. (d) Signal-transduction mechanism of the neuromast's stereociliary bundle in response to fluid flow. Reproduced with permission [43]. Copyright 2025, Wiley-VCH GmbH.

Both SNs and CNs undergo two stages, including the conversion of external flow into local flow and local flow triggering neuromast response [65]. SNs are better suited for detecting continuous, uniform flows and low-frequency disturbances, whereas CNs are more sensitive to high-frequency and non-uniform flows (e.g., vibrations or water waves generated by nearby fish) [66]. Thus, SNs and CNs enable fish to comprehensively and sensitively perceive a wide range of hydrodynamic stimuli in their surrounding environment.

2.2 | Coral Tentacles Sensory System

Coral lacks a centralized nervous system, but its specialized tentacle structures and multimodal signal processing enable dynamic interaction with the environment. As the primary sensory organs, Coral tentacles exhibit high flexibility and integrated functionality. Each tentacle comprises ectodermal, mesogleal, and endodermal layers enriched with specialized sensory and effector cells [67] (see Figure 3a). Richard N. Mariscal [68] employed scanning electron microscopy (SEM) to systematically characterize the sensory architecture on the tentacle surface of California sea ball coral. He identified abundant "ciliary cones," each formed by a central cilium surrounded by a ring of shorter stereocilia located in regions rich in nematocysts and spirula cells [69, 70]. These ciliary cones morphologically resemble the hair-cell bundles of vertebrate lateral-line and auditory systems, suggesting a mechanoreceptive role. In addition, single long cilia and microvilli scattered between nematocyst-bearing and non-nematocyst regions have been observed, likely contributing to the detection of flow and vibration [71].

Coral tentacles adapt to complex marine environments through multimodal sensing. Experimental studies have shown that the tentacle's intrinsic elasticity can oscillate out of phase with ambient currents, increasing mass-transfer efficiency at the tip by approximately 25% (Figure 3b(I)) [72]. Its mechanosensory function depends on surface cilia and nematocysts, triggering exploratory vibrations under weak flow and inducing defensive nematocyst discharge under strong flow (Figure 3 b(II)) [73, 74]. Moreover, tentacles optimize fluid mixing and sensing efficiency according to flow conditions with the help of switching between pinnate extension and finger-like contraction (Figure 3b(III)) [71]. Corals also detect dissolved amino acids to guide predation, maintain symbiosis with zooxanthellae-derived metabolites, and mount physiological responses to heavy-metal contamination

2365709x, 0, Downloaded from https://advanced.onlinelibrary.wiley.com/doi/10.1002/admt.202502446 by Tongji University, Wiley Online Library on [05/02/2026]. See the Terms and Conditions (https://onlinelibrary.wiley.com/terms-and-conditions) on Wiley Online Library for rules of use; OA articles are governed by the applicable Creative Commons License

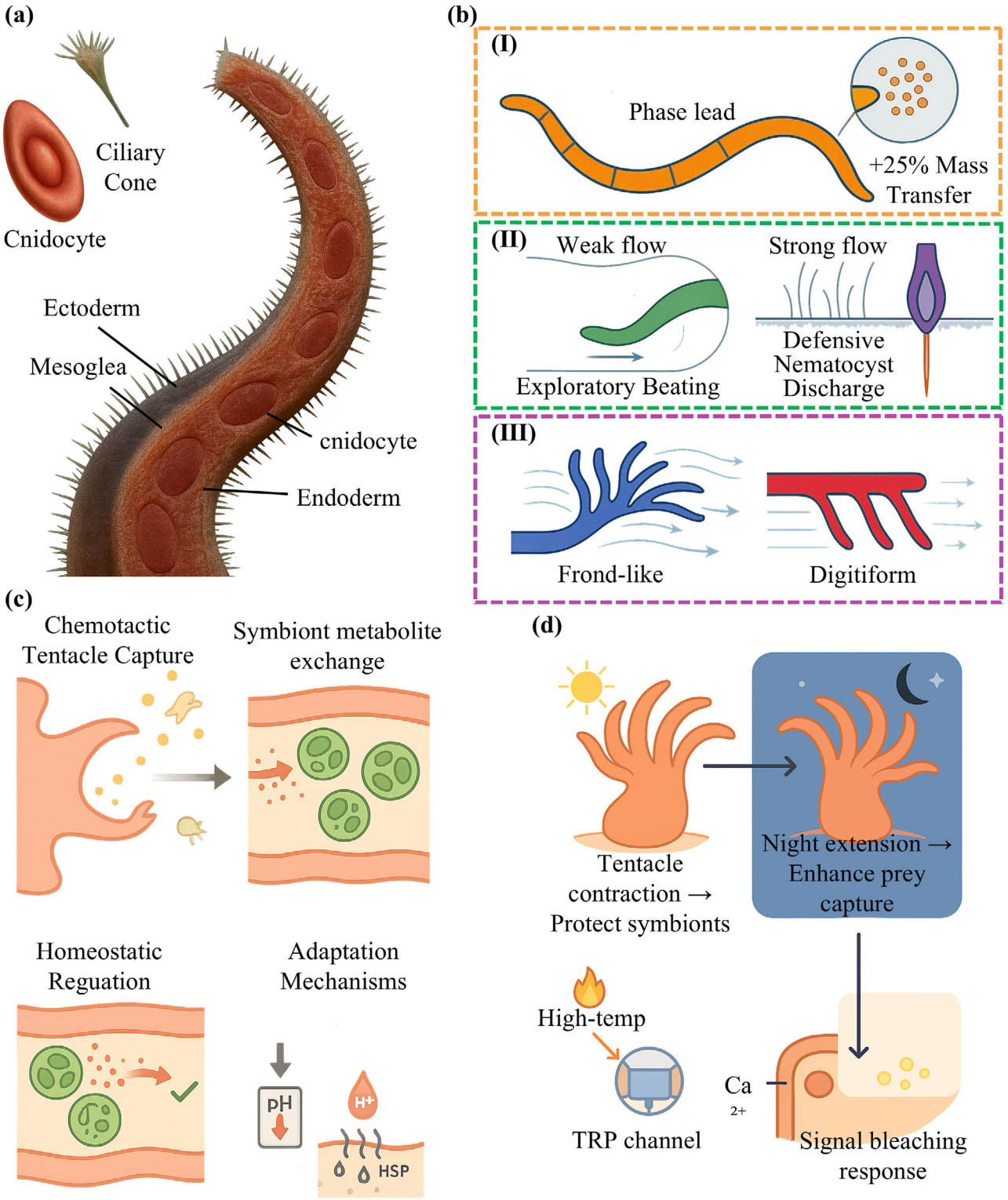

FIGURE 3 | Structural composition and multimodal sensing mechanisms of coral tentacles. (a) Cross-sectional anatomy showing ectoderm, mesoglea, and endoderm with embedded sensory cells. (b) Mechanical sensing modalities: I. Phase-lag oscillation of the tentacle's elastic structure in ambient flow. II. Ciliary cone and nematocyst-mediated exploratory vibration vs. defensive discharge under varying flow strengths. III. Morphological switching between pinnate extension and finger-like contraction to optimize fluid mixing and signal capture. (c) Chemosensory and symbiotic signaling: detection of dissolved amino acids, metabolite exchange with zooxanthellae, and responses to pH/heavy-metal stress. (d) Photoreceptive and thermosensitive regulation: diurnal contraction–extension driven by light-sensitive proteins, and heat-shock/TRP-channel activation under thermal stress.

2365709x, 0, Downloaded from https://advanced.onlinelibrary.wiley.com/doi/10.1002/admt.202502446 by Tongji University, Wiley Online Library on [05/02/2026]. See the Terms and Conditions (https://onlinelibrary.wiley.com/terms-and-conditions) on Wiley Online Library for rules of use; OA articles are governed by the applicable Creative Commons License

and ocean acidification, thereby enabling feeding, symbiotic balance, and environmental adaptation (Figure 3c). Finally, photoreceptive proteins in the epidermis and tentacles mediate diurnal contraction–extension rhythms—contracting during the day to protect symbionts and enhance photosynthesis [75], extending at night to improve prey capture [76]—while thermosensitive channels (e.g., TRP) and heat-shock proteins initiate molecular stress responses under thermal challenge, offering mechanisms for bleaching warning and heat-tolerance regulation (Figure 3d) [77].

The sensory signals of coral tentacles are processed in a distributed neural network [78], propagating rapidly to surrounding cells via electrotonic spread to trigger coordinated responses. Tactile stimulation can induce synchronous contraction of neighboring tentacles as a defensive reflex [79]. Neural signals drive antagonistic action between the ring and longitudinal muscles within the tentacle to enact morphological adjustments, such as contraction (to protect the oral region) or extension (to expand the feeding range).

2.3 | Octopus Tentacle Sensory System

Octopuses, as soft-bodied marine organisms, exhibit exceptional environmental sensing and manipulation capabilities via their highly evolved arms. Each arm features a muscular-hydrostat architecture composed of longitudinal, transverse, and oblique muscle fibers, enabling extreme flexibility and multi-degree-of-freedom motion. [80].The axial nerve cord within the arm is segmented into multiple ganglia, where each ganglia interface with a cluster of suckers, as shown in Figure 4a. This modular architecture enables local sensing and reflexive response independent of central brain control, forming a distributed tactile perception system (Figure 4b) [81].

Two primary types of sensory cells, like chemoreceptors and mechanoreceptors, form the basis of the arm's multimodal perception capabilities. Bellono and colleagues [82] identified a population of chemoreceptors in the sensory epithelium of each sucker using cell isolation, electrophysiology, and transcriptomics methods. These cells feature long, slender dendritic endings and specifically express cephalopod-unique chemical receptor proteins (CRs) that assemble into homo- or heteromeric ion-channel complexes. Upon binding hydrophobic terpene compounds released by prey, these channels produce inward-rectifying currents. The binding of terpenes to CRs induces conformational changes that open the ion pore; because different CR subtypes vary in ion selectivity (some permitting only monovalent cations, others also permeable to Ca^{2+}). This results in the ion flux altering the cell's membrane potential, and generates tonic electrical signals encoding stimulus intensity and duration (Figure 4c(I,II)). Mechanoreceptors are primarily located at the rim epithelium of each sucker and possess short, bulbous dendritic endings with high expression of the conserved mechanosensitive channel protein NompC. Mechanical deflection rapidly activates NompC, producing transient inward currents and phase-locked action potentials that mediate swift discrimination of object shape and stiffness (Figure 4c(III)). The mechanical cues localize contact events, while chemical cues characterize prey identity. This mechanism enables the octopus to perform autonomous behaviors without central-brain intervention. For example, mechanoreceptors first detect contour and initiate a grasp, and subsequent terpene detection by chemoreceptors reinforces edible-prey recognition, triggering further suction-cup engagement [83].

Figure 4d,e shows the circumferential muscle at the sucker rim detecting surface hardness through contraction force, while pressure variations within the sucker chamber map the texture of the contact interface [84]. This spatiotemporal encoding of tactile signals enables the octopus to discriminate prey species at the very moment of encirclement. Moreover, the arm's muscular flexibility allows dynamic adjustment of contact pressure. When it handles soft prey, the sucker modulates its negative-pressure gradient to avoid tissue damage (Figure 4f). Against crustacean prey, the arm applies localized high-frequency vibrations (~50 Hz) to exploit resonant effects, locate shell weak points, and concentrate force to fracture them (Figure 4g) [85]. In visually unassisted navigation, octopus arms construct three-dimensional spatial maps via tactile contact [86]. Figure 4h demonstrates helical muscle architecture enables millimeter-scale conformance to irregular surfaces, while the suction-cup array records environmental geometry through the spatiotemporal pattern of pressure distribution [87, 88]. From a bioinspired perspective, the octopus arm represents a model of decentralized, highly adaptive tactile sensing. Its combination of flexible actuation, local chemical–mechanical feedback, and distributed neural control offers powerful design inspiration for soft robotic manipulators in unstructured underwater environments.

2.4 | Sea Otter Palm Sensory System

Sea otters only rely on forelimb tactile sensing to perform fine manipulations. Strobel et al. employed a two-alternative forced-choice paradigm to measure the texture-discrimination thresholds of sea otter (Enhydra lutris) forepaws and whiskers in air and underwater, finding that their decision times are approximately 30 times faster than those of humans [89]. This rapid and precise tactile processing derives from a specialized fleshy palm pad evolved in the forelimb. Figure 5a shows that surface micro-protrusions embed into crevices of prey shells to create mechanical anchoring, while underlying multilayered receptors decode key prey features from instantaneous contact, enabling millimeter-scale localization even in turbid water or with closed eyes [28]. Dynamic tactile feedback precisely controls force and angle to avoid damaging prey during foraging, which demonstrates seamless integration of tactile perception and motor execution in Figure 5b.

The extraordinary tactile acuity of the sea otter palm derives from its unique anatomical design. The palm pad's epidermis is composed of highly keratinized, stratified squamous epithelium whose nipple-like protrusions amplify micro-strain signals at the contact interface [28]. Pacinian corpuscles and Merkel discs in the subcutaneous layer are distributed in a graded density to form a multimodal mechanoreceptive network, as shown in Figure 5c. The coordinated action of these two receptor types across both temporal and spatial dimensions endows the sea otter's tactile system with exceptionally high sensitivity and a broad dynamic range. For example, when the palm pad contacts a shell, Merkel discs first record the initial contact pressure and

2365709x, 0, Downloaded from https://advanced.onlinelibrary.wiley.com/doi/10.1002/admt.202502446 by Tongji University, Wiley Online Library on [05/02/2026]. See the Terms and Conditions (https://onlinelibrary.wiley.com/terms-and-conditions) on Wiley Online Library for rules of use; OA articles are governed by the applicable Creative Commons License

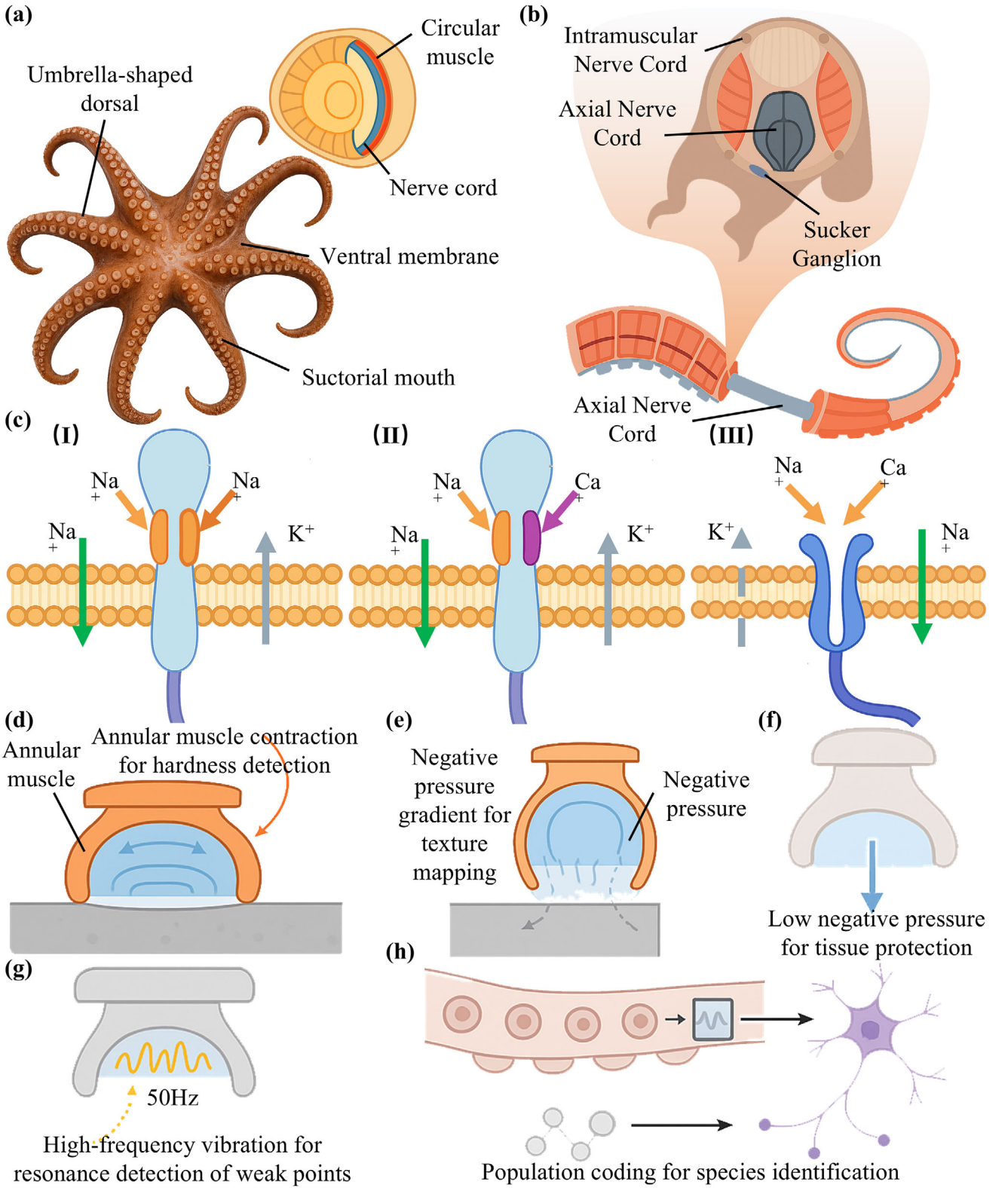

FIGURE 4 | Structural composition and multimodal sensing mechanisms of octopus tentacles. (a) Schematic of arm and sucker distribution. (b) Distributed perception–response mechanism of the "neural-node–muscle-unit" architecture. (c) Chemical and mechanoreceptor signal transduction: (I, II) terpene compound detection and tonic electrical signal generation by chemoreceptors; (III) mechanoreceptor activation and phasic electrical encoding. (d) Sensing mechanism of ring-muscle contraction mapping substrate hardness. (e) Sensing mechanism of sucker-chamber pressure variations encoding surface texture. (f) Negative-pressure gradient control state for handling soft prey. (g) High-frequency vibration detection and force-application mechanism for crustacean prey. (h) Spatial perception mechanism for reconstructing 3D environmental geometry via the arm's sucker array.

2365709x, 0, Downloaded from https://advanced.onlinelibrary.wiley.com/doi/10.1002/admt.202502446 by Tongji University, Wiley Online Library on [05/02/2026]. See the Terms and Conditions (https://onlinelibrary.wiley.com/terms-and-conditions) on Wiley Online Library for rules of use; OA articles are governed by the applicable Creative Commons License

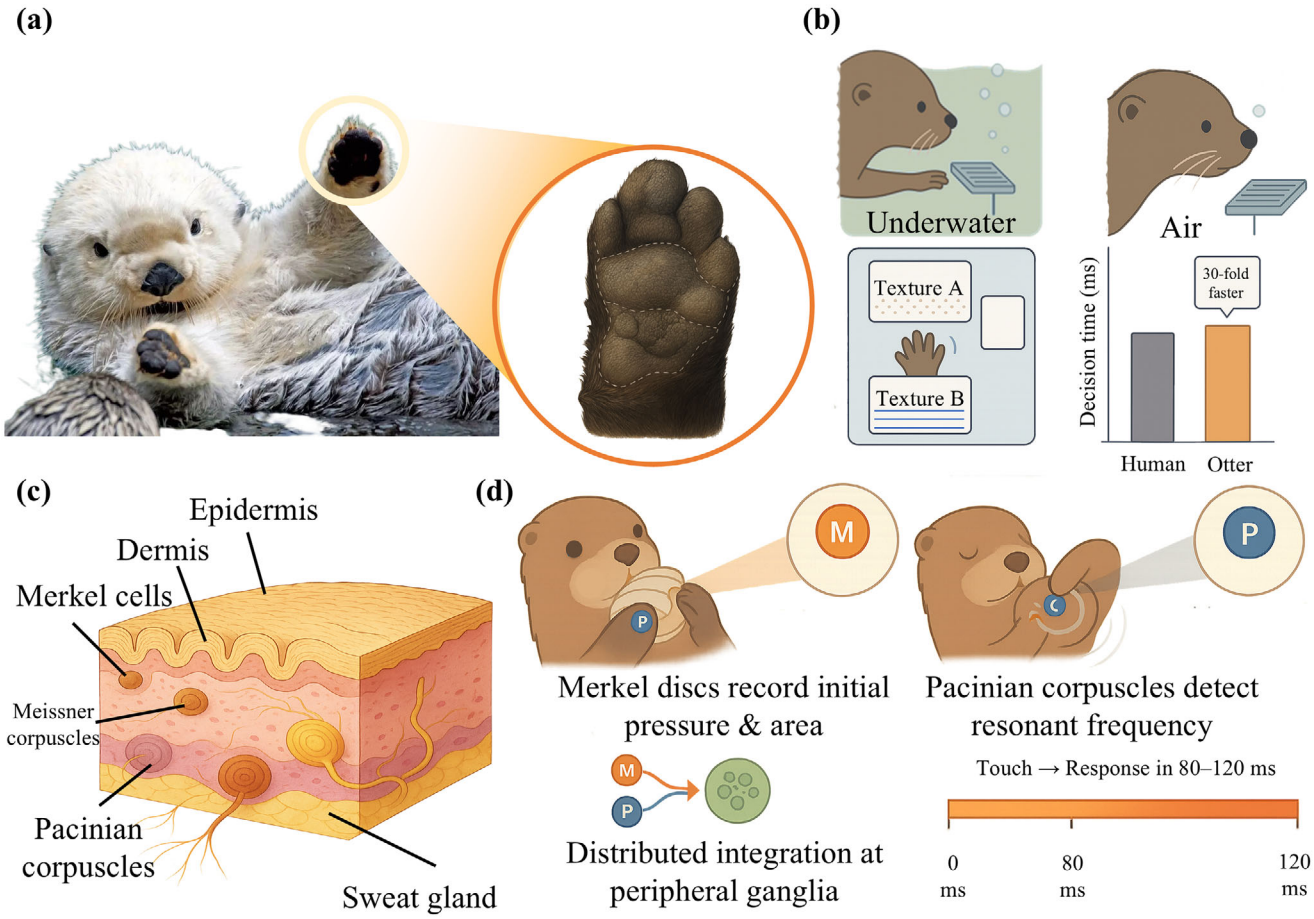

FIGURE 5 | Tactile structure and sensing mechanisms of the sea otter forepaw palm. (a) Schematic of the micro-protrusions on the surface of the fleshy palm pad. (b) The dynamic process of tactile feedback modulating striking strategy during foraging. (c) Graded density distribution of Pacinian corpuscles and Merkel discs in the subcutaneous layer of the palm pad. (d) Tactile signal latency from stimulus onset to motor response.

contact area to estimate prey size. Pacinian corpuscles detect the characteristic resonant frequency produced by internal cavity vibrations during shell tapping, allowing assessment of shell thickness and crack propagation. Neural signal integration occurs at the level of peripheral ganglia rather than relying solely on the central nervous system. This distributed processing mechanism greatly reduces tactile feedback latency, with the interval from contact stimulus to motor response measured at just 80–120 ms, as illustrated in Figure 5d.

2.5 | Seal Whisker Sensory System

Seals are marine mammals endowed with exceptional underwater sensing abilities, efficiently executing foraging and navigation tasks even in low-light or completely dark conditions [90–92]. Early biological observations reported blind yet long-lived, healthy individuals, indicating that seals do not rely solely on vision when hunting [93, 94]. Subsequent research has progressively revealed that the seal vibrissal system serves as their underwater sensory organ, which is capable of detecting extremely minute flow disturbances in the surrounding water.

As early as 1979, Renouf hypothesized that seals might rely on their vibrissae to sense and track prey [95, 96]. Building on Dehnhardt's team's foundational work [97, 98], Schulte-Pelkum et al. refined the experimental design by having one seal swim to generate a wake while training a second seal without vision and hearing to follow that wake [99] (Figure 6a). They tracked the wake along a near-straight path in about 63%, and they followed a zigzag trajectory, intercepting the wake multiple times in 34% of trials, which demonstrates exceptional vortex-sensing ability (Figure 6b).

This exceptional underwater sensing capability is largely attributable to the unique structural features of seal whiskers. In 2010, Hanke et al. [100] first demonstrated that the undulatory geometry of harbor seal whiskers can effectively disrupt the formation of regular Kármán vortex streets in the flow, thereby significantly suppressing vortex-induced vibrations (VIV). The wavy contour inhibits such self-induced VIV at its source through three core mechanisms: first, it disrupts the regular generation and coherent motion of vortices—its periodically varying thickness and cross-sectional shape shifts fluid separation positions constantly, preventing synchronous vortex formation along the vibrissa length, while inducing lateral fluid flow to break the two-dimensional (2D) vortex street into a fragmented three-dimensional (3D) structure where vortices interfere, merge, or break apart, failing to sustain vibration; second, it displaces the vortex generation region significantly

2365709x, 0, Downloaded from https://advanced.onlinelibrary.wiley.com/doi/10.1002/admt.202502446 by Tongji University, Wiley Online Library on [05/02/2026]. See the Terms and Conditions (https://onlinelibrary.wiley.com/terms-and-conditions) on Wiley Online Library for rules of use; OA articles are governed by the applicable Creative Commons License

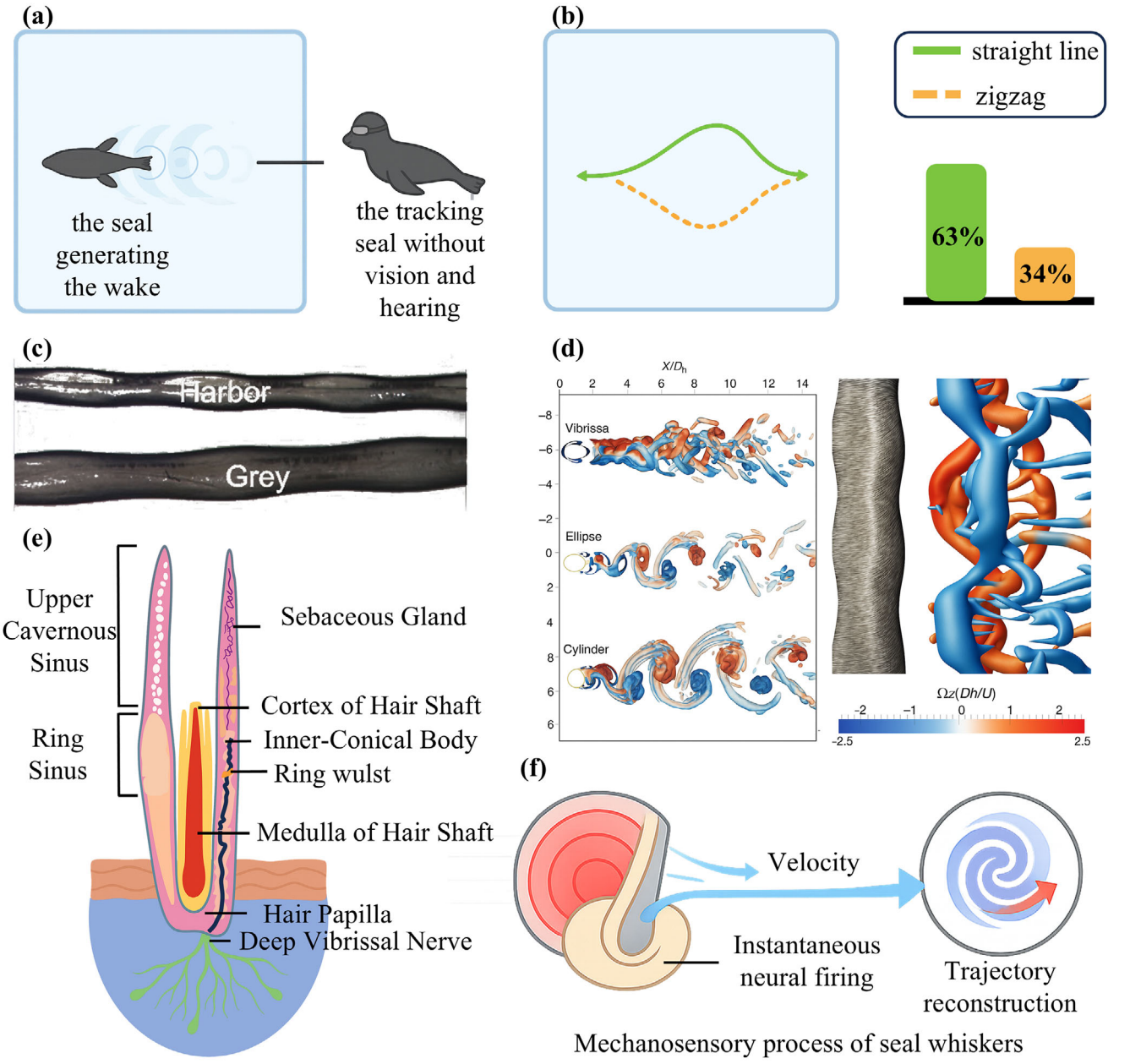

FIGURE 6 | Underwater sensing mechanism of the seal vibrissal system. (a) Schematic of the experimental setup in which a seal tracks a wake under visual and auditory deprivation. (b) Illustration of straight-line and zigzag tracking trajectories recorded during wake-following trials. (c) Diagram of the undulatory ripple geometry on the whisker surface. Reproduced with permission [101]. Copyright 2017, Wiley. (d) Validation of vortex-induced vibration suppression via particle image velocimetry (PIV) and computational fluid dynamics (CFD). Reproduced with permission [100]. Copyright 2022, The Company of Biologists Ltd. (e) Cross-sectional view of the follicle–sinus complex and embedded mechanoreceptor network inside a seal whisker. (f) Schematic of the seal whisker's vortex detection and localization process.

downstream, creating a gap that attenuates the pressure effects of vortices on the vibrissa and diminishes vortex strength as they mix with surrounding fluid and dissipate energy; third, it promotes uniform pressure distribution on the vibrissa surface, as pressure extrema at different cross-sections are staggered to cancel out periodic fluctuations, and lateral vortices disperse pressure changes spatially. Notably, this wavy structure only suppresses "self-induced vibration noise" without compromising responsiveness to external useful signals, as these cues stem from direct flow perturbations independent of the vibrissa's own vortex formation. Figure 6c illustrates this wavy structure, which attenuates vortex coherence in the wake. The structure displaces self-generated hydrodynamic disturbances away from the whisker shaft and restores pressure symmetry in the wake region, resulting in enhancing signal-to-noise ratio and flow-sensing accuracy. This mechanism has been further validated via particle image velocimetry (PIV) and computational fluid dynamics (CFD), as shown in Figure 6d.

Each whisker contains a hair follicle sinus complex, a dense network of nerve endings, and multiple mechanoreceptors (Figure 6e). Smodlaka et al. [102] used light and transmission

2365709x, 0, Downloaded from https://advanced.onlinelibrary.wiley.com/doi/10.1002/admt.202502446 by Tongji University, Wiley Online Library on [05/02/2026]. See the Terms and Conditions (https://onlinelibrary.wiley.com/terms-and-conditions) on Wiley Online Library for rules of use; OA articles are governed by the applicable Creative Commons License

electron microscopy to show that the Northern elephant seal whisker follicle is enclosed by a dermal sheath of densely packed, irregular connective tissue, with a capillary-rich dermal papilla at its base. The follicle comprises an outer root sheath, an inner root sheath, and a single-cell-layered keratinized layer. Surrounding the follicle are multiple sinus chambers, including the cavernous sinus, ring sinus, and lower cavernous sinus. When underwater prey generates a wake, the whisker's undulatory surface geometry first suppresses self-induced vortex-induced vibrations. Thereafter, the follicle's mechanoreceptors and their abundant afferent endings swiftly detect minute pressure and velocity changes in the water. This information enables seals to precisely identify and track vortex direction, strength, and trajectory for highly efficient underwater target perception and localization (Figure 6f).

2.6 | Other Biological Sensing Mechanisms

Water striders (Gerridae) are insects exquisitely adapted to the water-surface niche, celebrated for their unique ability to walk and skim across the water (Figure 7a). Their success in colonizing the interface stems from a specialized body morphology, an efficient locomotor mechanism, and a highly refined sensory system. When a dragonfly crashes into the water and thrashes, water striders rapidly detect the disturbance through surface-mounted mechanoreceptors and initiate predatory strikes. Social behaviors such as group signaling and mate recognition depend on arrays of sensory hairs distributed over their body surface.

David et al. [103] experimentally showed that water striders rely on surface tension to support their weight and propel themselves by rowing with their middle legs, which generates hemispherical vortices rather than surface waves to transfer momentum (Figure 7b). This discovery resolved Denny's paradox of juvenile striders' inability to propel at low leg-beat speeds. Perez Goodwyn et al. [104] then used optical, transmission-electron, and scanning-electron microscopy to map the morphology of tarsal-tip sensory hairs (Figure 7c), while recording their neuro-electrophysiological responses to vibrational stimuli. They found that the long tarsal hairs on the middle and hind legs not only detect flow but also exhibit distinct vibration sensitivity. Xin [105] proposed a hair-shaft–elastic-tissue biostructure (Figure 7d), comprising the hair shaft, elastic ligament, exoskeleton, surrounding tissue, and embedded neurons. The hair shaft deflects under fluid loading and transmits force to the elastic tissue via arthroidal elastic proteins, deforming subadjacent tissue and disrupting local ion balances to produce a bioelectric signal. Periodic loading causes cyclic deformation of the elastic tissue, and the hemolymph-filled cavity at the hair base is rhythmically compressed and relaxed, driving ionic currents that trigger action potentials in the sensory neurons. Intrinsic damping then restores the shaft to its upright position. Through this mechanism, water striders achieve rapid, sensitive detection of external fluid disturbances.

Sea stars' tube feet are key multifunctional organs enabling locomotion, attachment, feeding, and environmental sensing in benthic habitats; their tactile sensing mechanisms are closely tied to unique structural and physiological features (see Figure 7e). Theodora et al. [106], through experiments, mathematical modeling, and robotic simulation, systematically investigated the locomotion mechanism of sea stars. They found that, under varying underwater load conditions, sea stars adapt by recruiting more tube feet synchronously into their power stroke to form a "jumping" gait. As load increases, the proportion of tube feet engaged in propulsion rises significantly, while horizontal speed decreases only slightly. These results indicate that sea star movement relies on the distributed coordination of tube feet, dynamically regulated via vertical body oscillations without central-nervous-system control.

The structural basis of the tube foot is illustrated in Figure 7f. Structurally, a tube foot is a hollow, tubular extension of the body wall connected internally to the water-vascular system and often terminating in a suction-cup-like structure [107]. Both the surface of the tube foot and the suction disc are densely populated with specialized sensory cells—including mechanoreceptors and chemoreceptors—whose cilia or microvilli directly interface with the environment to sensitively detect mechanical stimuli and chemical cues. Mechanistically, when a tube foot contacts an external object, mechanical deformation of these sensory cells induces membrane-potential changes that generate neural signals [108], as depicted in Figure 7g. These signals are conducted via neural fibers within the tube foot to the sea star's radial nerves and central nervous system, thereby controlling tube foot contraction, extension, or suction-cup adhesion. Moreover, tactile feedback works in concert with hydraulic regulation by the water-vascular system: sensory input adjusts internal hydrostatic pressure so that the suction disc can dynamically modulate adhesion force according to substrate roughness, ensuring both secure attachment and rapid release—an essential capability for locomotion and survival on complex benthic terrain.

The neuromasts in the fish lateral line convert mechanical stimuli of the flow field into neural signals to address the challenge of flow field perception under low visibility; coral tentacles achieve multimodal perception (mechanical, chemical, optical, and thermal) to adapt to the multi-signal response requirements of complex marine environments; octopus tentacles rely on a distributed nerve-sucker system to solve the problem of precise manipulation and sensing coupling in unstructured environments; the micro-protrusions and graded receptors on sea otter palm pads break through the bottleneck of millimeter-scale texture recognition in turbid water; seal whiskers combine vibration suppression via wavy structures with follicle nerves to overcome the difficulties in extracting weak wake signals and reducing noise; the elastic structures of water strider tarsal hairs adapt to the demand for rapid detection of weak disturbances on water surfaces; sea star tube feet realize the coordination of hydraulics and sensing to meet the coupled needs of attachment and environmental perception in complex substrates.

To clearly present the core tactile-sensing features of representative aquatic organisms—fish, coral, octopus, sea otter, seal, water strider, and sea star—Table 1 systematically summarizes their sensing mechanisms and key characteristics. The table compares each species' core sensory structures, primary sensing capabilities, and functional traits, providing an intuitive overview of the tactile specialization strategies shaped by evolution and offering multidimensional biological prototypes for the design of underwater biomimetic tactile sensors.

2365709x, 0, Downloaded from https://advanced.onlinelibrary.wiley.com/doi/10.1002/admt.202502446 by Tongji University, Wiley Online Library on [05/02/2026]. See the Terms and Conditions (https://onlinelibrary.wiley.com/terms-and-conditions) on Wiley Online Library for rules of use; OA articles are governed by the applicable Creative Commons License

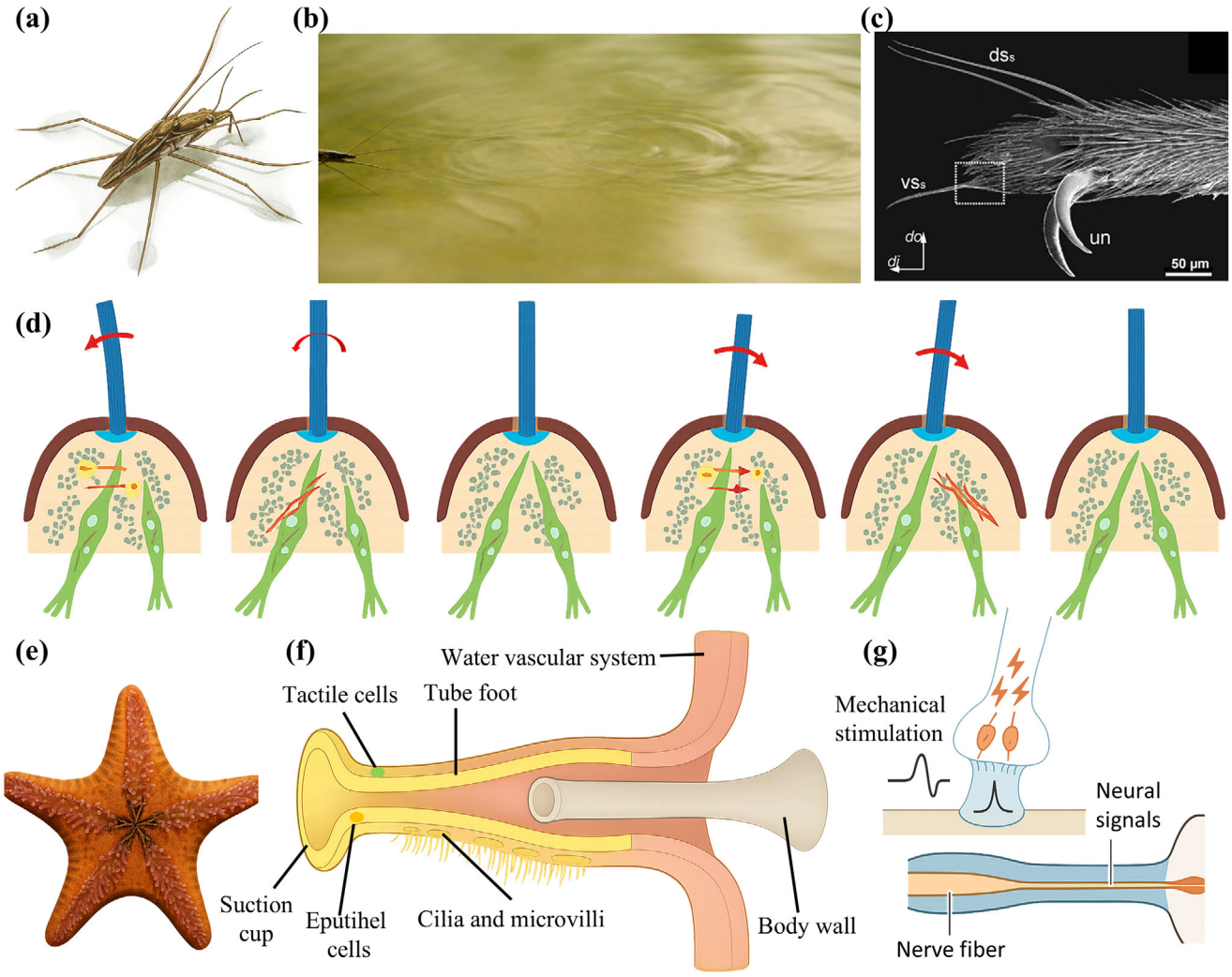

FIGURE 7 | Sensory structures and mechanisms of water striders and sea stars. (a) Schematic of water strider morphology on the water surface. (b) Hemispherical vortex generated by middle-leg rowing for propulsion [103]. (c) External architecture of a water strider's tarsal sensory hair. Reproduced with permission [104]. Copyright 2009, Elsevier. (d) "Hair-shaft–elastic tissue" biostructure of water strider sensory hairs. Reproduced with permission [105]. Copyright 2022, Wiley-VCH GmbH. (e) Morphology of a sea star and its tube feet. (f) Structural basis of the sea star tube foot (hollow tube and suction-cup end). (g) Mechanotransduction in the sea star tube foot: sensory-cell deflection and neural-signal conversion.

3 | Progress on Underwater Bionic Tactile Sensors

Based on in-depth analyses of marine organisms' tactile sensing mechanisms, researchers have translated these bio-inspired principles into practical designs, yielding a suite of underwater biomimetic tactile sensors. Addressing core needs such as hydrodynamic signal capture and multimodal perception, these devices exploit triboelectric, piezoelectric, and piezoresistive mechanisms and leverage fabrication techniques—including 3D printing, micro–nano processing, and flexible composites—to produce lateral-line-inspired sensors, whisker-inspired vortex detectors, tentacle-inspired multimodal units, and more. Some enhance sensitivity by replicating biological microstructures; others harness novel material properties to boost environmental resilience; and still others integrate multiple transduction principles for synergistic signal interpretation—together driving underwater tactile sensing from laboratory prototypes toward real-world applications.

3.1 | Working Principles and Fabrication Techniques

Different transduction principles serve as the core drivers of innovation in underwater biomimetic tactile sensing, and the degree to which they align with marine organisms' sensory mechanisms directly determines both the fidelity with which sensors replicate biological functions and the scope of their extended capabilities [109]. From energy-conversion schemes such as triboelectric and piezoelectric to signal-modulation modes like piezoresistive and capacitive, each mechanism mirrors a specific mechanical–signal transduction pathway found in natural sensory systems. Selecting and optimizing these principles requires not only a deep adherence to the underlying logic of biological perception but also careful consideration of manufacturing feasibility to realize functional breakthroughs. Together, these efforts build the critical bridge from biological mechanism to technological implementation, laying a solid foundation for subsequent process

2365709x, 0, Downloaded from https://advanced.onlinelibrary.wiley.com/doi/10.1002/admt.202502446 by Tongji University, Wiley Online Library on [05/02/2026]. See the Terms and Conditions (https://onlinelibrary.wiley.com/terms-and-conditions) on Wiley Online Library for rules of use; OA articles are governed by the applicable Creative Commons License

TABLE 1 | Comparison of tactile-sensing structures and characteristics of representative aquatic organisms.

Biological species	Core sensory structure	Primary sensing capability	Sensory characteristics
Fish (Lateral-Line System)	Superficial Neuromasts (SN), Canal Neuromasts (CN)	SN: flow velocity, vertical flow, low-frequency disturbancesCN: pressure gradients, high-frequency disturbances	SN suited for broad-scale flow detection; CN sensitive to high-frequency, non-uniform flows; together enable comprehensive hydrodynamic sensing
Coral (Tentacles)	Ciliary cones, nematocysts, photoreceptive proteins, thermosensitive receptors	Flow, vibration, chemical cues (e.g., amino acids), light intensity, temperature	Weak flows trigger exploratory vibrations; strong flows induce defensive nematocyst discharge; circadian control of extension–contraction
Octopus (Tentacles)	Suction-cup chemoreceptors (CRs), mechanoreceptors (NompC), axial nerve cord	Object shape, hardness, hydrophobic metabolites (terpenes); multimodal integration	Chemical signals encode intensity and duration; mechanical signals rapidly detect physical features; distributed neural control enables local autonomous response
Sea Otter (Palm Pad)	Papillary protrusions, Pacinian corpuscles, Merkel discs	Rapid texture discrimination, pressure sensing, prey-feature analysis (e.g., shell crevices, thickness)	Decision speed ∼30× faster than humans; 80–120 ms sensory-motor latency; combines high sensitivity with wide dynamic range
Seal (Whiskers)	Undulating whiskers, follicle–sinus complex, nerve-ending network	Minute vortex (e.g., prey wake) detection; flow velocity and direction	Undulating geometry suppresses VIV, enhances SNR; enables efficient wake-tracking under sensory deprivation
Wates Strider (Sensory Hairs)	Tarsal-tip sensory hairs (hair-shaft–elastic-tissue structure)	Flow, vibration, water-surface disturbance signals	Hair deflection triggers bioelectric signals, enabling rapid detection of prey-disturbance cues
Sea star (Tube Feet)	Suction-disc sensory cells (mechanoreceptors/chemoreceptors), water-vascular system	Mechanical stimuli (texture, pressure), chemical cues; hydraulic adhesion control	Distributed tube-foot coordination for environment sensing; adjusts suction force and locomotion without central control

innovations and performance leaps. As illustrated in Figure 8, this section will highlight recent exemplary advances in material design and fabrication techniques for tactile sensors.

3.1.1 | Triboelectric Nanogenerator

Triboelectric materials, by virtue of harvesting energy directly from minute mechanical disturbances in the environment without external power, show tremendous promise for self-powered sensors. Based on the coupling of contact electrification and electrostatic induction, the Triboelectric Nanogenerator (TENG) can transfer charge under various mechanical modes—contact–separation, sliding, rotation, etc.—and output measurable voltage or current signals to achieve efficient mechanical-to-electrical energy conversion [124]. The physical essence of a TENG can be described in terms of the electric displacement field D and displacement current in Maxwell's equations. When two materials come into contact, differences in their work functions generate equal and opposite surface charge densities $\pm\sigma$, which manifest as a polarization P source. Under these conditions, the displacement field satisfies Gauss's law:

$$\nabla \cdot D = \rho_{free}, D = \varepsilon_0 E + P \tag{1}$$

where D is the electric displacement field ($C{\cdot}m^{-2}$), ρ_{free} is the free charge density ($C{\cdot}m^{-3}$), ε_0 is the vacuum permittivity ($F{\cdot}m^{-1}$), E is the electric field intensity ($V{\cdot}m^{-1}$), and P is the polarization ($C{\cdot}m^{-2}$).

In the Absence of Free Current ($J_{free} = 0$), the Ampère–Maxwell Equation Becomes:

$$\nabla \times H = J_{free} + \frac{\partial D}{\partial t} \Rightarrow \nabla \times H = \frac{\partial D}{\partial t} \tag{2}$$

Here, H is the magnetic field intensity ($A{\cdot}m^{-1}$) and J_{free} is the free current density ($A{\cdot}m^{-2}$). This shows that the time-varying displacement field $\partial D/\partial t$ itself can be treated as a "displacement current" flowing in the external circuit to deliver energy output.

Common triboelectric materials include polytetrafluoroethylene (PTFE), polydimethylsiloxane (PDMS), polyimide (PI), and natural rubber. These materials typically exhibit excellent flexibility, facile processability, and high surface electronegativity, all of

2365709x, 0, Downloaded from https://advanced.onlinelibrary.wiley.com/doi/10.1002/admt.202502446 by Tongji University, Wiley Online Library on [05/02/2026]. See the Terms and Conditions (https://onlinelibrary.wiley.com/terms-and-conditions) on Wiley Online Library for rules of use; OA articles are governed by the applicable Creative Commons License

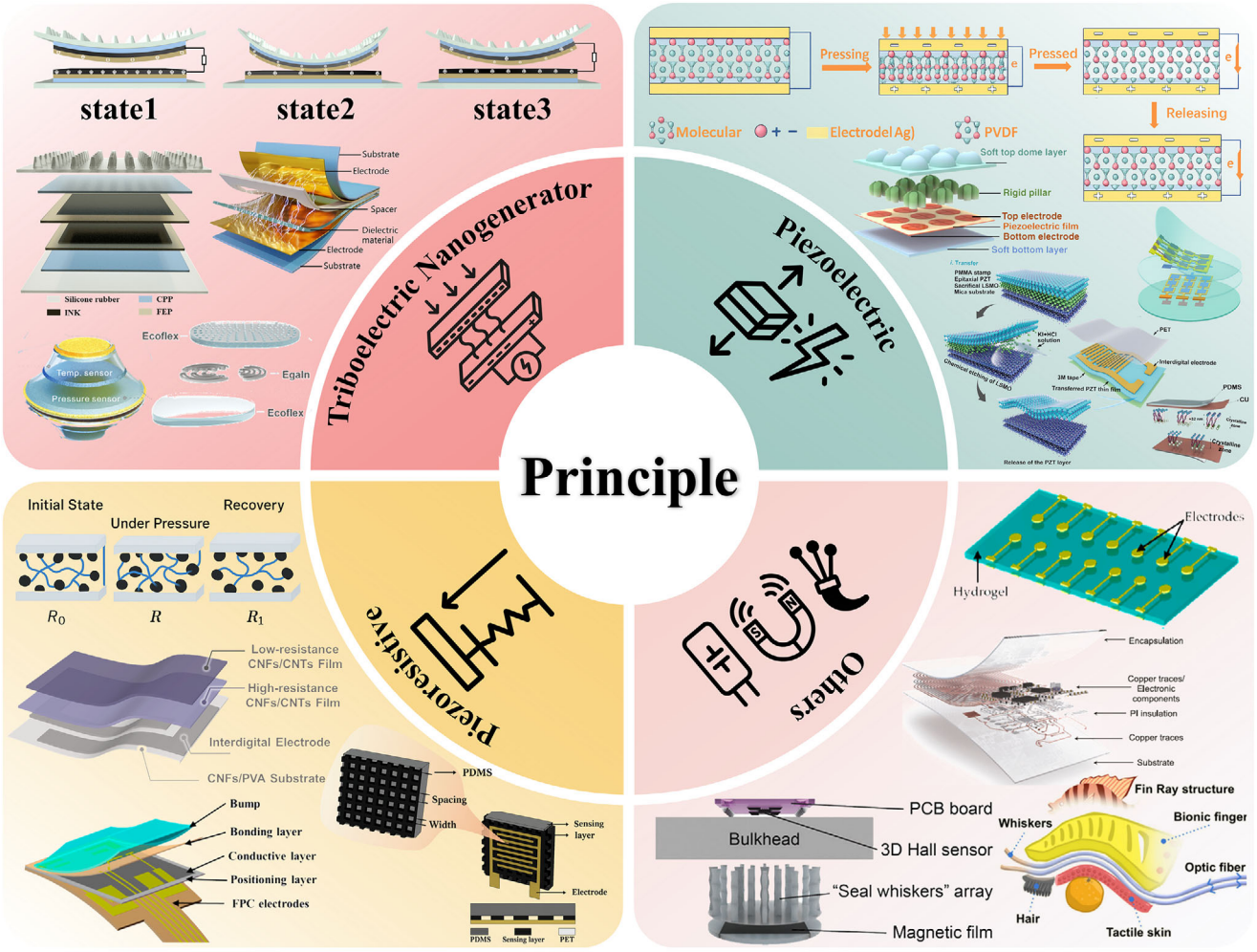

FIGURE 8 | Schematic of principles and fabrication process innovations for underwater biomimetic tactile sensors. Reproduced with permission [49]. Copyright 2022, Springer Nature. Reproduced with permission [53, 119]. Copyright 2023, Elsevier. Reproduced with permission [110]. Copyright 2022, Royal Society of Chemistry. Reproduced with permission [111, 113, 121]. Copyright 2025, Springer Nature. Reproduced with permission [112, 116]. Copyright 2020, Elsevier. Reproduced with permission [114, 122]. Copyright 2021, Wiley-VCH GmbH. Reproduced with permission [115, 117]. Copyright 2024, Wiley-VCH GmbH. Reproduced with permission [118]. Copyright 2024, MDPI. Reproduced with permission [120]. Copyright 2022, MDPI. Reproduced with permission [123]. Copyright 2024, Wiley-VCH GmbH.

which enhance triboelectric output performance. In particular, PTFE—due to its strong electronegativity—is often paired with metals or other highly electropositive materials to achieve greater charge density. PDMS offers outstanding compliance and biocompatibility, making it ideal for flexible or wearable sensor applications. Triboelectric induction can be realized in various working modes, primarily including contact–separation, sliding, single-electrode, and freestanding-layer modes [125]. The contact–separation mode is well suited for detecting vertical micro-motions; the sliding mode excels at sensing shear-direction disturbances; and the single-electrode mode simplifies device structure. Each mode is tailored to specific mechanical-disturbance characteristics in sensing tasks.

Xu et al. proposed a Triboelectric Nanogenerator-based, sea-otter-palm-inspired triboelectric tactile sensor (TPTS) [49]. As shown in Figure 9a, its design mimics the leathery micro-texture of the otter's palm: a strongly electronegative FEP film contacts and separates from conductive ink, generating voltage and current signals via contact electrification and electrostatic induction. Five symmetrically arranged sensing units (four squares surrounding one circle) enable differential signal analysis to precisely resolve the magnitude, direction, and location of applied forces.

Subsequently, Li et al. developed a sea-otter-palm-inspired underwater triboelectric tactile sensor using liquid metal (UPTS) [50]. Figure 9b depicts this device: hydrogel and a Ga–In–Sn liquid-metal alloy serve as the positive and negative triboelectric layers, respectively, with a silicone spacer forming the contact–separation structure. Under external load, triboelectrification between hydrogel and liquid metal and subsequent electrostatic induction produce a self-powered potential difference.

The fabrication process (Figure 9c) begins by mixing Dragon Skin 10 silicone parts A and B in a 1:1 ratio, casting them into a 3D-printed mold, and curing at 45°C for at least 30 min to form a flexible silicone support and cover. The five silicone covers are then snapped onto the support, and Ga–In–Sn alloy is injected via pre-formed holes and sealed with silicone caps. On the cover's

2365709x, 0, Downloaded from https://advanced.onlinelibrary.wiley.com/doi/10.1002/admt.202502446 by Tongji University, Wiley Online Library on [05/02/2026]. See the Terms and Conditions (https://onlinelibrary.wiley.com/terms-and-conditions) on Wiley Online Library for rules of use; OA articles are governed by the applicable Creative Commons License

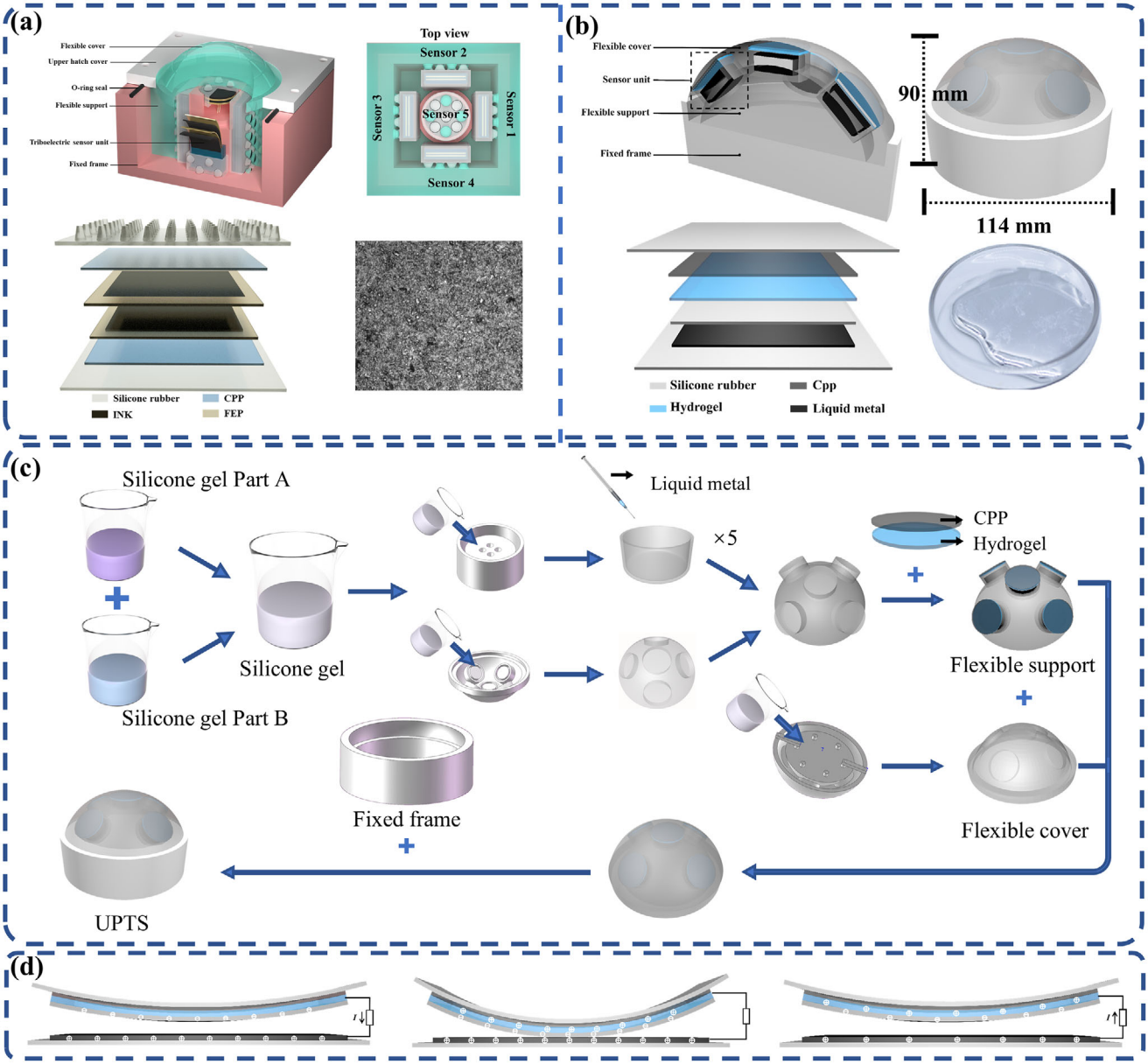

FIGURE 9 | Structure, fabrication process, and signal-generation mechanism of the sea-otter-palm-inspired triboelectric tactile sensor. (a) Appearance and distribution of the five sensing units in the Triboelectric Nanogenerator-based, otter-palm mimic sensor (TPTS). Reproduced with permission [49]. Copyright 2022, Springer Nature. (b) Structural schematic of the underwater, liquid-metal-based triboelectric tactile sensor (UPTS). Reproduced with permission [50]. Copyright 2024, Springer Nature. (c) Fabrication workflow for the UPTS device: (i) silicone mold casting, (ii) liquid-metal injection, (iii) hydrogel electrode integration, and (iv) final assembly. Reproduced with permission [50]. Copyright 2024, Springer Nature. (d) "Crocodile-tooth" five-unit array signal-generation and force-perception mechanism in the UPTS sensor. Reproduced with permission [50]. Copyright 2024, Springer Nature.

reverse side, hydrogel electrode films and CPP polymer shielding membranes are affixed in designated recesses before securing the cured covers to the support and mounting the assembly.

Figure 9d illustrates the signal-generation process: the "crocodile-tooth" five-unit array uses differential measurements to resolve force magnitude, direction (error < 5°), and contact area. Compared to Xu et al.'s sensor, Li et al.'s UPTS incorporates a liquid-metal/hydrogel electrode pairing, granting superior tensile, compressive, and deformation resilience in harsh underwater conditions, and thereby enhancing the stability and durability of mechanical-to-electrical signal conversion.

3.1.2 | Piezoelectric

With the advancement of sensing technology, piezoelectric materials—owing to their self-powered operation and high responsiveness—have been widely employed as sensing elements in intelligent sensors [126]. The piezoelectric effect refers to

2365709x, 0, Downloaded from https://advanced.onlinelibrary.wiley.com/doi/10.1002/admt.202502446 by Tongji University, Wiley Online Library on [05/02/2026]. See the Terms and Conditions (https://onlinelibrary.wiley.com/terms-and-conditions) on Wiley Online Library for rules of use; OA articles are governed by the applicable Creative Commons License

the linear coupling between mechanical stress and electrical properties in certain non-centrosymmetric crystals or ceramic materials. It comprises both the direct piezoelectric effect and the converse piezoelectric effect [127].

When a Mechanical Stress **T** Is Applied to a Piezoelectric Material, an Electric Displacement Field **D** Is Generated across Its Two Faces, Namely:

$$D_i = d_{ij} T_j \tag{3}$$

Here, D_i is the iiith component of the electric displacement, d_{ij} is the piezoelectric coefficient tensor (units: $C \cdot N^{-1}$ or $m \cdot V^{-1}$) with i,j = 1…6 corresponding to different mechanical and electrical directions, and T_j is the jjjth stress component.

When an Electric Field **E** Is Applied to a Piezoelectric Material, an Internal Strain **S** Is Generated within the Material, Given by:

$$S_k = d_{kl} E_l \tag{4}$$

where S_k is the iiith component of strain, and E_l is the jjjth component of the electric field.

Common piezoelectric materials include piezoelectric ceramics (PZT), polyvinylidene fluoride (PVDF), and piezoelectric fiber composites (MFC). PZT offers a high piezoelectric strain constant and energy-conversion efficiency, making it the top-performing piezoelectric material, but its brittleness limits its use in large-strain environments. PVDF is a flexible polymer suitable for applications involving large deformations, though its piezoelectric performance is relatively low. MFC strikes a balance between flexibility and moderate piezoelectric response. Additionally, piezoelectric thin-film materials such as ZnO and AlN are employed in high-frequency and broadband devices, but their fabrication typically requires complex processes like vapor deposition or magnetron sputtering. The primary operational modes of piezoelectric materials are d_{31} (bending), d_{33} (compression), and d_{15} (shear). Generally, the d_{33} mode exhibits a stronger response than the d_{31} mode—particularly in PZT—while the d_{15} mode becomes significant only under combined bending and torsional strains [128].

Shi et al. designed a four-unit array piezoelectric MEMS vector hydrophone (FPVH), mimicking the hair-cell stereocilia of the fish lateral-line system [129]. The core principle combines the piezoelectric effect with arrayed cooperative gain: each sensing unit consists of a polyvinyl chloride (PVC) "cilia" pillar—whose density closely matches water—mounted on an intersecting-beam inertial structure (Figure 10a). Under underwater acoustic excitation, the PVC cilia oscillate, driving rotation of the central inertia mass and vibration of the cantilever beams (Figure 10b). A lead–zirconate–titanate (PZT) thin film coated on the cantilevers generates charge separation upon deformation, producing an electrical output. By summing the signals from all four units, the array achieves a ~12 dB sensitivity gain, resolving the usual trade-off between single-element sensitivity and bandwidth. Fabrication uses standard MEMS processes: PZT thin-film microstructures are deposited and patterned on a silicon substrate; PVC cilia are then affixed to the inertial masses; finally, the device is encapsulated with a polyurethane acoustic window, stainless-steel housing, and silicone-oil coupling for waterproofing.

Guo et al. proposed a seal-whisker-inspired piezoelectric wave-whisker sensor [53]. This device comprises a wavy PDMS substrate overlaid with screen-printed silver electrodes and a PVDF piezoelectric film (Figure 10c). In vortex flows, the PDMS geometry converts fluid disturbances into mechanical strain, which the PVDF layer transduces into an electric signal (Figure 10d). The undulatory profile effectively suppresses self-induced vortex-induced vibrations, so only external vortices elicit a response—dramatically improving signal-to-noise ratio. As shown in Figure 10e, fabrication involves mixing PDMS base and curing agent at a 9:1 ratio, degassing, and casting into a 3D-printed mold; integrating prefabricated PVDF electrodes; vacuum-degassing and heat curing; and finally encapsulating in a PDMS shell with CPP tape for electrostatic shielding. These two works, in the realms of miniaturized underwater acoustics and hydrodynamic sensing, respectively, exemplify the innovative integration of biomimetic structures with piezoelectric functional materials.

3.1.3 | Piezoresistive

Piezoresistive materials occupy a key position in smart sensing owing to their simple structure, low cost, and ease of integration [130]. Under the piezoresistive effect, a material's resistivity changes with applied strain, allowing mechanical signals to be detected by monitoring resistance variations without complex energy-conversion mechanisms [131]. Common piezoresistive materials include semiconductor silicon, metal strain gauges, carbon-nanotube composites, and graphene. Silicon offers high sensitivity and good linearity, making it the prototypical piezoresistive sensor material, but its temperature sensitivity requires additional compensation circuitry. Metal strain gauges provide strong stability and mature fabrication processes—suitable for industrial environments—but their gauge factor is relatively low (≈2), limiting the detection of minute deformations. Carbon-nanotube composites and graphene excel in flexible and wearable devices due to their high compliance and large gauge factors (>100), though their cost and scalability remain challenges. Additionally, metal–ceramic composite thin films (e.g., NiCr alloys) are employed for pressure sensing in high-temperature environments, but their fabrication demands vacuum deposition techniques and entails greater process complexity. The primary operational modes for piezoresistive sensors are axial tension/compression and shear: the axial mode delivers a direct response and is easy to model for most conventional stress measurements [132], while the shear mode is sensitive to tangential strain and is commonly used in multi-axis force sensor designs [133]. Generally, carbon-based composites maintain stable responses at large strains (>10%) [134], whereas metal-based materials are better suited for high-precision measurements at small strains (<2%).

Liu et al. designed a biomimetic whisker sensor that mimics the undulatory geometry of seal vibrissae, combining vortex-induced vibration (VIV) suppression with piezoresistive sensing via CNT/AgNPs-filled microchannels [52]. As shown in Figure 11a,

2365709x, 0, Downloaded from https://advanced.onlinelibrary.wiley.com/doi/10.1002/admt.202502446 by Tongji University, Wiley Online Library on [05/02/2026]. See the Terms and Conditions (https://onlinelibrary.wiley.com/terms-and-conditions) on Wiley Online Library for rules of use; OA articles are governed by the applicable Creative Commons License

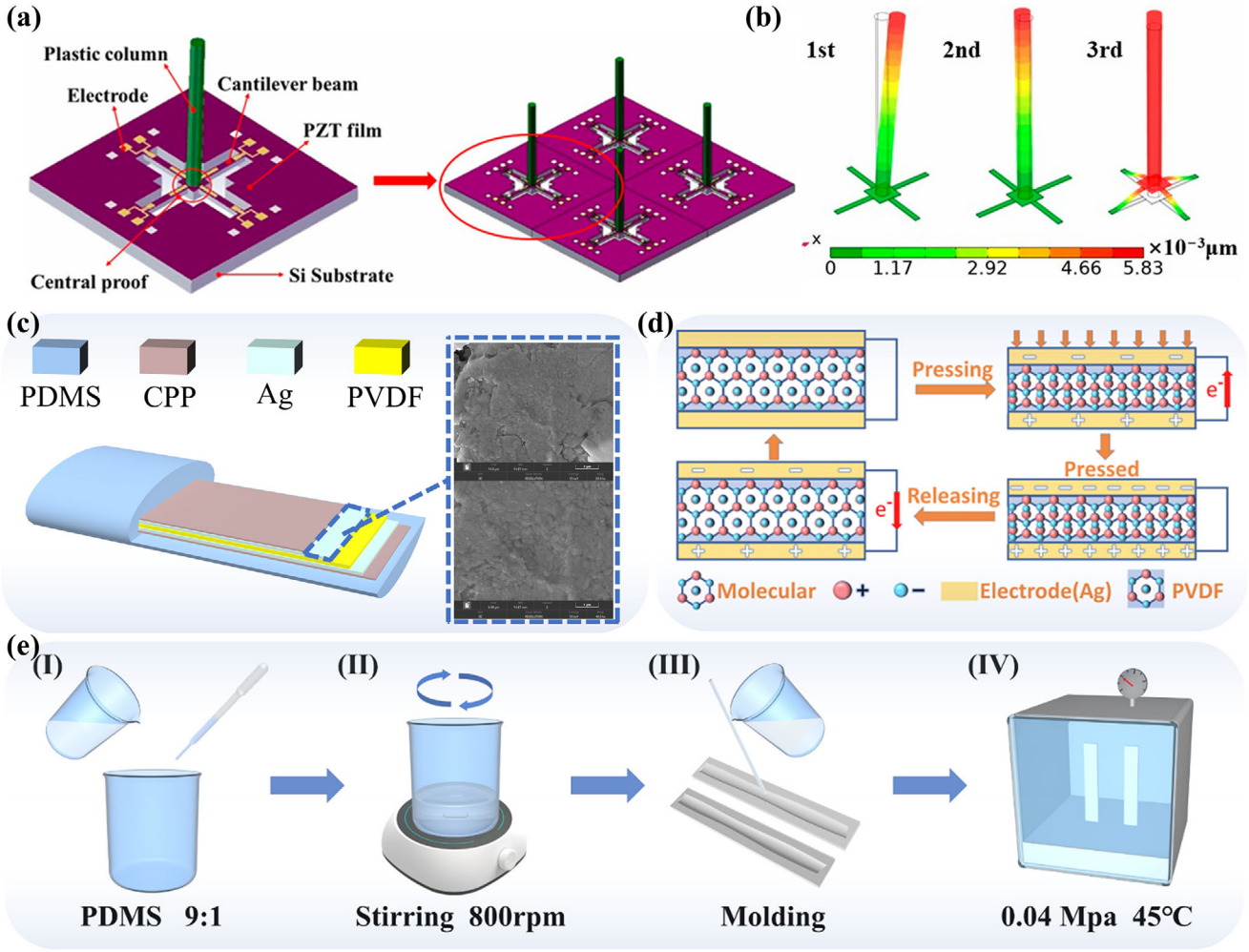

FIGURE 10 | Structure, working mechanism, and fabrication process of biomimetic piezoelectric sensors. (a) Core structure of the four-unit array MEMS vector hydrophone (FPVH), replicating fish lateral-line stereocilia with intersecting-beam "cilia" and central inertia masses. Reproduced with permission [129]. Copyright 2022, MDPI. (b) Oscillation of PVC "cilia" and resulting cantilever-beam vibration under underwater acoustic excitation in the FPVH device. Reproduced with permission [129]. Copyright 2022, MDPI. (c) Structural schematic of the seal-whisker-inspired piezoelectric wave-whisker sensor, featuring a wavy PDMS substrate with screen-printed silver electrodes and PVDF film. Reproduced with permission [53]. Copyright 2023, Elsevier. (d) Signal-generation mechanism of the wave-whisker piezoelectric sensor in vortex flows. Reproduced with permission [53]. Copyright 2023, Sensors and Actuators A: Physical. (e) Fabrication process flow for the wave-whisker sensor. Reproduced with permission [53]. Copyright 2023, Elsevier.

the sensor's wavy whisker is 3D-printed in PDMS to disrupt coherent vortex shedding and reduce self-induced flow noise. Its PDMS base integrates four Ω-shaped microchannels loaded with a CNT/AgNPs ink: when flow-induced bending strains these channels, their resistance changes, which is used to infer flow parameters. Fabrication (Figure 11b) employs 3D printing of the whisker and mold, casting PDMS (10:1 base to curing agent) to form the microchanneled base, then using Directed Liquid Spreading (DLS) to infill CNT/AgNPs ink—capillary action in inclined grooves ensures uniform deposition (Figure 11c–f)—and finally spraying a PDMS waterproof layer.

In parallel, Dusek et al. developed an underwater piezoresistive pressure-sensor array based on closed-cell carbon-black–doped PDMS (CBPDMS) foam [135]. Figure 11g depicts the array: when compressed, the foam's carbon particles make increased contact, lowering resistance; a four-probe measurement captures this change to sense pressure. Silver–carbon-black–PDMS composite electrodes provide low-resistance pathways, while a pure PDMS substrate ensures flexibility and waterproofing (Figure 11h,i). Fabrication involves molding composite electrodes (silver powder, carbon black, PDMS) with embedded leads, casting carbon-black-doped silicone foam into the inter-electrode gaps, and sealing with a thin PDMS overcoat. This simple, low-cost process yields an array capable of stable sensing over a wide dynamic pressure range, demonstrating the promise of flexible, scalable piezoresistive biomimetic sensors.

3.1.4 | Other Working Principles

Beyond the three major sensor types—triboelectric, piezoelectric, and piezoresistive—there are several "other" tactile sensing schemes, principally capacitive, fiber-optic speckle-imaging, and magneto-sensitive methods.

2365709x, 0, Downloaded from https://advanced.onlinelibrary.wiley.com/doi/10.1002/admt.202502446 by Tongji University, Wiley Online Library on [05/02/2026]. See the Terms and Conditions (https://onlinelibrary.wiley.com/terms-and-conditions) on Wiley Online Library for rules of use; OA articles are governed by the applicable Creative Commons License

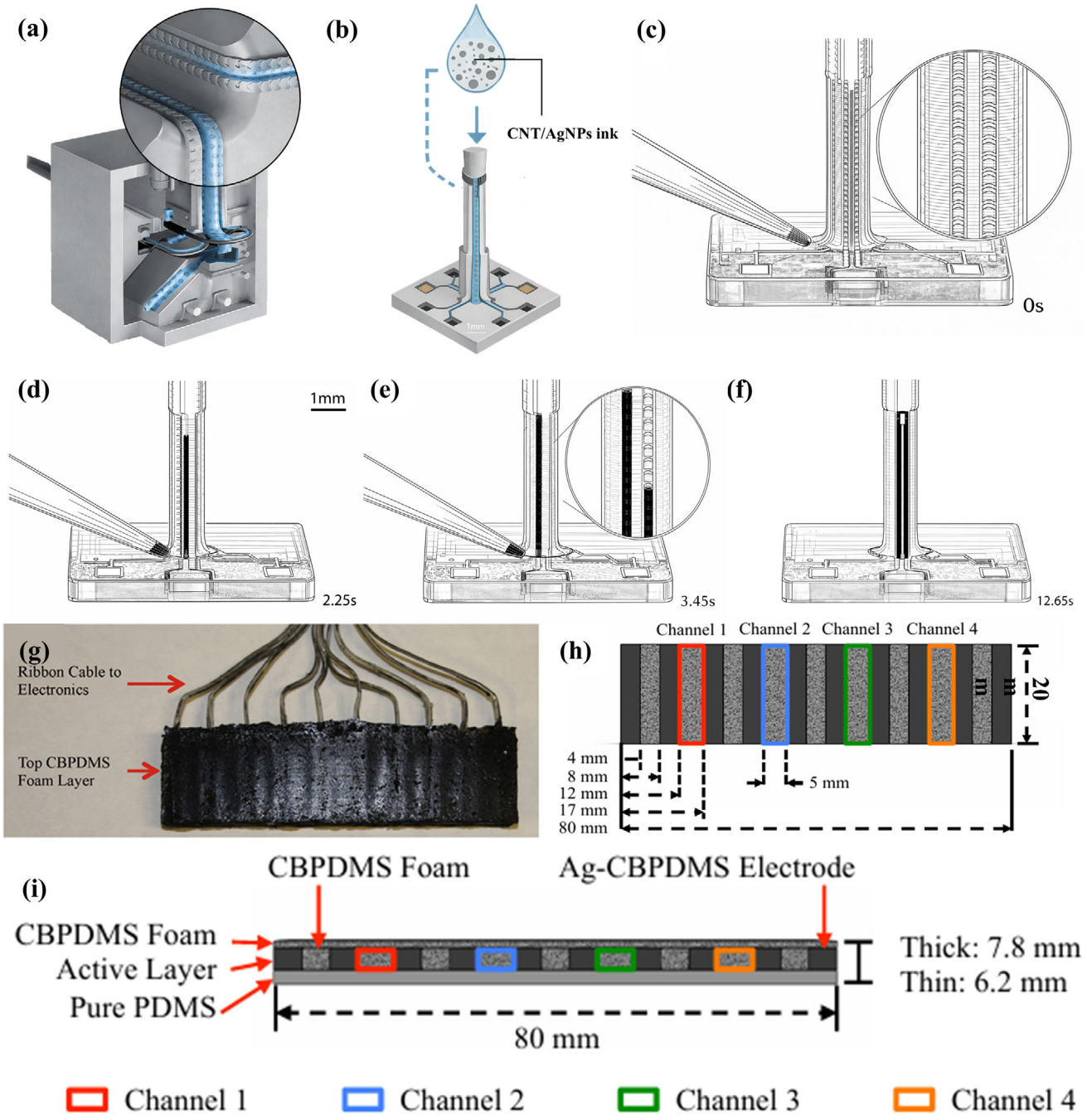

FIGURE 11 | Structure, fabrication process, and working mechanism of piezoresistive biomimetic tactile sensors. (a) 3D-printed mold and PDMS substrate preparation for the seal-whisker-inspired wavy piezoresistive sensor [52]. (b) Directed Liquid Spreading (DLS) technique for capillary infusion of CNT/AgNPs ink into the Ω-shaped microchannels [52]. (c–f) Sequential capillary-driven spreading of CNT/AgNPs ink within the microchannels, as guided by inclined groove geometry [52]. (g) Underwater piezoresistive pressure-sensor array based on closed-cell carbon-black-doped PDMS (CBPDMS) foam. Reproduced with permission [135]. Copyright 2016, Elsevier. (h, i) Conductive-pathway architectures in the CBPDMS foam sensor, showing silver–carbon–PDMS composite electrodes and foam embedded percolation networks. Reproduced with permission [135]. Copyright 2016, Elsevier.

Kanhere et al. developed a flexible, hydrogel-based capacitive pressure sensor [120], shown in Figure 12a. A self-crosslinked, fully swollen DMAA hydrogel film is sandwiched between Cr/Au electrodes. The hydrogel's tunable microporous network delivers high water retention, underwater stability, and acoustic-impedance matching, yielding a linear, high-sensitivity capacitive response. A patterned electrode array design further enables large-area "smart skin" coverage for underwater vehicles. Fabrication involves: (1) preparing the swollen DMAA hydrogel film; (2) sputtering Cr/Au electrodes on a silicon substrate; (3) epoxy-bonding connection wires; and (4) assembling and sealing the hydrogel between the electrodes. This sensor is well suited for pressure detection in underwater "smart skins" and soft robotics.

Inspired by electric fish's active electrolocation, Zhou et al. created a transparent, flexible electronic skin [121], whose architec-

2365709x, 0, Downloaded from https://advanced.onlinelibrary.wiley.com/doi/10.1002/admt.202502446 by Tongji University, Wiley Online Library on [05/02/2026]. See the Terms and Conditions (https://onlinelibrary.wiley.com/terms-and-conditions) on Wiley Online Library for rules of use; OA articles are governed by the applicable Creative Commons License

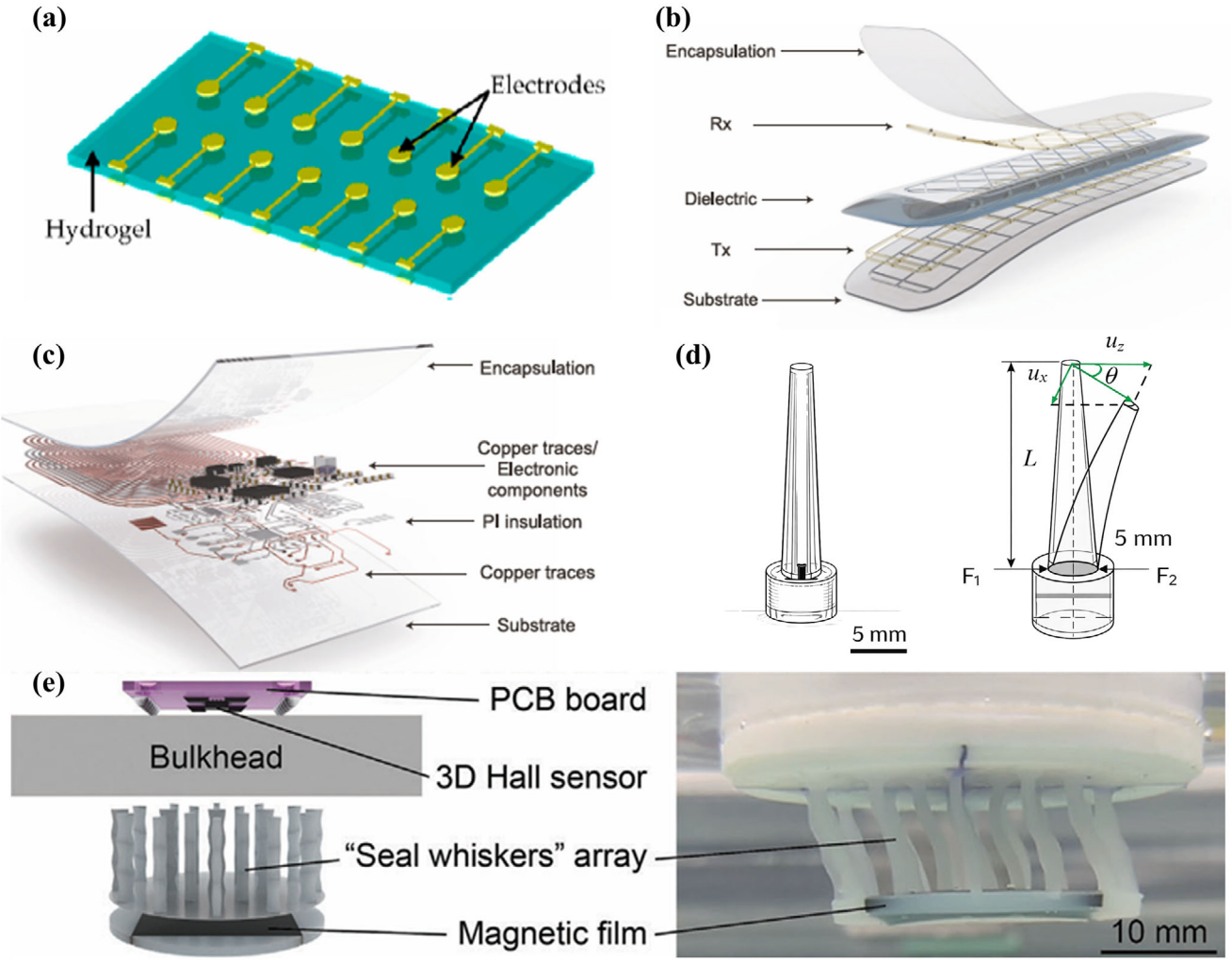

FIGURE 12 | Structural schematics and sensing mechanisms of capacitive, fiber-optic, and magneto-sensitive underwater biomimetic tactile sensors. (a) Flexible hydrogel-based capacitive pressure sensor with patterned Cr/Au electrode array. Reproduced with permission [120]. Copyright 2017, MDPI. (b) Transparent, flexible electronic skin inspired by electric fish's active electrolocation. Reproduced with permission [121]. Copyright 2024, Springer Nature. (c) Dual-electrode circuit and electric-field detection principle of the biomimetic e-skin. Reproduced with permission [121]. Copyright 2024, Springer Nature. (d) Biocompatible agarose–glycerol hydrogel "whisker" fiber-optic tactile sensor for speckle-based displacement and direction sensing [136]. (e) 3D hydrodynamic magneto-sensitive sensor mimicking seal-whisker waves: Ecoflex "whisker" array with embedded NdFeB/silicone film and 3D Hall-sensor readout. Reproduced with permission [122]. Copyright 2024, Wiley-VCH GmbH.

ture is shown in Figure 12b. Utilizing a biomimetic dual-electrode system (Figure 12c)—with one electrode actively emitting a 100 kHz electric field and the other detecting field distortions caused by nearby objects—it achieves non-contact 3D localization. Fabrication comprises: (1) injecting a biogel into PDMS microchannels to form stretchable electrodes; (2) integrating laser-cut flexible circuitry and miniature electronic components; and (3) encapsulating the assembly in a 1.4 mm-thick PDMS shell. Electrode perforation and dielectric-layer porosity optimizations boost sensitivity by over 40%, and the device supports real-time wireless transmission of three-dimensional coordinates for applications in robotic-arm control, UAV obstacle avoidance, and underwater-robot exploration.

Fujiwara et al. developed a biocompatible agarose–glycerol hydrogel "whisker" fiber-optic tactile sensor [136], as shown in Figure 12d. A conical hydrogel probe is embedded within an MMF–SMF–MMF optical path; when an external force bends the probe, it induces mode coupling in the single-mode fiber core, producing changes in the speckle pattern. Using a zero-normalized cross-correlation (ZNCC) algorithm, both displacement (≈0.7 mm) and direction (≈13°) can be determined. Fabrication involves molding and curing the agar–glycerol hydrogel into conical whiskers, fusion-splicing multimode and single-mode fibers to form the sensing optical path, and finally embedding the fiber within the probe and sealing the device. This sensor combines high resolution, arrayability, and excellent biocompatibility, making it suitable for medical diagnostics and tactile perception in soft robotics.

Dai et al. designed a three-dimensional hydrodynamic sensor inspired by the wavy geometry of seal whiskers [122]. As shown in Figure 12e, a radially magnetized NdFeB/silicone composite film is embedded at the base of an Ecoflex wave-shaped "whisker" array, with the wavy profile suppressing self-induced vortex-induced vibrations. Flow impinges on the whisker array and

2365709x, 0, Downloaded from https://advanced.onlinelibrary.wiley.com/doi/10.1002/admt.202502446 by Tongji University, Wiley Online Library on [05/02/2026]. See the Terms and Conditions (https://onlinelibrary.wiley.com/terms-and-conditions) on Wiley Online Library for rules of use; OA articles are governed by the applicable Creative Commons License

TABLE 2 | Performance comparison and applicable sensor types for underwater biomimetic tactile sensors based on different transduction principles.

Principle	Advantages	Disadvantages	Applicable scenarios
Triboelectric	Self-powered without External Energy; Harvesting Energy from Subtle Mechanical Disturbances; Flexible and Easy-to-process Materials	Output Signals Easily Influenced by Environmental Humidity; Long-term Stability Needs Improvement	Suitable for Scenarios Requiring Self-powering and Detecting Subtle Vertical or Shear Movements, Such as Force Sensing during Underwater Object Grasping
Piezoelectric	High Sensitivity, no external power required; High Energy Conversion Efficiency	Brittle Materials (e.g., PZT) Unsuitable for large-strain environments; Flexible Materials (e.g., PVDF) Exhibit Lower Piezoelectric Performance	Fish-inspired Lateral Line Vector Hydrophones, Seal-whisker-inspired Vortex Sensors, Suitable for Micro-scale Underwater Acoustic Perception and Hydrodynamic Disturbance Detection
Piezoresistive	Simple structure, Low Cost; Easy Integration; Straightforward Signal Processing	Semiconductor Materials Sensitive to Temperature, Requiring Temperature Compensation; Metal Strain Gauges Have Low Gauge Factors, Challenging to Detect Small Deformations	Seal-whisker-inspired Wavy Sensors, Suitable for Cost-sensitive Applications and Scenarios Requiring Regular Stress Detection or Large Strains
Capacitive	Good Linear Response; High Sensitivity; Flexible Structural Design	Susceptible to Environmental Interference (e.g., temperature, humidity); Demanding Waterproof Encapsulation	Underwater Smart Skins, Soft Robotic Pressure Sensors, Suitable for Large-area and Highly Sensitive Pressure Sensing Scenarios
Optical fiber	High Resolution; Array-compatible; Good Biocompatibility	Relatively Complex Structure; Strict Optical Alignment Requirements	Medical Detection, Soft Robotic Tactile Sensors, Suitable for Scenarios with High Biocompatibility Requirements
magnetosensitive	Strong Anti-interference Capability; High Measurement Accuracy; no Complex Calibration Needed	Affected by Magnetic Field Environments; Relatively High Material Costs	Seal-whisker-inspired 3D Hydrodynamic Sensors, Suitable for High-precision Detection of Flow Speed, Direction, and Vortex Frequency

magnetic film, producing tri-axial displacements that distort the surrounding magnetic field. A 3D Hall-sensor array behind the film captures these field changes, and a pre-established decoupling model—using parameters R_x, R_y, and S_z corresponding to X, Y, and Z displacements—directly computes flow velocity, direction, and vortex frequency without complex calibration.

Fabrication proceeds as follows: (1) mix NdFeB micro-powder with silicone and cast into films, then pulse-magnetize; (2) cast Ecoflex into a 3D-printed mold to form the wavy whisker structures while embedding and curing the magnetic films; (3) integrate the whisker array with the Hall sensors and encapsulate the assembly in a waterproof housing. Under testing, the sensor achieves accuracies better than 0.061 m/s for steady flow velocity, 0.05 Hz for vortex frequency, and 7° for flow-direction detection.

In summary, triboelectric, piezoelectric, piezoresistive, capacitive, fiber-optic speckle-imaging, and magneto-sensitive principles each play distinct roles in the development of underwater biomimetic tactile sensors. Triboelectric and piezoelectric approaches, with their self-powering capabilities, suit a wide range of bioinspired sensing scenarios; piezoresistive sensors, thanks to their structural simplicity, dominate cost-sensitive applications; and other methods are deployed for specialized needs such as biocompatibility and high-precision detection. By integrating these transduction mechanisms with novel materials and biomimetic architectures, sensor technology is moving toward multimodal, highly integrated platforms. Their respective strengths, limitations, and applicable sensor types are summarized in Table 2.

3.2 | Biomimetic Tactile Sensor Types

Based on the unique sensory structures of various marine organisms, underwater biomimetic tactile sensors can be categorized into three main types: lateral-line-inspired sensors, tentacle-inspired sensors, and whisker-inspired sensors. These sensor types respectively replicate the flow-sensing logic of fish lateral lines, the multimodal interaction mechanisms of octopus or coral tentacles, and the vortex-capturing characteristics of seal whiskers. Through targeted structural designs and principal adaptations, they reproduce the biological sensing capabilities. The following sections detail the design principles, performance characteristics, and application scenarios of each sensor type.

2365709x, 0, Downloaded from https://advanced.onlinelibrary.wiley.com/doi/10.1002/admt.202502446 by Tongji University, Wiley Online Library on [05/02/2026]. See the Terms and Conditions (https://onlinelibrary.wiley.com/terms-and-conditions) on Wiley Online Library for rules of use; OA articles are governed by the applicable Creative Commons License

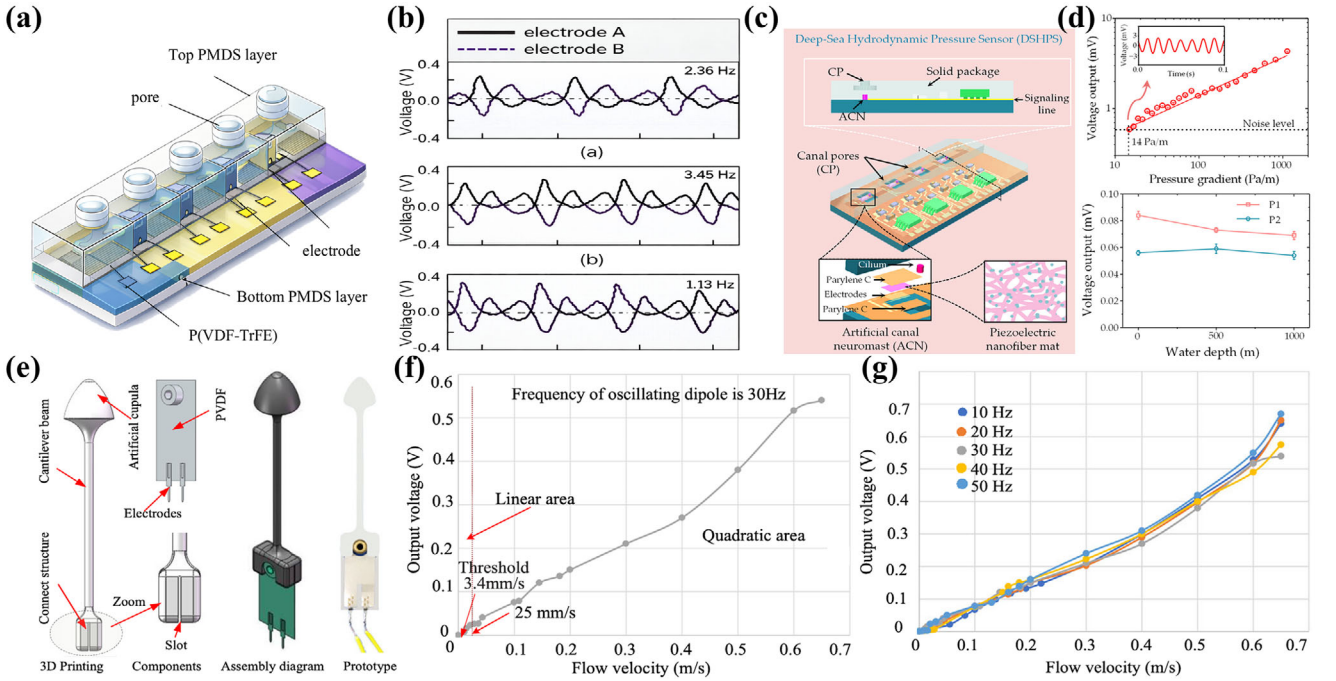

FIGURE 13 | Design and Performance Validation Diagrams of Fish-Inspired Lateral Line Underwater Tactile Sensors. (a) Schematic of the canal artificial lateral line (CALL) sensor array based on highly oriented P(VDF-TrFE) nanofibers [137]. (b) Diagram showing output voltage trends of the CALL sensor under vibrations at different frequencies [137]. (c) Schematic of the deep-sea hydrodynamic pressure sensor (DSHPS) based on P(VDF-TrFE)/BTO nanofibers. Reproduced with permission [138]. Copyright 2024, MDPI. (d) Diagram showing the stable operation of the DSHPS at various water depths. Reproduced with permission [138]. Copyright 2024, MDPI. (e) Schematic of the biomimetic lateral line sensor based on PVDF film for oscillatory flow sensing. Reproduced with permission [139]. Copyright 2022, IEEE. (f–g) Experimental results illustrating the oscillatory flow detection performance of the PVDF-based lateral line sensor. Reproduced with permission [139]. Copyright 2022, IEEE.

3.2.1 | Fish-Inspired Lateral Line Sensors

In recent years, inspired by the lateral line system (LLS) of fish, researchers have proposed various biomimetic artificial lateral line sensors aimed at achieving highly sensitive detection of weak disturbances in underwater environments.

Gong et al. developed a canal artificial lateral line (CALL) sensor array based on highly oriented P(VDF-TrFE) nanofibers [137], as illustrated in Figure 13a. They improved the conventional far-field electrospinning process by combining a rotating drum and parallel-electrode collector to produce highly oriented P(VDF-TrFE) nanofibers, which were annealed at 140°C for 2 h to enhance β-phase crystallinity. The sensor array mimicked the structural design of the fish lateral line system. Experiments demonstrated that, under a 0.6 mm displacement vibration, the output voltage gradually increased as the frequency rose from 2.38 Hz to 5.13 Hz, as shown in Figure 13b. Electrodes A and B produced opposite polarities, forming a differential signal that improved the signal-to-noise ratio, validating its feasibility for underwater pressure sensing.

Hu et al. developed a deep-sea hydrodynamic pressure sensor (DSHPS) [138], as shown in Figure 13c. They used P(VDF-TrFE)/BTO nanofibers as the sensing material and optimized the electrode configuration, sensor element dimensions, and other parameters. The sensor was encapsulated using a high Young's modulus packaging strategy inspired by fish skulls. Experimental results showed that it could detect a minimum pressure difference of approximately 0.11 Pa and had a pressure gradient detection limit of 14 Pa/m. It maintained stable operation at water depths of 0 m, 500 m, and 1000 m, as illustrated in Figure 13d, and demonstrated consistent performance in locating spherical targets, confirming its effectiveness in deep-sea dynamic pressure sensing.

Tan et al. developed a biomimetic lateral line sensor based on polyvinylidene fluoride (PVDF) films for oscillatory flow sensing [139], as shown in Figure 13e. Through computational fluid dynamics and piezoelectric analysis, they optimized the artificial cupula shape (parabolic) and the cantilever beam length (60 mm), and fabricated the sensor using 3D printing along with a waterproofing design. Figure 13f,g presents the experimental results, indicating that the sensor had a flow velocity detection threshold of 3.4 mm s^{-1} at 30 Hz oscillatory flow, with a sensitivity of 0.75 V/(m·s^{-1}). It responded stably within the 10–50 Hz frequency range and could operate at a water depth of 30 meters, demonstrating its effectiveness.

Scott E and Hauert S developed a macroscopic biomimetic lateral line sensor designed to detect vortices shed by upstream robots or obstacles [140], as shown in Figure 14a. Inspired by the fish lateral line system, they enhanced the sensor's performance through optimized design—such as adopting circular canals, backward-facing pores, and increased pore spacing. Simulation analysis was conducted using openfoam, and the sensor prototype was fabricated via 3D printing. Experimental validations were carried out in still water and a custom flow tank.

2365709x, 0, Downloaded from https://advanced.onlinelibrary.wiley.com/doi/10.1002/admt.202502446 by Tongji University, Wiley Online Library on [05/02/2026]. See the Terms and Conditions (https://onlinelibrary.wiley.com/terms-and-conditions) on Wiley Online Library for rules of use; OA articles are governed by the applicable Creative Commons License

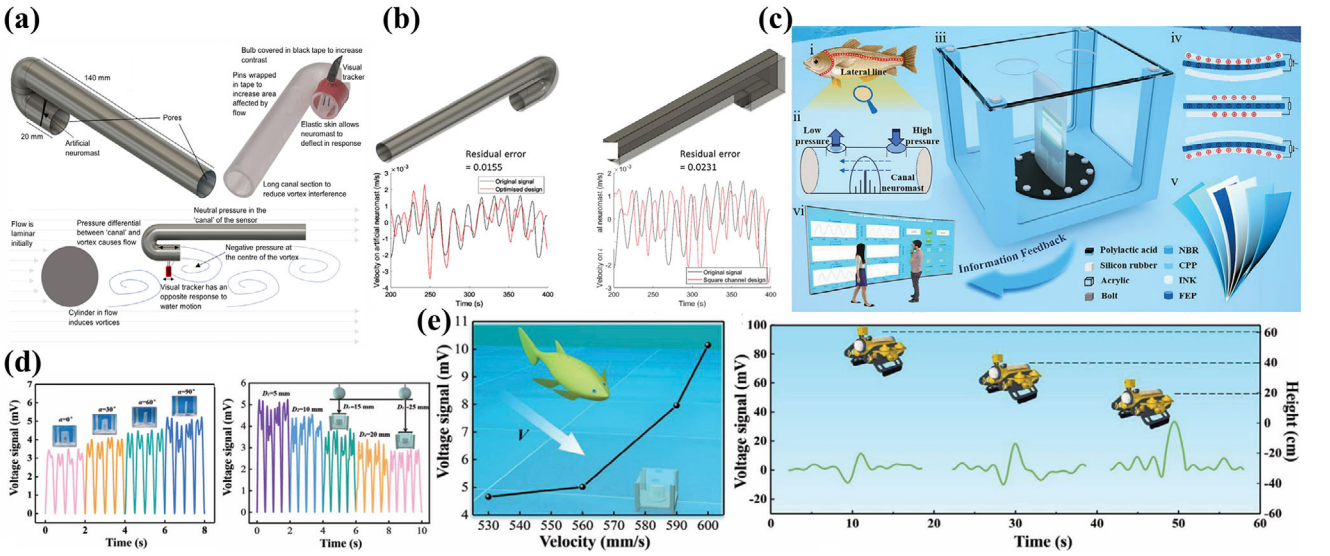

FIGURE 14 | Design and Performance Validation Diagrams of Fish-Inspired Lateral Line Underwater Tactile Sensors. (a) Schematic of the macroscopic biomimetic lateral line sensor for vortex detection. Reproduced with permission [140]. Copyright 2022, IOP Publishing. (b) Simulation error comparison diagram of the optimized design for the macroscopic biomimetic lateral line sensor. Reproduced with permission [140]. Copyright 2022, IOP Publishing. (c) Structural schematic of the biomimetic lateral line sensor (BLLS) based on a triboelectric nanogenerator. Reproduced with permission [42]. Copyright 2023, Wiley-VCH GmbH. (d) Diagram showing dynamic pressure monitoring using the BLLS. Reproduced with permission [42]. Copyright 2023, Wiley-VCH GmbH. (e) Diagram showing the BLLS's capability in identifying underwater object types and motion parameters. Reproduced with permission [42]. Copyright 2023, Wiley-VCH GmbH.

Simulation results showed that the optimized design reduced residual errors by at least 20% compared to sensors lacking key structural elements, with circular canals reducing errors by nearly 40% compared to square canals. These findings are illustrated in Figure 14b. Physical experiments confirmed that the sensor could effectively filter out background flow generated by its own motion. In still water, it successfully detected vortices generated by a moving cylinder, and in the flow tank, it consistently detected vortices at distances of 10 and 20 cm from the cylinder, with the highest detection consistency observed near the cylinder's centerline. Furthermore, the sensor remained effective across a flow velocity range of 0.1–1 m/s, with a 15 mm canal diameter identified as the optimal dimension.

Inspired by the fish lateral line system, Liu et al. developed a biomimetic lateral line sensor (BLLS) based on the principle of a triboelectric nanogenerator (TENG) for underwater dynamic pressure monitoring and trajectory perception [42], as shown in Figure 14c. They fabricated the PLA substrate and connecting disks using 3D printing, encapsulated the sensing unit—composed of strongly electronegative fluorinated ethylene propylene (FEP) and strongly electropositive conductive ink—with Ecoflex20 silicone rubber, and incorporated an acrylic cover plate to achieve waterproofing. The sensor's performance was experimentally validated.

Figure 14d shows the relevant experimental setup. The BLLS achieved optimal sensing performance at a 90° angle of attack, with an open-circuit voltage reaching 5.0 mV and exhibiting a strong linear correlation with the effective diameter (R^2 = 0.98944). The response to disturbance distance followed the fitting equation U = −0.112D + 5.62 (R^2 = 0.99492), where distances from 5.0 to 25.0 mm corresponded to voltages of 5.0 to 2.7 mV, as illustrated in Figure 14d. The response to disturbance frequency in the 1.0–2.0 Hz range followed the fitting equation U = 3.21622f − 1.4973 (R^2 = 0.99604).

Figure 14e demonstrates the sensor's recognition capabilities: it can identify types of underwater objects, measure robotic fish speed (530–600 mm/s corresponding to 4.7–10.1 mV), and detect the height of an ROV. The sensor array can monitor both linear and angular trajectories. Moreover, the sensor maintained stable performance underwater for six months, with no significant decay in the initial 5.0 mV voltage output, making it a promising supplement for sensing in complex underwater environments.

3.2.2 | Tentacle-Inspired Sensors

Bio-tentacle-inspired sensors are a class of biomimetic tactile sensing devices designed by mimicking the structural features, tactile perception mechanisms, and environmental adaptability of natural biological tentacles. Typically integrating flexible, stretchable, and multifunctional materials, these sensors replicate the softness, dexterity, and high-sensitivity tactile perception inherent to biological tentacles.

Wang et al. developed a self-powered biomimetic coral wave sensor (BCWS) for ocean wave monitoring, based on the principle of a triboelectric nanogenerator (TENG) and inspired by coral structures [141], as shown in Figure 15a. They fabricated components such as the polylactic acid (PLA) base using 3D printing and encapsulated the friction-based sensing unit (60 × 10 × 1.5 mm)—composed of fluorinated ethylene propylene (FEP) and conductive ink—with Ecoflex20 silicone rubber. The system also integrates buoyancy trays and counterweight mechanisms, as

2365709x, 0, Downloaded from https://advanced.onlinelibrary.wiley.com/doi/10.1002/admt.202502446 by Tongji University, Wiley Online Library on [05/02/2026]. See the Terms and Conditions (https://onlinelibrary.wiley.com/terms-and-conditions) on Wiley Online Library for rules of use; OA articles are governed by the applicable Creative Commons License

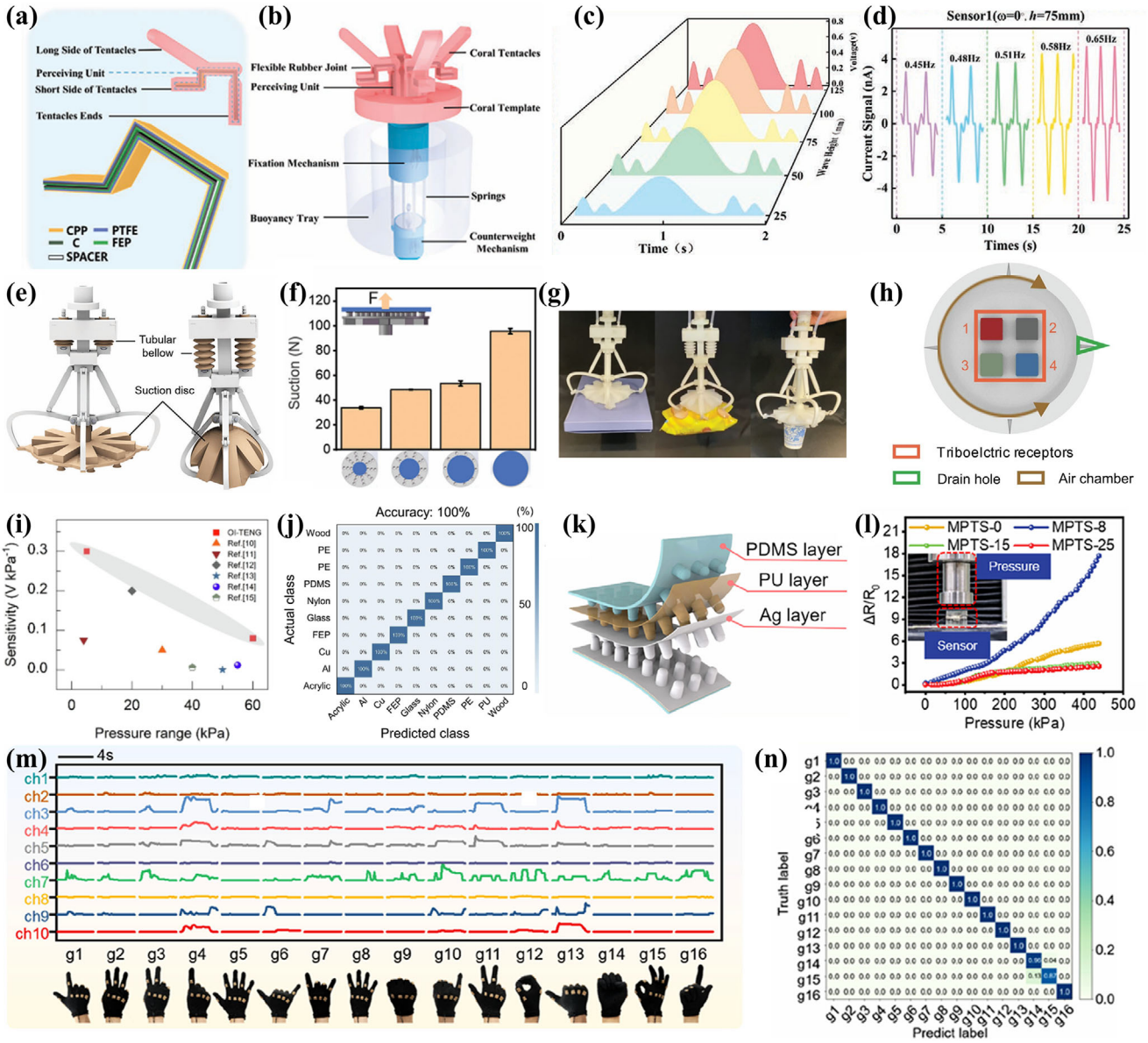

FIGURE 15 | Tentacle-Inspired Underwater Biomimetic Tactile Sensors and Performance Test Diagrams (a) Structural schematic of the self-powered biomimetic coral wave sensor (BCWS) based on the TENG principle. Reproduced with permission [141]. Copyright 2021, Wiley-VCH GmbH. (b) Diagram of BCWS components, including the triboelectric sensing unit, buoyancy tray, etc. Reproduced with permission [141]. Copyright 2021, Wiley-VCH GmbH. (c), (d) Performance data diagrams of BCWS for wave height and frequency sensing. Reproduced with permission [141]. Copyright 2021, Wiley-VCH GmbH. (e) Structural schematic of the soft robotic gripper inspired by bioluminescent octopus suckers. Reproduced with permission [142]. Copyright 2022, Wiley-VCH GmbH. (f) Performance data of the soft robotic gripper's suction force and actuation force [142]. (g) Diagram of the gripper grasping different objects in various scenarios. Reproduced with permission [142]. Copyright 2022, Wiley-VCH GmbH. (h) Structural schematic of the octopus-inspired multi-channel tactile sensor (OI-TENG) based on TENG. Reproduced with permission [143]. Copyright 2025, Elsevier. (i) Output voltage and sensitivity performance data diagram of the OI-TENG. Reproduced with permission [143]. Copyright 2025, Elsevier. (j) Underwater material recognition accuracy of OI-TENG combined with CNN. Reproduced with permission [143]. Copyright 2025, Elsevier. (k) Schematic of the gesture recognition glove (GRG) with integrated micro-pillar tactile sensors (MPTS), inspired by starfish tube feet. Reproduced with permission [144]. Copyright 2024, American Chemical Society. (l) Pressure response range and sensitivity performance data of MPTS. Reproduced with permission [144]. Copyright 2024, American Chemical Society. (m), (n) Diagrams of GRG gesture recognition accuracy and classification performance. Reproduced with permission [144]. Copyright 2024, American Chemical Society.

illustrated in Figure 15b, and its performance was verified through simulation and experiments.

Figure 15c,d shows that the BCWS produced output voltages ranging from 0.3255 V to 0.8162 V in response to wave heights between 25 and 125 mm, with a linear correlation coefficient of R = 0.97132. For wave frequencies between 0.45 and 0.65 Hz, the output current increased from 3.2 to 4.78 nA, with a linear correlation coefficient of R = 0.9906. The sensor demonstrated millimeter-level precision in detecting wave height and

23656798, 0, Downloaded from https://advanced.onlinelibrary.wiley.com/doi/10.1002/admt.202502446 by Tongji University, Wiley Online Library on [05/02/2026]. See the Terms and Conditions (https://onlinelibrary.wiley.com/terms-and-conditions) on Wiley Online Library for rules of use; OA articles are governed by the applicable Creative Commons License

period. The voltage and current signals from its four tentacle-like structures varied symmetrically with angle, enabling accurate wave direction recognition. In real ocean environments, the sensor remained stable when anchored with a mooring chain and successfully collected and wirelessly transmitted data via an Arduino module, with a total power consumption of 4.26 W.

Wu et al., inspired by bioluminescent octopus suckers, developed a soft robotic gripper for underwater adaptive grasping and sensing [142], as shown in Figure 15e. They fabricated the linkage mechanism using 3D printing and employed a modular silicone molding technique to create soft suction cups. Tubular bellows were integrated as actuators, and the gripper's performance was experimentally validated.

As shown in Figure 15f, the gripper achieved a maximum suction force of approximately 100 N—three times greater than that of a fingerless gripper of the same contact area. The tubular bellows produced a maximum pulling force of 24.3 N and a pushing force of 46.7 N, enabling the opening and closing of the suction cups. The gripper was capable of grasping flat objects, objects beyond its direct grasping range (e.g., a 2.5 kg water bottle), and irregularly shaped items. It could also simultaneously pick up multiple dispersed objects, as illustrated in Figure 15g.

In turbid underwater environments, the sensor function was realized by monitoring flow variations inside the suction cups using a turbine flow meter, allowing differentiation between objects of different sizes (e.g., flat plates, knives, etc.). Furthermore, it was capable of gently and non-destructively grasping live turtles and small fish, demonstrating its applicability in complex environments. This gripper presents an effective solution for tasks such as underwater manipulation.

Inspired by octopus suckers, Hao et al. developed an octopus-inspired multi-channel tactile sensor (OI-TENG) based on triboelectric nanogenerator (TENG) technology for underwater material recognition [143], as shown in Figure 15h. They fabricated the suction cup structure using 3D-printed thermoplastic polyurethane (TPU) and integrated four types of triboelectric materials—FEP, PE, and others—as sensory elements. These were treated with inductively coupled plasma (ICP) to create a superhydrophobic surface with a contact angle of 130°. A machine learning-based underwater material identification system (UMIS) was also constructed.

Experiments showed that the sensor's voltage output increased by 67%, achieving a sensitivity of 0.195 V/kPa. The relevant performance data are presented in Figure 15i. The sensor had a response time of 85 ms and maintained stable performance after 3,500 test cycles. It remained consistent under pressures ranging from 5 to 60 N, with minimal output variation across different water depths.

As shown in Figure 15j, a convolutional neural network (CNN) was used to process sensor signals for 10 different materials, achieving 100% accuracy on the training set and 98% on the test set. The sensor functioned reliably in both freshwater and seawater, offering an effective solution for intelligent perception in underwater robotics.

Inspired by the flexible structure of starfish tube feet, Liu et al. developed a gesture recognition glove (GRG) integrated with micro-pillar tactile sensors (MPTS) for underwater immersive communication via hand gesture recognition [144], as shown in Figure 15k. They fabricated the PDMS micro-pillar substrate using two-photon laser direct writing. After N_2 plasma treatment, a layer of water-based polyurethane (WPU) was spray-coated, and silver (Ag) was deposited via magnetron sputtering to form the sensing structure. Ten MPTS units were sewn onto the glove at corresponding finger joints, and a fully connected neural network (FC-NN) algorithm was employed for gesture recognition.

As shown in Figure 15l, the MPTS with an 8° tilt angle exhibited optimal performance: its working range covered 5 Pa to 450 kPa, with a sensitivity of 0.024 kPa^{-1} in the 0–200 kPa range and 0.04 kPa^{-1} from 200–450 kPa. It had a fast response time of 23 ms and maintained stable signals after 10 000 test cycles. In the 20–40 °C temperature range, the resistance variation was only 0.8%, demonstrating excellent waterproof capability.

Figure 15m shows that the GRG captured resistance change signals for 16 different hand gestures, and after processing by the FC-NN model, achieved a recognition accuracy of 99.8%. Figure 15n presents the recognition results. This system enables stable underwater communication and offers a reliable technological solution for divers and other underwater operators.

3.2.3 | Whisker-Inspired Sensors

Based on the sensory mechanisms of seal whiskers, researchers at home and abroad have developed various types of whisker-inspired sensors. As early as 2010, Stocking et al. [145] proposed a capacitive biomimetic sea otter whisker sensor that integrated a rigid artificial whisker into a novel conical parallel-plate capacitor covered with a PDMS film. Numerical simulations predicted a capacitance change of approximately 1 pF under flow velocities ranging from 0–1 m/s, but experimental differences between the baseline and response indicated the need for structural optimization.

In 2015, Beam et al. [146, 147] utilized 3D printing and stereolithography to construct a biomimetic sea otter whisker model, upon which they designed a piezoelectric sensor. Through whisker vibration, multidirectional strain gauges were actuated to achieve multi-dimensional perception of flow disturbances.

In 2018, Gul et al. [148] achieved 360° displacement detection and resistance response using a fully 3D-printed, multi-material design composed of a polyurethane rod and graphene-patterned circuitry.

Inspired by seal whiskers, Wang et al. developed an underwater biomimetic whisker sensor (UBWS) based on a triboelectric nanogenerator (TENG) for passive vortex detection [149], as shown in Figure 16a. They 3D-printed artificial whiskers using PDMS and encapsulated the triboelectric sensing unit—comprising fluorinated ethylene propylene (FEP) and conductive ink—within a silicone bubble structure. Experimental validation demonstrated stable output under varying motion parameters: as the

2365709x, 0, Downloaded from https://advanced.onlinelibrary.wiley.com/doi/10.1002/admt.202502446 by Tongji University, Wiley Online Library on [05/02/2026]. See the Terms and Conditions (https://onlinelibrary.wiley.com/terms-and-conditions) on Wiley Online Library for rules of use; OA articles are governed by the applicable Creative Commons License

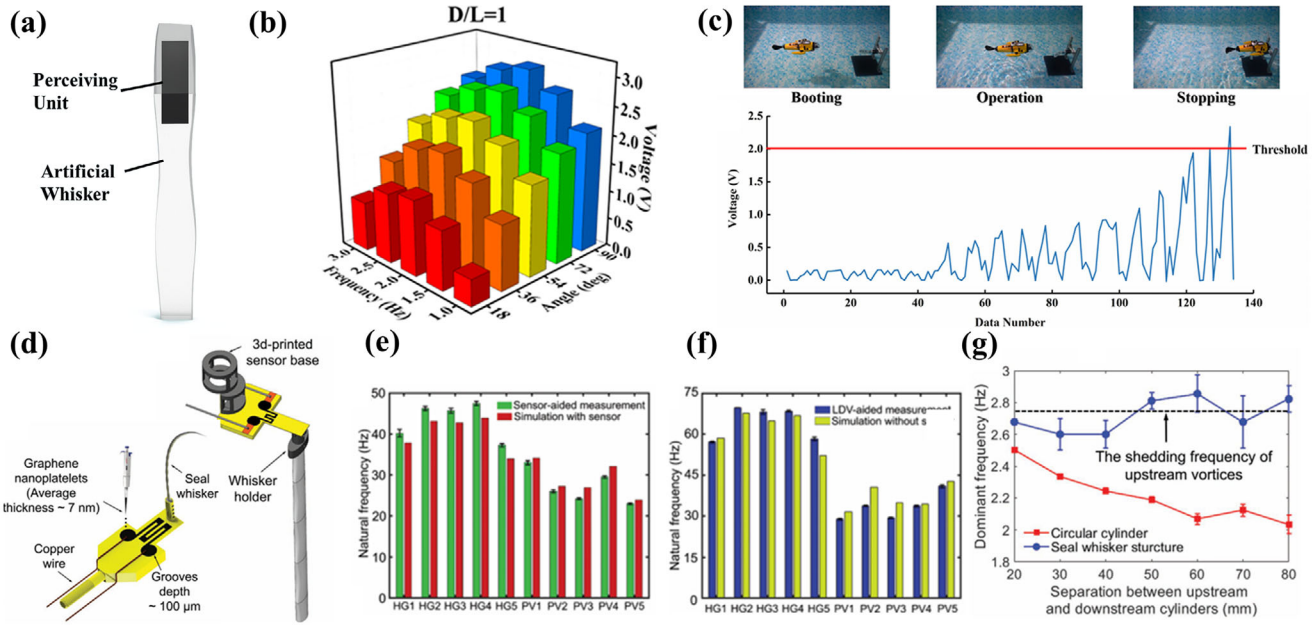

FIGURE 16 | Design and Performance Validation Diagrams of Seal Whisker-Inspired Underwater Biomimetic Tactile Sensors. (a) Structural schematic of the underwater biomimetic whisker sensor (UBWS) based on a triboelectric nanogenerator (TENG). Reproduced with permission [149]. Copyright 2022, Elsevier. (b) Diagram showing output voltage variations of the UBWS under different dimensionless distances, oscillation angles, and frequencies. Reproduced with permission [149]. Copyright 2022, Elsevier. (c) Application scenarios of UBWS, including external module control and robotic fish target tracking. Reproduced with permission [149]. Copyright 2022, Elsevier. (d) Structural schematic of the 3D-printed graphene-based piezoresistive MEMS whisker sensor. Reproduced with permission [150]. Copyright 2022, Wiley-VCH GmbH. (e), (f) Comparative diagrams of experimental and simulated natural frequencies of whiskers from different seal species. Reproduced with permission [150]. Copyright 2022, Wiley-VCH GmbH. (g) Vibration response diagram of the graphene piezoresistive sensor in long-distance wake detection. Reproduced with permission [150]. Copyright 2022, Wiley-VCH GmbH.

dimensionless distance (D/L) increased from 1 to 5, the output voltage decreased linearly (correlation coefficient: 0.99459); as the oscillation angle increased from 18° to 90°, the output voltage followed a quadratic trend (correlation coefficient: 0.99815); and a peak output was observed near the 2 Hz resonant frequency (correlation coefficient: 0.99276), as shown in Figure 16b. The sensor exhibited only a 10% performance drop underwater and maintained stable performance over 30 days of durability testing.

As shown in Figure 16c, the sensor can be used to control external modules in real time, monitor target motion, and be integrated into robotic fish for underwater target tracking, providing an effective sensing solution for underwater robotics.

Zheng et al. developed a 3D-printed graphene-based piezoresistive microelectromechanical system (MEMS) sensor, inspired by the hypersensitive wake-tracking ability of seal whiskers [150], as shown in Figure 16d. They fabricated the cantilever structure using stereolithographic 3D printing technology and formed high-gauge-factor piezoresistive elements by drop-casting graphene nanosheets. The system integrates both real and 3D-printed seal whisker structures and was validated through laser Doppler vibrometry (LDV) and COMSOL simulations.

Experimental results showed that the natural frequency of gray seal whiskers was measured to be 43 ± 4 Hz, and that of harbor seals was 27 ± 4 Hz. These results, presented in Figure 16e,f, aligned well with both LDV measurements and simulation data, with errors ranging from 1 to 6 Hz. In angle-of-attack tests, vortex-induced vibration (VIV) was minimal at 0°, but increased significantly when the angle exceeded 30°.

During long-range wake detection, the sensor exhibited wake-induced vibration (WIV) amplitudes 2 to 10 times higher than its intrinsic VIV when placed at distances ranging from 2.5 to 10 times the whisker diameter. Moreover, the vibration frequency was locked to the upstream vortex shedding frequency of 2.75 Hz, as illustrated in Figure 16g. This sensor provides an efficient solution for long-range wake sensing in underwater robotics.

Glick et al. developed a fiber-optic seal-whisker-inspired sensor array based on fiber Bragg gratings (FBG) for tracking hydrodynamic disturbances [153], as shown in Figure 17a. They used 80 mm-long, 250 μm-diameter quartz optical fibers, embedding an 8 mm FBG at the base to serve as a strain sensor (monitoring bending stress), and a second FBG at the tip to provide temperature compensation (eliminating temperature interference). A helical array layout was designed to reduce collinearity, and the signals were processed using generalized cross-correlation (GCC) and polygon-based localization algorithms, as illustrated in Figure 17b.

Figure 17c–e shows that the sensor array performed effectively under flow velocities ranging from 5 to 25 cm/s, with a wavelength shift detection threshold of 0.012 nm (noise ±0.006 nm). For disturbances at distances of 200–300 mm, the root-mean-square error (RMSE) in direction of arrival (DoA) estimation was 3.5° and 3.7°, respectively. The helical array layout yielded the best

2365709x, 0, Downloaded from https://advanced.onlinelibrary.wiley.com/doi/10.1002/admt.202502446 by Tongji University, Wiley Online Library on [05/02/2026]. See the Terms and Conditions (https://onlinelibrary.wiley.com/terms-and-conditions) on Wiley Online Library for rules of use; OA articles are governed by the applicable Creative Commons License

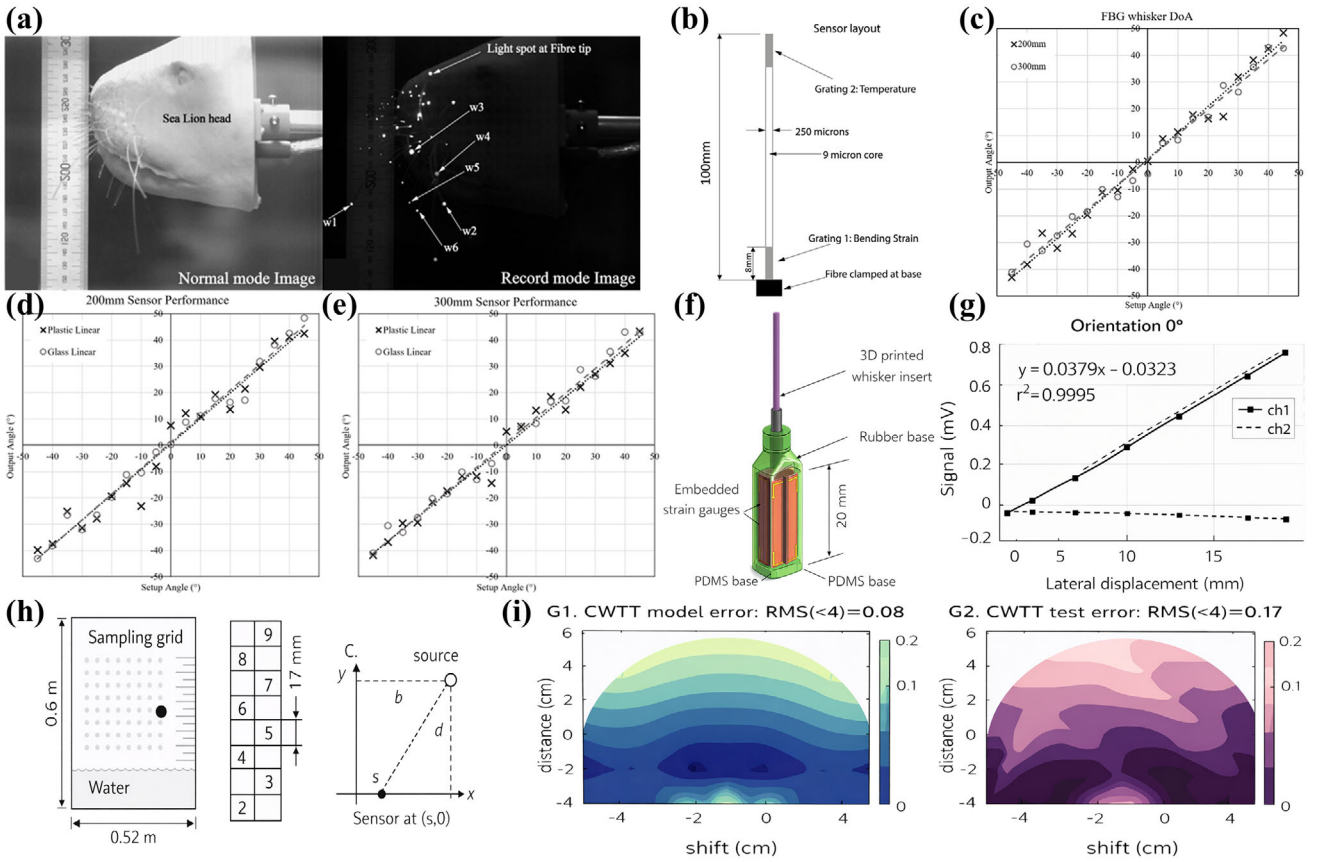

FIGURE 17 | Design and Performance Validation Diagrams of Seal Whisker-Inspired Underwater Biomimetic Tactile Sensors. (a) Structural schematic of the seal whisker-inspired sensor array based on fiber Bragg grating (FBG). Reproduced with permission [151]. Copyright 2024, University of London Institutional Repository. (b) Diagram of the FBG sensor array's helical layout and signal processing algorithm. Reproduced with permission [151]. Copyright 2024, University of London Institutional Repository. (c)–(e) Diagrams illustrating the FBG sensor's flow velocity response, disturbance direction estimation error, and performance comparison of array configurations. Reproduced with permission [151]. Copyright 2024, University of London Institutional Repository. (f) Structural schematic of the low-cost biomimetic seal whisker flow sensor [152]. (g) Experimental results showing the flow velocity detection sensitivity and linear response of the whisker flow sensor [152]. (h) Layout and dimensions of the 9-element whisker sensor array [152]. (i) Prediction results of underwater bipolar source positions using the sensor array [152].

performance, with an RMSE as low as 1.9°. The signal-to-noise ratio (SNR) was approximately 2 dB, and the computational efficiency was 40% higher than that of conventional visual tracking methods. This sensor reliably identifies vortex rings and cylinder wakes, providing a robust solution for environmental perception in underwater robotics.

Geng et al. proposed a low-cost, easily mass-producible biomimetic seal whisker flow sensor for passive underwater sensing of flow velocity and direction [152], as shown in Figure 17f. The device was fabricated by first precisely replicating the geometry of a seal whisker using 3D printing, then embedding two adjacent and perpendicular metal foil strain gauges within a flexible PDMS substrate to enable bidirectional measurement of both bending amplitude and direction during whisker deflection.

Experimental results, shown in Figure 17g, indicated that the sensor exhibited extremely low self-noise in still water and was capable of reliably detecting flow velocities as low as 0.5 mm/s—approaching the sensitivity of biological whiskers (~0.25 mm/s). Within the low-frequency range (≤35 Hz), the output signal maintained a high degree of linearity with flow velocity (R^2 > 0.99), had a response time under 100 ms, and demonstrated excellent repeatability and fatigue resistance after thousands of test cycles.

To validate its applicability in arrayed configurations, the research team built a 9-element sensor array and employed an artificial neural network for data interpretation. Figure 17h shows the layout and dimensions of the array, which successfully achieved accurate localization of underwater bipolar sources, as illustrated in Figure 17i.

4 | Applications of Underwater Bionic Tactile Sensing

Building upon the continuous evolution of material systems and sensor types, biomimetic underwater tactile sensors are gradually transitioning from laboratory research to real-world applications. Their flexibility, high sensitivity, and strong anti-interference capabilities grant them unique advantages in complex underwater environments. With the advancement of marine technology—particularly the rise of intelligent underwater systems—these

2365709x, 0, Downloaded from https://advanced.onlinelibrary.wiley.com/doi/10.1002/admt.202502446 by Tongji University, Wiley Online Library on [05/02/2026]. See the Terms and Conditions (https://onlinelibrary.wiley.com/terms-and-conditions) on Wiley Online Library for rules of use; OA articles are governed by the applicable Creative Commons License

sensors have not only expanded the boundaries of traditional sensing methods but also provided new technological pathways for various critical scenarios. The following sections will focus on their specific applications in representative areas such as underwater robotics, marine scientific monitoring, and military and emergency rescue operations.

4.1 | Underwater Flow Field Sensing

Underwater flow field sensing is fundamental to enabling critical tasks such as autonomous navigation, obstacle avoidance, and target tracking [154–156]. Inspired by the highly sensitive tactile systems of marine organisms like seal whiskers, fish lateral lines, and coral tentacles, researchers are developing a range of flexible biomimetic sensors capable of high-resolution, multidimensional, and real-time detection of subtle flow velocities, vortices, and flow directions.

Liu et al. developed a deep learning-assisted triboelectric whisker sensor array (TWSA) for underwater applications [51], as shown in Figure 18a. Inspired by seal whiskers, the sensor features a high aspect-ratio elliptical whisker shaft, four sensing units at the base, and a flexible corrugated joint. Based on the triboelectric nanogenerator principle, it converts micro-disturbances into electrical signals. The sensor exhibits a response time of 19 ms, sensitivity of 0.2 V/ms, and a signal-to-noise ratio of 58 dB. It can identify 3D flow velocity and direction in underwater environments, track upstream vortex shedding frequencies, and achieve a minimum detection accuracy of 81.2%. When integrated into remotely operated vehicles (ROVs) and combined with a hybrid model of convolutional neural networks (CNNs) and long short-term memory networks (LSTMs), it enables 3D trajectory estimation. Figure 18b–d shows the trajectory estimation process and results, achieving a root-mean-square error (RMSE) of approximately 0.02, while also detecting nearby obstacles. This technology provides effective support for near-field sensing and autonomous navigation of underwater vehicles. Figure 18e illustrates its application scenarios, showing significant potential in marine research, underwater search and rescue, and environmental monitoring.

Wang et al. developed a seal-whisker-inspired flow sensor using a mechanical-to-magnetic signal conversion mechanism, which physically separates the whisker drag element from the electronic components, ensuring good waterproofing and corrosion resistance [157], as shown in Figure 18f. Its modular design allows for optimization of sensitivity and sensing range by adjusting the shape of the drag element (e.g., rod, plate, cross-shaped). An analytical model was used to quantify the impact of whisker shape and cross-sectional area on sensor performance. This sensor can be integrated into surface robots such as commercial remote-controlled boats, as shown in Figure 18g,h. In field tests, when installed on a remote-controlled boat for speed estimation, it successfully captured various speed changes. Compared to the ground truth measured by a laser prism system, the sensor achieved a minimum RMSE of 0.06 m s^{-1}, as shown in Figure 18i. This provides an effective solution for flow sensing and speed estimation in underwater robotics, enhancing their perception and navigation capabilities.

Liu et al. also developed a triboelectric biomimetic lateral line sensor (TBLS), inspired by the neuromasts in fish lateral line systems. The sensor consists of a flexible sensing unit and a biomimetic canal and operates based on the triboelectric nanogenerator principle [43], as shown in Figure 18j. In propeller wake thickness measurements, it achieved only 5.7% error, and demonstrated a pressure gradient sensitivity of 2.1 mV·Pa^{-1}·m^{-1}. When paired with the H_2O Auto-ML algorithm, the sensor achieved 100% accuracy in identifying oscillatory flow signals, as shown in Figure 18k. It can be integrated into underwater robots (e.g., ROVs) to assist in flow field sensing under low-light or complex conditions, such as detecting propeller wakes and oscillatory flows—filling the gap left by visual sensors. Additionally, the sensor was combined with an unmanned surface vehicle (USV) to build a monitoring platform, as illustrated in Figure 18l. In real marine environments, the system transmitted underwater disturbance data wirelessly to a receiving terminal 117 meters away, as shown in Figure 18m. This technology offers a new approach to enhancing flow field perception and operational capabilities of underwater robots.

4.2 | Underwater Operations

In underwater operations, robotic manipulators, grippers, and inspection platforms must obtain accurate force and flow field information under complex hydrodynamic and contact conditions. The use of biomimetic flexible tactile sensors can significantly enhance operational stability, safety, and efficiency.

Xu et al. developed a self-powered underwater tactile sensor (TPTS) based on a contact–separation-type triboelectric nanogenerator (TENG) and inspired by the structure of sea otter paw pads. They successfully integrated the sensor into various underwater operation platforms, demonstrating broad application potential [49], as shown in Figure 19a. In pipeline non-destructive testing, the sensor was used to collect clamping force signals in real time to identify cracks and corrosion defects, as illustrated in Figure 19b. In closed-loop grasping experiments, the system precisely adjusted gripping force based on the hardness and shape of the target, enabling high-accuracy classification of soft spheres and geometric objects while avoiding damage, as shown in Figure 19c–f. In autonomous grasping demonstrations, the sensor guided obstacle avoidance and navigation via LED indicators and a deep learning model. Its high-frequency stability and excellent directional resolution also make it suitable for providing real-time tactile feedback for underwater monitoring, sampling, and remote manipulation by AUVs/ROVs, making it an ideal low-cost and self-powered solution.

Chen et al. developed a biomimetic underwater octopus tactile gripper (UOTG) based on the triboelectric nanogenerator principle. Inspired by octopus sensing and grasping mechanisms, the gripper consists mainly of a suction cup-like structural network and embedded triboelectric sensors [47], as shown in Figure 19g. Its fully flexible structure adapts to objects of various shapes and sizes, and generates electrical signals through contact–separation effects to provide tactile information such as pressure and deformation. Figure 19h,i shows the integration of the gripper with a remotely operated underwater vehicle (ROV). It is capable of sensing grip force, detecting object slippage, estimating object

2365709x, 0, Downloaded from https://advanced.onlinelibrary.wiley.com/doi/10.1002/admt.202502446 by Tongji University, Wiley Online Library on [05/02/2026]. See the Terms and Conditions (https://onlinelibrary.wiley.com/terms-and-conditions) on Wiley Online Library for rules of use; OA articles are governed by the applicable Creative Commons License

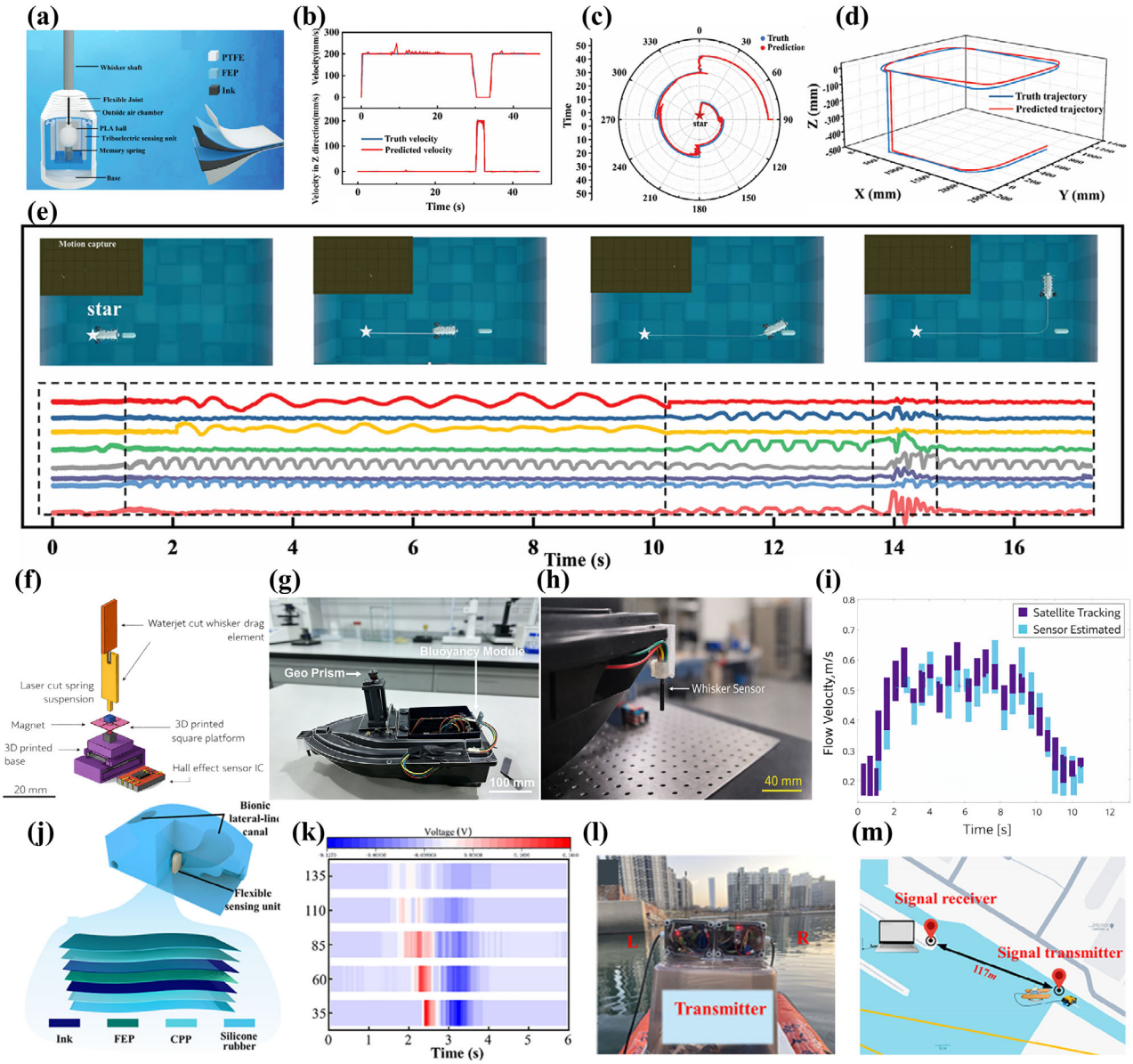

FIGURE 18 | Diagrams of biomimetic underwater flow field sensing sensors and their applications. (a) Structural schematic of the deep learning-assisted triboelectric underwater whisker sensor array (TWSA). Reproduced with permission [51]. Copyright 2024, Wiley-VCH GmbH. (b)–(d) Diagrams showing the 3D trajectory estimation process and results of TWSA integrated into an unmanned underwater vehicle. Reproduced with permission [51]. Copyright 2024, Wiley-VCH GmbH. (e) Application scenario of TWSA for near-field perception and autonomous navigation of an unmanned underwater vehicle. Reproduced with permission [51]. Copyright 2024, Wiley-VCH GmbH. (f) Structural schematic of the seal-whisker-inspired flow sensor based on a mechanical-to-magnetic signal conversion mechanism [152]. (g), (h) Diagrams showing integration of the seal-whisker-inspired flow sensor into a commercial remote-controlled boat [152]. (i) Diagram comparing sensor-based speed estimation results with ground-truth measurements [157]. (j) Structural schematic of the triboelectric biomimetic lateral line sensor (TBLS). Reproduced with permission [43]. Copyright 2025, Wiley-VCH GmbH. (k) Performance data diagram of TBLS, including propeller wake measurement error and oscillatory flow identification accuracy. Reproduced with permission [43]. Copyright 2025, Wiley-VCH GmbH. (l) Schematic of a monitoring platform combining TBLS with an unmanned surface vehicle (USV). Copyright 2025, Wiley-VCH GmbH. (m) Diagram of TBLS wireless data transmission in real marine environments. Reproduced with permission [43]. Copyright 2025, Wiley-VCH GmbH.

volume, and recognizing object shape and hardness. Figure 19j,k presents the corresponding recognition results, with accuracies of 98.3% for shape and 98.0% for hardness. Furthermore, the gripper generated distinctive signals when grasping underwater biological models such as crabs and sea cucumbers, indicating its significant potential for applications in underwater salvage, archaeology, and marine debris removal.

This section focuses on the development and application of biomimetic underwater tactile sensors, introducing a variety of sensors inspired by marine organisms such as seal whiskers, fish lateral lines, sea otter paw pads, and octopus tentacles. These sensors, utilizing principles such as triboelectric nanogenerator and mechanical-to-magnetic conversion, have demonstrated excellent performance in flow field sensing and underwater

2365709x, 0, Downloaded from https://advanced.onlinelibrary.wiley.com/doi/10.1002/admt.202502446 by Tongji University, Wiley Online Library on [05/02/2026]. See the Terms and Conditions (https://onlinelibrary.wiley.com/terms-and-conditions) on Wiley Online Library for rules of use; OA articles are governed by the applicable Creative Commons License

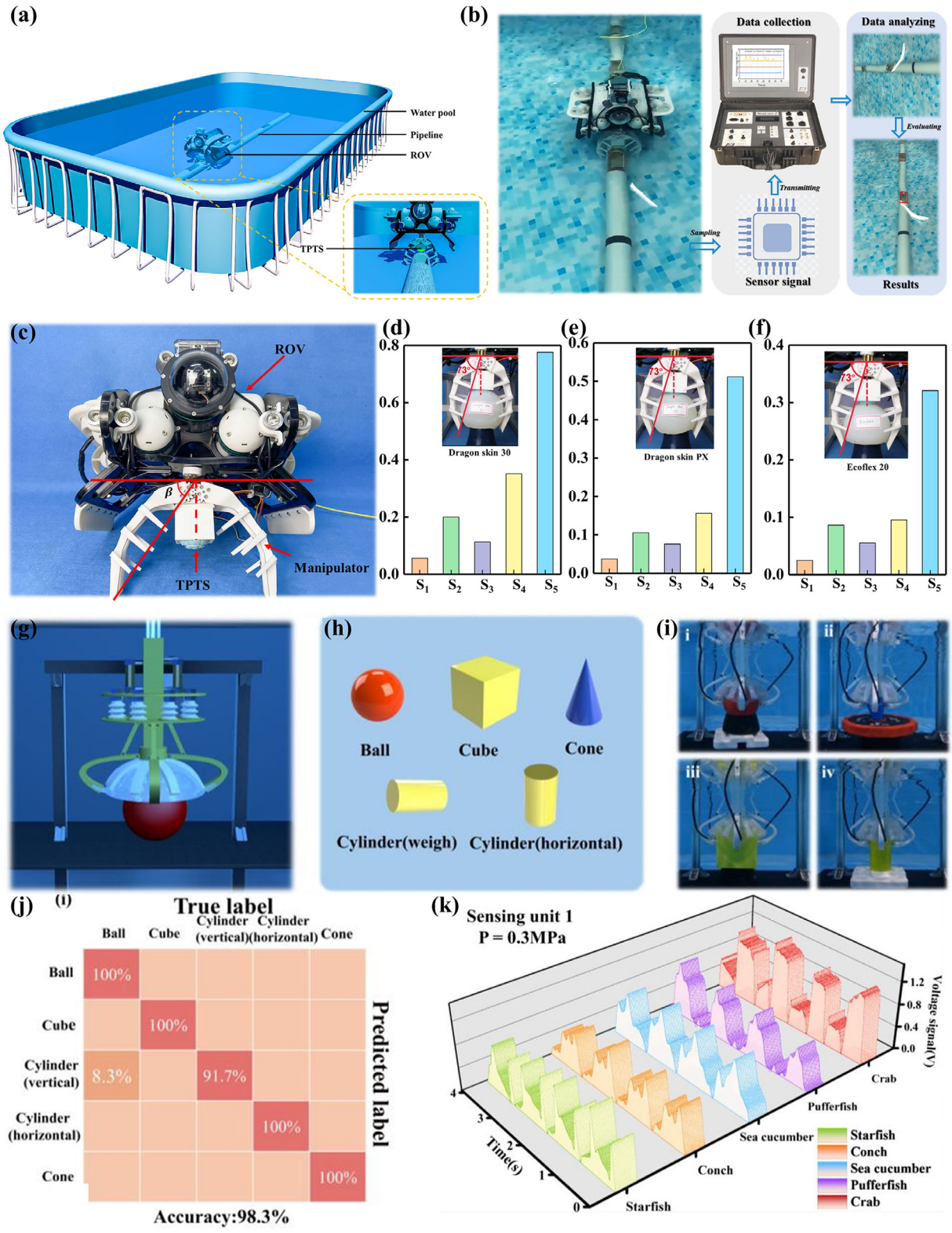

FIGURE 19 | Illustrations of biomimetic underwater tactile sensor integration in operational platforms. (a) Schematic of the sea otter paw pad-inspired self-powered underwater tactile sensor (TPTS) based on the TENG principle and its integration into an operational platform. Reproduced with permission [49]. Copyright 2022, Springer Nature. (b) Diagram showing the use of TPTS to collect clamping force signals for defect detection during pipeline non-destructive testing. Reproduced with permission [49]. Copyright 2022, Springer Nature. (c)–(f) Diagrams showing the process and outcomes of TPTS adjusting gripping force in closed-loop grasping experiments for different target objects. Reproduced with permission [49]. Copyright 2022, Springer Nature. (g) Structural schematic of the biomimetic underwater octopus tactile gripper (UOTG) based on a triboelectric nanogenerator. Reproduced with permission [47]. Copyright 2025, Elsevier. (h,i) Diagrams showing the integration of UOTG into a remotely operated underwater vehicle (ROV). Reproduced with permission [47]. Copyright 2025, Elsevier. (j,k) Diagrams showing UOTG's recognition performance for object shape and hardness. Reproduced with permission [47]. Copyright 2025, Elsevier.

2365709x, 0, Downloaded from https://advanced.onlinelibrary.wiley.com/doi/10.1002/admt.202502446 by Tongji University, Wiley Online Library on [05/02/2026]. See the Terms and Conditions (https://onlinelibrary.wiley.com/terms-and-conditions) on Wiley Online Library for rules of use; OA articles are governed by the applicable Creative Commons License

TABLE 3 | Comparison table of performance metrics and application scenarios of biomimetic underwater tactile sensors.

Sensor name	Biological inspiration	Performance metrics	Application scenarios
Underwater Triboelectric Whisker Sensor Array (TWSA)	Seal whiskers	Response Time: 19 Ms; Sensitivity: 0.2 V/Ms; SNR: 58 dB; Flow Velocity and Direction Accuracy: 81.2%; Trajectory Estimation RMSE: ∼0.02	Near-field Sensing and Autonomous Navigation for AUVs; Marine Research; Underwater Rescue; Environmental Monitoring
Seal-Whisker-Inspired Flow Sensor	Seal whiskers	Minimum RMSE: 0.06 M/s; Performance Tunable by Adjusting Whisker Shape	Flow Sensing and Speed Estimation for Surface/Underwater Robots; Enhanced Navigation and Perception
Triboelectric Biomimetic Lateral Line Sensor (TBLS)	Fish lateral line neuromasts	Propeller Wake Thickness Error: 5.7%; Pressure Gradient Sensitivity: 2.1 $mV \cdot Pa^{-1} \cdot M^{-1}$; Oscillatory Flow Recognition Accuracy: 100%; Transmission Range: 117 M	Flow Field Sensing (propeller wakes, oscillatory flows) in Low-light Environments for Underwater Robots; Integrated with USVs for Monitoring Platforms
Self-Powered Underwater Tactile Sensor (TPTS)	Sea otter paw pads	High-frequency Stability; Excellent Directional Resolution; Precise Grip Force Adjustment	Pipeline Non-destructive Testing; Object Classification, Monitoring, Sampling, and Remote Operation for Underwater Robots
Biomimetic Underwater Octopus Tactile Gripper (UOTG)	Octopus tentacles	Shape Recognition Accuracy: 98.3%; Hardness Recognition Accuracy: 98.0%; Detects Gripping Force, Slippage, and Volume	Underwater Salvage, Archaeology, Debris Removal; Grasping of Marine Biological Models (e.g., crabs, sea cucumbers)

operations, addressing diverse needs such as autonomous navigation and object manipulation. Detailed information and application scenarios of these sensors are summarized in Table 3.

5 | Challenges and Future Trends

Although Underwater Biomimetic Tactile Sensors Show Great Promise in the Field of Marine Perception, Current Technological Development Still Faces Multiple Challenges, Which Limit Their Widespread Deployment in Complex Ocean Environments.

5.1 | Current Technological Bottlenecks

As shown in Figure 20, material performance represents the most challenging corein the underwater biomimetic tactile sensing technology. Material characterized by excellent flexibility, biocompatibility, and corrosion resistance simultaneously remains difficult. Surrounding this core are four interrelated layers of technical barriers, including sensing performance, interference coupling, structural replication, and signal processing. These four modules are both independent and intertwined. For example, the microstructure of materials determines the upper limit of sensitivity, and environmental disturbances amplify signal noise. Thus, any breakthrough in one aspect may trigger new complications, resulting in an interconnected system of technological obstacles.

Material performance is the cornerstone of underwater biomimetic tactile sensing technology. The simultaneous optimization of functional properties, biocompatibility, and environmental resilience remains an unresolved triadic dilemma. For instance, triboelectric tactile sensors inspired by sea otter paw pads can replicate the unique surface texture of otter palms, allowing real-time detection and differentiation of normal and shear loads, but their sensitivity and reliability are limited in high-temperature environments [158]. Humidity sensors with highly biocompatible materials based on Zn electrodes and biodegradable hydrogels are prone to structural breakdown in extreme pH or high-salinity underwater environments, such as swelling or rupture. This characteristic makes them unsuitable for long-term operation in harsh conditions [159]. Ionic polymer–metal composites, which exhibit good biocompatibility in aquatic environments, can achieve large bending deformations (>220%) under 3V activation in hydrated states, but suffer from low output force (only 1–5 MPa) and efficiency loss over repeated use [160]. These examples illustrate how the functional properties optimization, biocompatibility, and environmental resistance form the central node of the technological bottleneck network. Around this node, challenges related to sensing performance, interference coupling, structural replication, and signal processing further evolve into derivative technical layers.

Sensing performance in dynamic underwater environments involves inherent trade-offs among sensitivity, dynamic range, response speed, and multimodal decoupling capability. To detect weak signals such as biological wakes, sensors must be designed

2365709x, 0, Downloaded from https://advanced.onlinelibrary.wiley.com/doi/10.1002/admt.202502446 by Tongji University, Wiley Online Library on [05/02/2026]. See the Terms and Conditions (https://onlinelibrary.wiley.com/terms-and-conditions) on Wiley Online Library for rules of use; OA articles are governed by the applicable Creative Commons License

FIGURE 20 | The current challenge network faced by biomimetic underwater tactile sensing technology.

with extremely high gain to ensure high sensitivity [161]. Moreover, multimodal coupling introduces signal confusion. Physical quantities, such as pressure, vibration, and temperature, often act on the sensing elements through similar mechanisms, causing their signals to overlap and become indistinguishable at the sensor output, which significantly reduces signal resolvability [162].

Underwater environments are inherently unstable, where external and internal noise sources interact in ways that degrade sensor performance and reliability. For instance, Biological wakes and turbulence can have overlapping frequency spectra, especially in the low-frequency domain. This means that it is difficult to distinguish between fish swimming or crustacean motion and ambient flow using frequency-based identification algorithms [163].

Microstructures in biological tactile organs are key to their superior sensing capabilities. However, current fabrication technologies cannot precisely replicate such microstructures, leading to a bottleneck in structural replication. Mainstream manufacturing methods, such as photolithography, microfabrication, and 3D printing, face physical limitations when attempting to reproduce high aspect ratios, complex surfaces, and nanoscale features [164].

Signal processing faces significant algorithmic bottlenecks. Existing algorithms are often ill-equipped to handle compound disturbances from water flow, biofouling, and electromagnetic interference [165]. Moreover, the absence of standardized multi-source interference datasets leads to insufficient training, making it difficult to distinguish target signals from environmental noise [166]. This results in limiting the reliability of perception and hindering robustness improvements through algorithmic optimization [167].

These bottlenecks interact and amplify each other, forming a tightly coupled, self-reinforcing network of technical challenges. This systemic difficulty continues to constrain the advancement of biomimetic underwater tactile sensing technologies and hinders their path toward engineering-scale application.

5.2 | Future Research Directions

The Future Research of Underwater Biomimetic Tactile Sensing Technology Can Follow a Progressive Pathway of Materials Innovation, System Integration, Application Expansion, Gradually Overcoming the Material-centered Network of Challenges.

2365709x, 0, Downloaded from https://advanced.onlinelibrary.wiley.com/doi/10.1002/admt.202502446 by Tongji University, Wiley Online Library on [05/02/2026]. See the Terms and Conditions (https://onlinelibrary.wiley.com/terms-and-conditions) on Wiley Online Library for rules of use; OA articles are governed by the applicable Creative Commons License

Materials innovation is the primary breakthrough point. For example, in the case of hydrogel materials, introducing reinforcing phases such as cellulose nanocrystals can optimize the crosslinking network, which enhances mechanical properties and reduces the risks of swelling and degradation under extreme pH or salinity conditions [168, 169]. Additionally, specific material design strategies have been proposed to enhance sensor performance: Wang et al. prepared TPU/MOFs-801 composite nanofiber films via electrospinning, utilizing the porous structure and carboxyl groups of MOFs-801 to construct ion transport channels; combined with the sensing mechanism of "pressure-driven difference in ion migration rate" to amplify signal response, the sensitivity of the sensor was improved [170]. Liu et al. developed a seawater-resistant conductive hydrogel with ultra-high sensitivity and self-healing ability by introducing a skin-like heterogeneous structure, which was specifically constructed through surface hydrophobic modification via confined N-alkylation reaction; an underwater strain sensor fabricated based on this hydrogel further enhanced the sensitivity and pressure resistance of the sensor [171].

On the other hand, biomimetic micro/nano surfaces inspired by the structures of deep-sea organisms can be designed. For instance, mimicking the densely packed yet flexible arrangement of deep-sea fish scales, ordered microstructures can be fabricated on material surfaces using photolithography and 3D printing techniques. These structures can reduce lower water flow resistance, as well as improve the sensor's sensitivity to slight pressure changes. Alternatively, based on the drag-reduction mechanism of dolphin skin, adaptive surface materials can be developed that automatically adjust their surface morphology in response to variations in water flow and pressure [172, 173].

In response to high underwater pressure, special encapsulation structures made of pressure-resistant materials can be designed to isolate internal sensing components from the external environment. In terms of material algorithm coupling, dedicated signal processing algorithms should be developed for the characteristics of novel materials. For example, specific filtering algorithms of the nanocomposite sensors can be designed to remove intrinsic material noise and underwater environmental interference [174]. Machine learning algorithms can also be employed to build adaptive models based on the sensing data features of materials under different underwater environments, enabling real-time adjustment of signal processing parameters.

Material performance should be expanded toward application-oriented goals. In terms of multi-scenario customization, materials that are sensitive to bioelectrical and chemical signals and possess good biocompatibility should be developed to precisely monitor the behavior and physiological states of marine organisms. In the field of underwater archaeology and cultural heritage conservation, materials that are sensitive to subtle pressure and temperature changes and exhibit good anti-aging performance should be developed for the detection and protection of underwater artifacts [175]. In marine resource exploration, materials should be designed to withstand high temperature and high pressure, with selective responsiveness to specific minerals or chemicals, in order to improve the efficiency and accuracy of resource detection.

From the perspective of sustainable development, research should focus on biodegradable and recyclable sensing materials, such as degradable hydrogels based on natural biopolymers, which can naturally decompose in the marine environment after completing their sensing function [176]. Moreover, material recycling and reuse strategies should be explored to reduce costs. The strategies ensure that biomimetic underwater tactile sensing technology not only meets performance demands in long-term applications but also aligns with environmental protection and economic viability.

6 | Conclusion

The Deep Integration of Marine Biological Inspiration and Engineering Techniques Has Driven Remarkable Advancements in Biomimetic Underwater Tactile Sensing, Yielding Diverse Solutions to Address Key Challenges in Underwater Environmental Perception.

The core bottleneck limiting further development lies in the material-centered technical network, where balancing mechanical strength, sensing precision, and environmental adaptability remains unresolved. Future efforts should prioritize developing novel biomimetic composite materials: emulating the micro/nano surface structures and functional mechanisms of deep-sea organisms, and optimizing material interfacial properties to enhance anti-interference capability and tolerance to extreme conditions like high pressure and corrosion. A specific step involves incorporating cellulose nanocrystals into hydrogel matrices to reinforce mechanical stability while retaining flexibility, enabling long-term deployment in high-salinity or extreme pH environments.

Guided by material innovation, integrating miniaturized, low-power hardware with intelligent algorithms will enable precise filtering of multi-source interference, constructing integrated systems that balance environmental robustness and sensing resolution. These systems can be iteratively refined through real-scenario applications in deep-sea exploration, marine engineering, and biological observation—validating material performance, exposing weaknesses, and optimizing solutions.

Looking ahead, the coordinated advancement of multifunctional materials, micro/nano structural simulation, integrated module design, and data-driven intelligent signal processing will collectively overcome bottlenecks such as insufficient sensitivity, limited noise suppression, and inadequate structural precision. This holistic approach will equip marine engineering and underwater intelligent robotics with high-reliability, precision tactile sensing capabilities, unlocking new potentials for ocean resource development and environmental monitoring.

Funding

This work was supported in part by the National Natural Science Foundation of China (Nos. 52371345, 52401399), in part by the Postdoctoral Fellowship Program of China Postdoctoral Science Foundation (No. GZC20230062)

2365709x, 0, Downloaded from https://advanced.onlinelibrary.wiley.com/doi/10.1002/admt.202502446 by Tongji University, Wiley Online Library on [05/02/2026]. See the Terms and Conditions (https://onlinelibrary.wiley.com/terms-and-conditions) on Wiley Online Library for rules of use; OA articles are governed by the applicable Creative Commons License

Conflicts of Interest

The authors declare no conflicts of interest.

Data Availability Statement

The authors have nothing to report.

References

1. N. Krasnokutska, T. Danko, and N. Shyriaieva, "Ecosystem-based Technology Innovation Management in the European Renewable Energy Sector," in 2023 IEEE 4th KhPI Week on Advanced Technology (KhPI-Week) (IEEE, 2023), 1–6, https://doi.org/10.1109/KhPIWeek61412.2023.10312849.

2. A. K. Verma, "Influence of Climate Change on Balanced Ecosystem, Biodiversity and Sustainable Development: An Overview," *International Journal of Biological Innovations* 03, no. 02 (2021): 331–337, https://doi.org/10.46505/IJBI.2021.3213.

3. X. Ye, "Research on Biodiversity and Ecological Environment Cycle: Interaction and Balance Mechanisms," in SHS Web of Conferences (edp Sciences, 2024), 02029, https://doi.org/10.1051/shsconf/202420002029.

4. C. A. Obiorah, O. G. Ndubuisi, S. E. Ali, and U. T. Aku, "Preserving the Delicate Balance: Understanding the Interconnections Between Ecosystem and Biodiversity," *International Journal of Innovative Environmental Studies Research* 13, no. 2 (2025): 22–32, https://doi.org/10.5281/ZENODO.15153018.

5. M. F. Rabbi, J. Popp, D. Máté, and S. Kovács, "Energy Security and Energy Transition to Achieve Carbon Neutrality," *Energies* 15, no. 21 (2022): 8126, https://doi.org/10.3390/en15218126.

6. T. R. R. Pearman, K. Robert, A. Callaway, et al., "Spatial and Temporal Environmental Heterogeneity Induced by Internal Tides Influences Faunal Patterns on Vertical Walls within a Submarine Canyon," *Frontiers in Marine Science* 10 (2023): 1091855, https://doi.org/10.3389/fmars.2023.1091855.

7. Y. Li, C. Yu, W. Wang, H. Li, and X. Jiang, "A Review on Structural Failure of Composite Pressure Hulls in Deep Sea," *Journal of Marine Science and Engineering* 10, no. 10 (2022): 1456, https://doi.org/10.3390/jmse10101456.

8. R. Liu, L. Liu, and F. Wang, "The Role of Hydrostatic Pressure on the Metal Corrosion in Simulated Deep-Sea Environments — A Review," *Journal of Materials Science & Technology* 112 (2022): 230–238, https://doi.org/10.1016/j.jmst.2021.10.014.

9. B. Liu, X. Tang, R. Tharmarasa, T. Kirubarajan, R. Jassemi, and S. Hallé, "Underwater Target Tracking in Uncertain Multipath Ocean Environments," *IEEE Transactions on Aerospace and Electronic Systems* 56, no. 6 (2020): 4899–4915, https://doi.org/10.1109/TAES.2020.3003703.

10. Challenges, Limitations, and Measurement Strategies to Ensure Data Quality in Deep-sea Sensors, Accessed 2025, https://www.frontiersin.org/journals/marine-science/articles/10.3389/fmars.2023.1152236/full.

11. Review of Underwater Sensing Technologies and Applications, Accessed 2025, https://www.mdpi.com/1424-8220/21/23/7849.

12. Y. Liu, H. Lu, and Y. Cui, "A Review of Marine in Situ Sensors and Biosensors," *Journal of Marine Science and Engineering* 11, no. 7 (2023): 1469, https://doi.org/10.3390/jmse11071469.

13. M. Tang, M. Liu, S. Zhang, R. Zheng, S. Dong, and Z. Liu, "Distributed Target Tracking via UWSNs in the Presence of Multipath Interference," *Signal Processing* 236 (2025): 110041, https://doi.org/10.1016/j.sigpro.2025.110041.

14. H. Song, S. Zhang, H. Du, et al., "A Flexible Flow Velocity Sensor Based on Core-Sheath Structured Triboelectric Nanogenerator for Underwater Environmental Monitoring," *Advanced Materials Technologies* 10 (2025): 00704, https://doi.org/10.1002/admt.202500704.

15. N. Yang, M. R. Amini, M. Johnson-Roberson, and J. Sun, "Real-time Model Predictive Control for Energy Management in Autonomous Underwater Vehicle," in 2018 IEEE Conference on Decision and Control (CDC) (IEEE, 2018), 4321–4326, https://doi.org/10.1109/CDC.2018.8619844.

16. Z. Cooper-Baldock, S. Turnock, and K. Sammut, "Wake-informed 3D path planning for Autonomous Underwater Vehicles using A∗ and neural network approximations," *Ocean Engineering* 332 (2025): 121353, https://doi.org/10.1016/j.oceaneng.2025.121353.

17. Review of pH Sensing Materials from Macro-to Nano-scale: Recent Developments and Examples of Seawater Applications, 2025, https://scholar.google.com.hk/scholar?hl=zh-CN&as_sdt=0%2C5&q=Review+of+pH+sensing+materials+from+macro-to+nano-scale%3A+Recent+developments+and+examples+of+seawater+applications&btnG =.

18. S. Raz and D. Breitkopf, "Natural Perception Hypothesis: How Natural Selection Shapes Species-Specific Sensory Experiences and Influences Biodiversity," Global Journal of Ecology 9 no. 2, (2024): 132–144.

19. D. E. Edgley, M. Carruthers, N. P. Gabagambi, et al., "Lateral Line System Diversification during the Early Stages of Ecological Speciation in Cichlid Fish," *BMC Ecology and Evolution* 24, no. 1 (2024): 24, https://doi.org/10.1186/s12862-024-02214-5.

20. W. Han, S. Lei, Y. Chenguang, et al., "Development and Application of an Underwater Mass Spectrometer for in Situ Detection of Deep-sea Dissolved Gases," *Chinese Journal of Analytical Chemistry* 51, no. 9 (2023): 100299, https://doi.org/10.1016/j.cjac.2023.100299.

21. Y. Yang, Z. Dai, Y. Chen, Y. Yuan, Y. Yalikun, and C. Shang, "Emerging MEMS Sensors for Ocean Physics: Principles, Materials, and Applications," *Applied Physics Reviews* 11, no. 2 (2024): 021320, https://doi.org/10.1063/5.0194194.

22. J. F. Webb, "Structural and Functional Evolution of the Mechanosensory Lateral Line System of Fishes," *The Journal of the Acoustical Society of America* 154, no. 6 (2023): 3526–3542, https://doi.org/10.1121/10.0022565.

23. J. Baranyk, K. Malir, M. A. P. Silva, S. Rieck, G. Scheve, and N. Nakanishi, "Structural, Molecular and Developmental Evidence for Cell-type Diversity in Cnidarian Mechanosensory Neurons," *Nature Communications* 16, no. 1 (2025): 1514, https://doi.org/10.1038/s41467-025-56115-2.

24. W. Chang and M. E. Hale, "Mechanosensory Signal Transmission in the Arms and the Nerve Ring, an Interarm Connective, of Octopus Bimaculoides," *iScience* 26, no. 5 (2023): 106722, https://doi.org/10.1016/j.isci.2023.106722.

25. B. P. Chagnaud, H. Bleckmann, and J. Engelmann, "Neural Responses of Goldfish Lateral Line Afferents to Vortex Motions," *Journal of Experimental Biology* 209, no. 2 (2006): 327–342.

26. K. P. Sebens and M. A. R. Koehl, "Predation on Zooplankton by the Benthic Anthozoans *Alcyonium siderium* (Alcyonacea) and *Metridium senile* (Actiniaria) in the New England Subtidal," *Marine Biology* 81, no. 3 (1984): 255–271, https://doi.org/10.1007/BF00393220.

27. E. Papadakis, D. P. Tsakiris, and M. Sfakiotakis, "An Octopus-Inspired Soft Pneumatic Robotic Arm," *Biomimetics* 9, no. 12 (2024): 773.

28. S. M. Strobel, M. A. Miller, M. J. Murray, and C. Reichmuth, "Anatomy of the Sense of Touch in Sea Otters: Cutaneous Mechanoreceptors and Structural Features of Glabrous Skin," *The Anatomical Record* 305, no. 3 (2022): 535–555, https://doi.org/10.1002/ar.24739.

29. X. Zheng, A. M. Kamat, M. Cao, and A. G. P. Kottapalli, "Wavy Whiskers in Wakes: Explaining the Trail-Tracking Capabilities of Whisker Arrays on Seal Muzzles," *Advanced Science* 10, no. 2 (2023): 2203062, https://doi.org/10.1002/advs.202203062.

30. M. Bora, A. G. P. Kottapalli, J. Miao, and M. S. Triantafyllou, "Biomimetic Hydrogel-CNT Network Induced Enhancement of Fluid-Structure Interactions for Ultrasensitive Nanosensors," *NPG Asia Materials* 9, no. 10 (2017): e440–e440.

31. S. Liang, J. Li, F. Li, L. Hu, W. Chen, and C. Yang, "Flexible Tactile Sensing Microfibers Based on Liquid Metals," *ACS Omega* 7, no. 15 (2022): 12891–12899, https://doi.org/10.1021/acsomega.2c00098.

2365709x, 0, Downloaded from https://advanced.onlinelibrary.wiley.com/doi/10.1002/admt.202502446 by Tongji University, Wiley Online Library on [05/02/2026]. See the Terms and Conditions (https://onlinelibrary.wiley.com/terms-and-conditions) on Wiley Online Library for rules of use; OA articles are governed by the applicable Creative Commons License

32. J. Tie, Z. Mao, L. Zhang, Y. Zhong, X. Sui, and H. Xu, "Conductive Ionogel with Underwater Adhesion and Stability as Multimodal Sensor for Contactless Signal Propagation and Wearable Devices," *Composites Part B: Engineering* 232 (2022): 109612, https://doi.org/10.1016/j.compositesb.2022.109612.

33. G. Diraco, G. Rescio, P. Siciliano, and A. Leone, "Review on human Action Recognition in Smart Living: Sensing Technology, Multimodality, Real-time Processing, Interoperability, and Resource-constrained Processing," *Sensors* 23, no. 11 (2023): 5281, https://doi.org/10.3390/s23115281.

34. Y. Guo, P. Huo, S. Huang, G. Gou, and Q. Li, "Multi-Receptor Skin with Highly Sensitive Tele-Perception Somatosensory Flexible Electronics in Healthcare: Multimodal Sensing and AI-Powered Diagnostics," *Advanced Healthcare Materials* 14 (2025): 2502901, https://doi.org/10.1002/adhm.202502901.

35. C. Abah, A. L. Orekhov, G. L. Johnston, P. Yin, H. Choset, and N. Simaan, "A Multi-Modal Sensor Array for Safe Human-Robot Interaction and Mapping," in 2019 International Conference on Robotics and Automation (ICRA) (IEEE, 2019), 3768–3774, https://doi.org/10.1109/ICRA.2019.8793466.

36. X. Liu, K. Li, S. Qian, et al., "A High-sensitivity Flexible Bionic Tentacle Sensor for Multidimensional Force Sensing and Autonomous Obstacle Avoidance Applications," *Microsystems & Nanoengineering* 10, no. 1 (2024): 149.

37. A. Duan, Z. Zhu, M. Wang, et al., "Magnetic Arthropod Soft Robot with Triboelectric Bionic Antennae for Obstacle Identifying and Avoidance," *Materials & Design* 244 (2024): 113109, https://doi.org/10.1016/j.matdes.2024.113109.

38. J. Yu, K. Zhang, and Y. Deng, "Recent Progress in Pressure and Temperature Tactile Sensors: Principle, Classification, Integration and Outlook," *Soft Science* 1, no. 1 (2021): 6, https://doi.org/10.20517/ss.2021.05.

39. Q. Shu, Y. Pang, Q. Li, et al., "Flexible Resistive Tactile Pressure Sensors," *Journal of Materials Chemistry A* 12, no. 16 (2024): 9296–9321, https://doi.org/10.1039/D3TA06976A.

40. S. Park, Y. Park, and J. Bae, "Performance Evaluation of a Tactile and Kinesthetic Finger Feedback System for Teleoperation," *Mechatronics* 87 (2022): 102898, https://doi.org/10.1016/j.mechatronics.2022.102898.

41. T. Uthai, T. Zhou, Y. Ye, H. You, and J. Du, "Haptics-Based Robot Teleoperation for Soft Object Manipulation," *Journal of Construction Engineering and Management* 151, no. 5 (2025): 04025028, https://doi.org/10.1061/JCEMD4.COENG-15819.

42. J. Liu, P. Xu, B. Liu, et al., "Underwater Biomimetic Lateral Line Sensor Based on Triboelectric Nanogenerator for Dynamic Pressure Monitoring and Trajectory Perception," *Small* 20, no. 19 (2024): 2308491, https://doi.org/10.1002/smll.202308491.

43. J. Liu, B. Liu, Z. Xi, et al., "Highly Sensitive and Integratable Triboelectric Bionic Lateral Line Sensor for Flow Recognition of Underwater Vehicle," *Advanced Materials Technologies* 10, no. 13 (2025): 2500072, https://doi.org/10.1002/admt.202500072.

44. Q. Wang, P. Xiao, W. Zhou, et al., "Bioinspired Adaptive, Elastic, and Conductive Graphene Structured Thin-Films Achieving High-Efficiency Underwater Detection and Vibration Perception," *Nano-Micro Letters* 14 (2022): 62, https://doi.org/10.1007/s40820-022-00799-4.

45. T. Wang, Z. Guo, H. Jin, et al., "A Coral-inspired and Fully Self-powered Wave Monitoring System Based on Hybridized Triboelectric-electromagnetic Nanogenerator," *Sensors and Actuators A: Physical* 387 (2025): 116451, https://doi.org/10.1016/j.sna.2025.116451.

46. X. Wang, J. Liu, S. Wang, et al., "A Self-powered Triboelectric Coral-Like Sensor Integrated Buoy for Irregular and Ultra-Low Frequency Ocean Wave Monitoring," *Advanced Materials Technologies* 7 (2022): 2101098, https://doi.org/10.1002/admt.202101098.

47. H. Chen, Y. Li, P. Xu, et al., "Octopus-inspired Soft Gripper with Embedded Triboelectric Tactile Sensor for Underwater Target Recognition and Grasp," *Nano Energy* 140 (2025): 111007, https://doi.org/10.1016/j.nanoen.2025.111007.

48. C. Wei, S. Yu, Y. Meng, et al., "Octopus Tentacle-Inspired In-Sensor Adaptive Integral for Edge-Intelligent Touch Intention Recognition," *Advanced Materials* 37, no. 27 (2025): 2420501, https://doi.org/10.1002/adma.202420501.

49. P. Xu, J. Liu, X. Liu, et al., "A Bio-inspired and Self-powered Triboelectric Tactile Sensor for Underwater Vehicle Perception," *npj Flexible Electronics* 6, no. 1 (2022): 25, https://doi.org/10.1038/s41528-022-00160-0.

50. Y. Li, B. Liu, P. Xu, et al., "A Palm-like 3D Tactile Sensor Based on Liquid-metal Triboelectric Nanogenerator for Underwater Robot Gripper," *Nano Research* 17, no. 11 (2024): 10008–10016, https://doi.org/10.1007/s12274-024-6903-3.

51. B. Liu, B. Dong, H. Jin, et al., "Deep-Learning-Assisted Triboelectric Whisker Sensor Array for Real-Time Motion Sensing of Unmanned Underwater Vehicle," *Advanced Materials Technologies* 10, no. 3 (2025): 2401053, https://doi.org/10.1002/admt.202401053.

52. G. Liu, Y. Jiang, P. Wu, Z. Ma, H. Chen, and D. Zhang, "Artificial Whisker Sensor with Undulated Morphology and Self-Spread Piezoresistors for Diverse Flow Analyses," *Soft Robotics* 10, no. 1 (2023): 97–105, https://doi.org/10.1089/soro.2021.0166.

53. L. Guo, J. Liu, G. Wu, et al., "Piezoelectric Wavy Whisker Sensor for Perceiving Underwater Vortex from a Bluff Body," *Sensors and Actuators A: Physical* 365 (2024): 114875, https://doi.org/10.1016/j.sna.2023.114875.

54. M. A. Schwalbe, B. J. Sevey, and J. F. Webb, "Detection of Artificial Water Flows by the Lateral Line System of a Benthic Feeding Cichlid Fish," *Journal of Experimental Biology* 219, no. 7 (2016): 1050–1059, https://doi.org/10.1242/jeb.136150.

55. S. Dijkgraaf, "THE FUNCTIONING and SIGNIFICANCE OF THE LATERAL-LINE ORGANS," *Biological Reviews* 38, no. 1 (1963): 51–105, https://doi.org/10.1111/j.1469-185X.1963.tb00654.x.

56. H. Bleckmann and R. Zelick, "Lateral Line System of Fish," *Integrative Zoology* 4, no. 1 (2009): 13–25, https://doi.org/10.1111/j.1749-4877.2008.00131.x.

57. S. Coombs, H. Bleckmann, R. R. Fay, and A. N. Popper, The Lateral Line System. (Springer Handbook of Auditory Research) (Springer, 2014), https://doi.org/10.1007/978-1-4614-8851-4.

58. J. Engelmann, W. Hanke, J. Mogdans, and H. Bleckmann, "Hydrodynamic Stimuli and the Fish Lateral Line," *Nature* 408, no. 6808 (2000): 51–52, https://doi.org/10.1038/35040706.

59. C. Li, X. J. Wang, and J. K. Song, "Structure and function of the mechanosensory lateral line system in fish and biomimetic," *Chinese Science Bulletin* 62, no. 22 (2017): 2509–2519, https://doi.org/10.1360/N972016-00706.

60. R. R. Taylor and A. Forge, "Hair Cell Regeneration in Sensory Epithelia from the Inner Ear of a Urodele Amphibian," *Journal of Comparative Neurology* 484, no. 1 (2005): 105–120, https://doi.org/10.1002/cne.20450.

61. E. Y. Ma, E. W. Rubel, and D. W. Raible, "Notch Signaling Regulates the Extent of Hair Cell Regeneration in the Zebrafish Lateral Line," *The Journal of Neuroscience* 28, no. 9 (2008): 2261–2273.

62. J. C. Liao, "Organization and Physiology of Posterior Lateral Line Afferent Neurons in Larval Zebrafish," *Biology Letters* 6, no. 3 (2010): 402–405, https://doi.org/10.1098/rsbl.2009.0995.

63. H. Münz, "Morphology and Innervation of the Lateral Line System in*Sarotherodon niloticus* (L.) (Cichlidae, Teleostei," *Zoomorphologie* 93, no. 1 (1979): 73–86, https://doi.org/10.1007/BF02568676.

64. J. Song and R. G. Northcutt, "Morphology, Distribution and Innervation of the Lateral-Line Receptors of the Florida Gar, *Lepisosteus platyrhincus*," *Brain Behaviour and Evolution* 37 (1991), 24–37, https://doi.org/10.1159/000114344.

65. J. C. Montgomery, S. Windsor, and D. Bassett, "Behavior and Physiology of Mechanoreception: Separating Signal and Noise," *Integrative Zoology* 4, no. 1 (2009): 3–12, https://doi.org/10.1111/j.1749-4877.2008.00130.x.

2365709x, 0, Downloaded from https://advanced.onlinelibrary.wiley.com/doi/10.1002/admt.202502446 by Tongji University, Wiley Online Library on [05/02/2026]. See the Terms and Conditions (https://onlinelibrary.wiley.com/terms-and-conditions) on Wiley Online Library for rules of use; OA articles are governed by the applicable Creative Commons License

66. S. Kröther, J. Mogdans, and H. Bleckmann, "Brainstem Lateral Line Responses to Sinusoidal Wave Stimuli in Still and Running Water," *Journal of Experimental Biology* 205, no. 10 (2002): 1471–1484, https://doi.org/10.1242/jeb.205.10.1471.

67. Coral Disease & Health Consortium, Microscopic Anatomy, 2025, https://cdhc.noaa.gov/coral-biology/microscopic-anatomy/.

68. R. N. Mariscal, "Scanning Electron Microscopy of the Sensory Surface of the Tentacles of Sea Anemones and Corals," *Zeitschrift für Zellforschung und Mikroskopische Anatomie* 147, no. 2 (1974): 149–156, https://doi.org/10.1007/BF00582789.

69. A. Beckmann and S. Özbek, "The Nematocyst: A Molecular Map of the Cnidarian Stinging Organelle," *The International Journal of Developmental Biology* 56, no. 6–8 (2012): 577–582, https://doi.org/10.1387/ijdb.113472ab.

70. S. Kommareddy and M. Amiji, "Biodistribution and Pharmacokinetic Analysis of Long-Circulating Thiolated Gelatin Nanoparticles Following Systemic Administration in Breast Cancer-Bearing Mice," *Journal of Pharmaceutical Sciences* 96, no. 2 (2007): 397–407, https://doi.org/10.1002/jps.20813.

71. U. Shavit, T. Mass, and A. Genin, "The Small-Scale Flow Field around Dipsastraea Favus Corals," *Frontiers in Marine Science* 9 (2022): 857109, https://doi.org/10.3389/fmars.2022.857109.

72. D. Malul, R. Holzman, and U. Shavit, "Coral Tentacle Elasticity Promotes an *out-of-phase* Motion That Improves Mass Transfer," *Proceedings of the Royal Society B: Biological Sciences* 287, no. 1929 (2020): 20200180, https://doi.org/10.1098/rspb.2020.0180.

73. E. Tambutté, P. Ganot, A. A. Venn, and S. Tambutté, "A Role for Primary Cilia in Coral Calcification?," *Cell and Tissue Research* 383 (2021): 1093–1102, https://doi.org/10.1007/s00441-020-03343-1.

74. G. M. Watson and D. A. Hessinger, "Cnidocyte Mechanoreceptors Are Tuned to the Movements of Swimming Prey by Chemoreceptors," *Science* 243, no. 4898 (1989): 1589–1591, https://doi.org/10.1126/science.2564698.

75. B. M. Mason, M. Koyanagi, T. Sugihara, et al., "Multiple Opsins in a Reef-building Coral, Acropora Millepora," *Scientific Reports* 13, no. 1 (2023): 1628, https://doi.org/10.1038/s41598-023-28476-5.

76. K. P. Sebens and K. DeRiemer, "Diel Cycles of Expansion and Contraction in Coral Reef Anthozoans," *Marine Biology* 43, no. 3 (1977): 247–256, https://doi.org/10.1007/BF00402317.

77. B. Nilius and G. Owsianik, "The Transient Receptor Potential family of Ion Channels," *Genome Biology* 12, no. 3 (2011): 218, https://doi.org/10.1186/gb-2011-12-3-218.

78. F. Pallasdies, S. Goedeke, W. Braun, and R. M. Memmesheimer, "From Single Neurons to Behavior in the Jellyfish Aurelia aurita," *elife* 8 (2019): 50084, https://doi.org/10.7554/eLife.50084.

79. R. W. Meech, "Electrophysiology and Behavior of Cnidarian Nervous Systems," in *Oxford Research Encyclopedia of Neuroscience*, Accessed August 5, 2025 (2019), https://oxfordre.com/neuroscience/display/10.1093/acrefore/9780190264086.001.0001/acrefore-9780190264086-e-146.

80. W. M. Kier and M. P. Stella, "The Arrangement and Function of Octopus Arm Musculature and Connective Tissue," *Journal of Morphology* 268, no. 10 (2007): 831–843, https://doi.org/10.1002/jmor.10548.

81. Octopus Arms Have Segmented Nervous Systems to Power Extraordinary Movements | Biological Sciences Division. The University of Chicago, Accessed August 5, 2025, https://biologicalsciences.uchicago.edu/news/octopus-arms-segmented-nervous-system.

82. L. van Giesen, P. B. Kilian, C. A. Allard, and N. W. Bellono, "Molecular Basis of Chemotactile Sensation in Octopus," *Cell* 183, no. 3 (2020): 594–604.e14.

83. G. Sumbre, Y. Gutfreund, G. Fiorito, T. Flash, and B. Hochner, "Control of Octopus Arm Extension by a Peripheral Motor Program," *Science* 293, no. 5536 (2001): 1845–1848, https://doi.org/10.1126/science.1060976.

84. Sensational Sucker: the Neural Complexity of the Octopus Organ | Scientific American, Accessed 2025, https://www.scientificamerican.com/article/sensational-sucker/.

85. J. M. Kim, A. Coutinho, Y. J. Park, and H. Rodrigue, "Octopus-inspired Suction Cup Array for Versatile Grasping Operations," *IEEE Robotics and Automation Letters* 8, no. 5 (2023): 2962–2969, https://doi.org/10.1109/LRA.2023.3263377.

86. K. C. Buresch, N. D. Huget, W. C. Brister, et al., "Evidence for Tactile 3D Shape Discrimination by Octopus," *Journal of Comparative Physiology A* 210, no. 5 (2024): 815–823, https://doi.org/10.1007/s00359-024-01696-4.

87. A. Tekinalp, N. Naughton, S. H. Kim, et al., "Topology, Dynamics, and Control of an Octopus-analog Muscular Hydrostat," (2023), https://doi.org/10.48550/arXiv.2304.08413.

88. Octopus Arms Have Segmented Nervous Systems to Power Extraordinary Movements | Biological Sciences Division | The University of Chicago, 2025, https://biologicalsciences.uchicago.edu/news/octopus-arms-segmented-nervous-system.

89. S. M. Strobel, J. M. Sills, M. T. Tinker, and C. J. Reichmuth, "Active Touch in Sea Otters: In-air and Underwater Texture Discrimination Thresholds and Behavioral Strategies for Paws and Vibrissae," *Journal of Experimental Biology* 221, no. 18 (2018): jeb181347, https://doi.org/10.1242/jeb.181347.

90. M. E. Diamond and E. Arabzadeh, "Whisker sensory system – From receptor to decision," *Progress in Neurobiology* 103 (2013): 28–40, https://doi.org/10.1016/j.pneurobio.2012.05.013.

91. T. J. Prescott, M. E. Diamond, and A. M. Wing, "Active Touch Sensing," *Philosophical Transactions of the Royal Society B: Biological Sciences* 366, no. 1581 (2011): 2989–2995, https://doi.org/10.1098/rstb.2011.0167.

92. W. W. Au, K. J. Benoit-Bird, and R. A. Kastelein, "Modeling the Detection Range of Fish by Echolocating Bottlenose Dolphins and Harbor Porpoises," *The Journal of the Acoustical Society of America* 121, no. 6 (2007): 3954–3962, https://doi.org/10.1121/1.2734487.

93. T. C. Newby, F. M. Hart, and R. A. Arnold, "Weight and Blindness of Harbor Seals," *Journal of Mammalogy* 51, no. 1 (1970): 152–152, https://doi.org/10.2307/1378545.

94. H. Hyvärinen, "Diving in Darkness: Whiskers as Sense Organs of the Ringed Seal *(Phoca hispida saimensis)*," *Journal of Zoology* 218, no. 4 (1989): 663–678, https://doi.org/10.1111/j.1469-7998.1989.tb05008.x.

95. D. Renouf, "Fishing in Captive Harbour Seals (Phoca vitulina concolor): A Possible Role for Vibrissae," *Netherlands Journal of Zoology* 30, no. 3 (1979): 504–509.

96. D. Renouf, "Preliminary Measurements of the Sensitivity of the Vibrissae of Harbour Seals (*Phoca vitulina*) to Low Frequency Vibrations," *Journal of Zoology* 188, no. 4 (1979): 443–450, https://doi.org/10.1111/j.1469-7998.1979.tb03428.x.

97. G. Dehnhardt, B. Mauck, and H. Bleckmann, "Seal Whiskers Detect Water Movements," *Nature* 394, no. 6690 (1998): 235–236, https://doi.org/10.1038/28303.

98. G. Dehnhardt, B. Mauck, W. Hanke, and H. Bleckmann, "Hydrodynamic Trail-Following in Harbor Seals (*Phoca vitulina*)," *Science* 293, no. 5527 (2001): 102–104, https://doi.org/10.1126/science.1060514.

99. N. Schulte-Pelkum, S. Wieskotten, W. Hanke, G. Dehnhardt, and B. Mauck, "Tracking of Biogenic Hydrodynamic Trails in Harbour Seals (*Phoca vitulina*)," *Journal of Experimental Biology* 210, no. 5 (2007): 781–787, https://doi.org/10.1242/jeb.02708.

100. W. Hanke, M. Witte, L. Miersch, et al., "Harbor Seal Vibrissa Morphology Suppresses Vortex-induced Vibrations," *Journal of Experimental Biology* 213, no. 15 (2010): 2665–2672, https://doi.org/10.1242/jeb.043216.

101. X. Zheng, A. M. Kamat, M. Cao, and A. G. P. Kottapalli, "Creating Underwater Vision Through Wavy Whiskers: A Review of the Flow-Sensing Mechanisms and Biomimetic Potential of Seal Whiskers," *Journal of the Royal Society Interface* 18, no. 183 (2021), https://doi.org/10.1098/rsif.2021.0629.

2365709x, 0, Downloaded from https://advanced.onlinelibrary.wiley.com/doi/10.1002/admt.202502446 by Tongji University, Wiley Online Library on [05/02/2026]. See the Terms and Conditions (https://onlinelibrary.wiley.com/terms-and-conditions) on Wiley Online Library for rules of use; OA articles are governed by the applicable Creative Commons License

102. H. Smodlaka, I. Galex, L. Palmer, J. A. Borovac, and W. A. Khamas, "Ultrastructural, Sensory and Functional Anatomy of the Northern Elephant Seal (*Mirounga angustirostris*) Facial Vibrissae," *Anatomia, Histologia, Embryologia* 46, no. 5 (2017): 487–496, https://doi.org/10.1111/ahe.12293.

103. D. L. Hu, B. Chan, and J. W. Bush, "The Hydrodynamics of Water Strider Locomotion," *Nature* 424, no. 6949 (2003): 663–666, https://doi.org/10.1038/nature01793.

104. P. P. Goodwyn, A. Katsumata-Wada, and K. Okada, "Morphology and Neurophysiology of Tarsal Vibration Receptors in the Water Strider Aquarius paludum (Heteroptera: Gerridae)," *Journal of Insect Physiology* 55, no. 9 (2009): 855–861, https://doi.org/10.1016/j.jinsphys.2009.06.001.

105. Q. Q. Xin, Design and fabrication of bionic sensor based on the perception mechanism of water striders, Ph.D. Thesis, Jilin University, Changchun, China, (2023).

106. T. Po, E. Kanso, and M. J. McHenry, "Cooperative Transport in Sea Star Locomotion," *Current Biology* 34, no. 12 (2024): 2551–2557.e4, https://doi.org/10.5061/dryad.hqbzkh1p3.

107. R. Santos, D. Haesaerts, M. Jangoux, and P. Flammang, "Comparative Histological and Immunohistochemical Study of Sea Star Tube Feet (Echinodermata, Asteroidea)," *Journal of Morphology* 263, no. 3 (2005): 259–269, https://doi.org/10.1002/jmor.10187.

108. R. Santos, Â. Barreto, C. Franco, and A. V. Coelho, "Mapping Sea Urchins Tube Feet Proteome — A Unique Hydraulic Mechano-Sensory Adhesive Organ," *Journal of Proteomics* 79 (2013): 100–113, https://doi.org/10.1016/j.jprot.2012.12.004.

109. Y. Liu, R. Bao, J. Tao, J. Li, M. Dong, and C. Pan, "Recent Progress in Tactile Sensors and Their Applications in Intelligent Systems," *Science Bulletin* 65, no. 1 (2020): 70–88, https://doi.org/10.1016/j.scib.2019.10.021.

110. H. Zhao, H. Wang, H. Yu, et al., "Theoretical Modeling of Contact-separation Mode Triboelectric Nanogenerators from Initial Charge Distribution," *Energy & Environmental Science* 17, no. 6 (2024): 2228–2247, https://doi.org/10.1039/D3EE04143C.

111. Y. Liu, J. Wang, T. Liu, et al., "Triboelectric Tactile Sensor for Pressure and Temperature Sensing in High-temperature Applications," *Nature Communications* 16, no. 1 (2025): 383, https://doi.org/10.1038/s41467-024-55771-0.

112. X. Qu, J. Xue, Y. Liu, W. Rao, Z. Liu, and Z. Li, "Fingerprint-shaped Triboelectric Tactile Sensor," *Nano Energy* 98 (2022): 107324, https://doi.org/10.1016/j.nanoen.2022.107324.

113. J. Zhang, H. Yao, J. Mo, et al., "Finger-inspired Rigid-soft Hybrid Tactile Sensor with Superior Sensitivity at High Frequency," *Nature Communications* 13 (2022): 5076, https://doi.org/10.1038/s41467-022-32827-7.

114. W. Lin, B. Wang, G. Peng, Y. Shan, H. Hu, and Z. Yang, "Skin-Inspired Piezoelectric Tactile Sensor Array with Crosstalk-Free Row+Column Electrodes for Spatiotemporally Distinguishing Diverse Stimuli," *Advanced Science* 8, no. 3 (2021): 2002817, https://doi.org/10.1002/advs.202002817.

115. Q. Xu, M. Jia, P. Zhou, et al., "High-Performance Ultrasensitive Flexible Piezoelectric Thin Film Sensors via a Cost-Effective Transfer Strategy," *Advanced Functional Materials* 35, no. 4 (2025): 2414211, https://doi.org/10.1002/adfm.202414211.

116. L. Yang, S. Chi, S. Dong, et al., "Preparation and Characterization of a Novel Piezoelectric Nanogenerator Based on Soluble and Meltable Copolyimide for Harvesting Mechanical Energy," *Nano Energy* 67 (2020): 104220, https://doi.org/10.1016/j.nanoen.2019.104220.

117. X. Lin, Y. Teng, H. XUE, et al., "Janus Conductive Mechanism: An Innovative Strategy Enabling Ultra-Wide Linearity Range Pressure Sensing for Multi-Scenario Applications," *Advanced Functional Materials* 34, no. 32 (2024): 2316314, https://doi.org/10.1002/adfm.202316314.

118. Y. Zhang, J. Zeng, Y. Wang, and G. Jiang, "Flexible Three-Dimensional Force Tactile Sensor Based on Velostat Piezoresistive Films," *Micromachines* 15, no. 4 (2024): 486, https://doi.org/10.3390/mi15040486.

119. G. Canavese, S. Stassi, C. Fallauto, et al., "Piezoresistive Flexible Composite for Robotic Tactile Applications," *Sensors and Actuators A: Physical* 208 (2014): 1–9, https://doi.org/10.1016/j.sna.2013.11.018.

120. E. Kanhere, M. Bora, J. Miao, and M. Triantafyllou, "Flexible Hydrogel Capacitive Pressure Sensor for Underwater Applications," *Proceedings* 1 (2017): 360, https://doi.org/10.3390/proceedings1040360.

121. J. Zhou, J. Li, H. Jia, et al., "Mormyroidea-inspired Electronic Skin for Active Non-Contact Three-dimensional Tracking and Sensing," *Nature Communications* 15, no. 1 (2024): 9875, https://doi.org/10.1038/s41467-024-54249-3.

122. H. Dai, C. Zhang, H. Hu, et al., "Biomimetic Hydrodynamic Sensor with Whisker Array Architecture and Multidirectional Perception Ability," *Advanced Science* 11, no. 38 (2024): 2405276, https://doi.org/10.1002/advs.202405276.

123. B. Mao, K. Zhou, Y. Xiang, et al., "A Bioinspired Robotic Finger for Multimodal Tactile Sensing Powered by Fiber Optic Sensors," *Advanced Intelligent Systems* 6, no. 8 (2024): 2400175, https://doi.org/10.1002/aisy.202400175.

124. Y. Yu, Q. Gao, X. Zhang, et al., "Contact-sliding-separation Mode Triboelectric Nanogenerator," *Energy & Environmental Science* 16, no. 9 (2023): 3932–3941.

125. Z. Shi, Y. Zhang, J. Gu, et al., "Triboelectric Nanogenerators: State of the Art," *Sensors* 24, no. 13 (2024): 4298, https://doi.org/10.3390/s24134298.

126. Y. Zhou, J.-H. Zhang, F. Wang, et al., "Recent Advances in Flexible Self-Powered Sensors in Piezoelectric, Triboelectric, and Pyroelectric Fields," *Nanoenergy Advances* 4, no. 3 (2024): 235–257, https://doi.org/10.3390/nanoenergyadv4030015.

127. A. Aabid, M. A. Raheman, Y. E. Ibrahim, et al., "A Systematic Review of Piezoelectric Materials and Energy Harvesters for Industrial Applications," *Sensors* 21, no. 12 (2021): 4145, https://doi.org/10.3390/s21124145.

128. H. Shaukat, A. Ali, S. Bibi, W. A. Altabey, M. Noori, and S. A. Kouritem, "A Review of the Recent Advances in Piezoelectric Materials, Energy Harvester Structures, and Their Applications in Analytical Chemistry," *Applied Sciences* 13, no. 3 (2023): 1300, https://doi.org/10.3390/app13031300.

129. S. Shi, X. Zhang, Z. Wang, et al., "Design and Implementation of a Four-Unit Array Piezoelectric Bionic MEMS Vector Hydrophone," *Micromachines* 15, no. 4 (2024): 524, https://doi.org/10.3390/mi15040524.

130. X. Zong, N. Zhang, X. Ma, J. Wang, and C. Zhang, "Polymer-Based Flexible Piezoresistive Pressure Sensors Based on Various Micro/Nanostructures Array," *Composites Part A: Applied Science and Manufacturing* 190 (2025): 108648, https://doi.org/10.1016/j.compositesa.2024.108648.

131. D. D. L. Chung, "A Critical Review of Piezoresistivity and Its Application in Electrical-Resistance-Based Strain Sensing," *Journal of Materials Science* 55, no. 32 (2020): 15367–15396, https://doi.org/10.1007/s10853-020-05099-z.

132. A. D. Smith, F. Niklaus, A. Paussa, et al., "Piezoresistive Properties of Suspended Graphene Membranes Under Uniaxial and Biaxial Strain in Nanoelectromechanical Pressure Sensors," *ACS Nano* 10, no. 11 (2016): 9879–9886, https://doi.org/10.1021/acsnano.6b02533.

133. C. Hou, H. Gao, X. Yang, et al., "A Piezoresistive-Based 3-Axial MEMS Tactile Sensor and Integrated Surgical Forceps for Gastrointestinal Endoscopic Minimally Invasive Surgery," *Microsystems & Nanoengineering* 10, no. 1 (2024): 141, https://doi.org/10.1038/s41378-024-00774-6.

134. J. Yuan, Q. Li, L. Ding, et al., "Carbon Black/Multi-Walled Carbon Nanotube-Based, Highly Sensitive, Flexible Pressure Sensor," *ACS Omega* 7, no. 48 (2022): 44428–44437, https://doi.org/10.1021/acsomega.2c06548.

2365709x, 0, Downloaded from https://advanced.onlinelibrary.wiley.com/doi/10.1002/admt.202502446 by Tongji University, Wiley Online Library on [05/02/2026]. See the Terms and Conditions (https://onlinelibrary.wiley.com/terms-and-conditions) on Wiley Online Library for rules of use; OA articles are governed by the applicable Creative Commons License

135. J. E. Dusek, M. S. Triantafyllou, and J. H. Lang, "Piezoresistive Foam Sensor Arrays for Marine Applications," *Sensors and Actuators A: Physical* 248 (2016): 173–183, https://doi.org/10.1016/j.sna.2016.07.025.

136. E. Fujiwara, "Optical fiber Tactile Sensor Based on a Biocompatible Whisker-Inspired Transducer," *IEEE Sensors Journal* 24 (2024): 32229–32236, https://doi.org/10.1109/JSEN.2024.3451989.

137. L. Gong, J. Fu, Z. Ma, D. Zhang, and Y. Jiang, "Canal-type Artificial Lateral Line Sensor Array Based on Highly Aligned P (VDF-TrFE) Nanofibers," in *2016 IEEE 11th Annual International Conference on Nano/Micro Engineered and Molecular Systems (NEMS)* (IEEE, 2016), 423–426, https://doi.org/10.1109/NEMS.2016.7758282.

138. X. Hu, Z. Ma, Z. Gong, et al., "A Highly Sensitive Deep-sea Hydrodynamic Pressure Sensor Inspired by Fish Lateral Line," *Biomimetics* 9, no. 3 (2024): 190, https://doi.org/10.3390/biomimetics9030190.

139. T. Shizhe and W. Yijin, "An Artificial Lateral Line Sensor Using Polyvinylidene Fluoride (PVDF) Membrane for Oscillatory Flow Sensing," *IEEE Access* 10 (2022): 15771–15785, https://doi.org/10.1109/ACCESS.2022.3148165.

140. E. Scott and S. Hauert, "A Simple Macro-scale Artificial Lateral Line Sensor for the Detection of Shed Vortices," *Bioinspiration & Biomimetics* 17, no. 5 (2022): 055005, https://doi.org/10.1088/1748-3190/ac84b7.

141. X. Wang, J. Liu, S. Wang, et al., "A Self-powered Triboelectric Coral-Like Sensor Integrated Buoy for Irregular and Ultra-Low Frequency Ocean Wave Monitoring," *Advanced Materials Technologies* 7, no. 6 (2022): 2101098, https://doi.org/10.1002/admt.202101098.

142. M. Wu, X. Zheng, R. Liu, et al., "Glowing Sucker Octopus (Stauroteuthis syrtensis)-Inspired Soft Robotic Gripper for Underwater Self-Adaptive Grasping and Sensing," *Advanced Science* 9, no. 17 (2022): 2104382, https://doi.org/10.1002/advs.202104382.

143. Y. Hao, Y. Sun, J. Wen, et al., "Octopus-inspired Multichannel Tactile Sensor for Enhanced Underwater Material Identification," *Chemical Engineering Journal* 507 (2025): 160604, https://doi.org/10.1016/j.cej.2025.160604.

144. J. Liu, L. Wang, R. Xu, et al., "Underwater Gesture Recognition Meta-gloves for Marine Immersive Communication," *ACS nano* 18, no. 16 (2024): 10818–10828, https://doi.org/10.1021/acsnano.3c13221.

145. J. B. Stocking, W. C. Eberhardt, Y. A. Shakhsheer, B. H. Calhoun, J. R. Paulus, and M. Appleby, "A Capacitance-Based Whisker-like Artificial Sensor for Fluid Motion sensing," Sensors In *Proc. IEEE SENSORS 2010; IEEE: Waikoloa, HI, USA* (2010), 2224–2229, https://doi.org/10.1109/ICSENS.2010.5690637.

146. H. R. Beem and M. S. Triantafyllou, "Wake-induced 'Slaloming'response Explains Exquisite Sensitivity of Seal Whisker-like Sensors," *Journal of Fluid Mechanics* 783 (2015): 306–322, https://doi.org/10.1017/jfm.2015.513.

147. H. Beem, M. Hildner, and M. Triantafyllou, "Calibration and Validation of a Harbor Seal Whisker-Inspired Flow Sensor," *Smart Materials and Structures* 22, no. 1 (2012): 014012, https://doi.org/10.1088/0964-1726/22/1/014012.

148. J. Z. Gul, K. Y. Su, and K. H. Choi, "Fully 3D Printed Multi-Material Soft Bio-Inspired Whisker Sensor for Underwater-Induced Vortex Detection," *Soft Robotics* 5, no. 2 (2018): 122–132, https://doi.org/10.1089/soro.2016.0069.

149. S. Wang, P. Xu, X. Wang, et al., "Underwater Bionic Whisker Sensor Based on Triboelectric Nanogenerator for Passive Vortex Perception," *Nano Energy* 97 (2022): 107210, https://doi.org/10.1016/j.nanoen.2022.107210.

150. X. Zheng, A. M. Kamat, A. O. Krushynska, M. Cao, and A. G. P. Kottapalli, "3D Printed Graphene Piezoresistive Microelectromechanical System Sensors to Explain the Ultrasensitive Wake Tracking of Wavy Seal Whiskers," *Advanced Functional Materials* 32, no. 47 (2022): 2207274, https://doi.org/10.1002/adfm.202207274.

151. R. Glick, Flow Sensing with Arrays of Fibre-optic Whisker Sensors, (2024). Accessed August 9, 2025, https://openaccess.city.ac.uk/id/eprint/35267/.

152. B. Geng, Q. Xue, Z. Xu, et al., "Biomimetic Seal Whisker Sensors for High-sensitivity Wake Detection and Localization," *Bioinspiration & Biomimetics* 20, no. 3 (2025): 036013, https://doi.org/10.1088/1748-3190/adcddf.

153. R. Glick, Flow Sensing with Arrays of Fibre-optic Whisker Sensors, (2024). Accessed August 5, 2025, https://openaccess.city.ac.uk/id/eprint/35267/.

154. J. Xu, X. Irigoien, and M. S. Alouini, "State-of-the-Art Underwater Vehicles and Technologies Enabling Smart Ocean: Survey and Classifications," *arXiv preprint* (2024), arXiv:2412.18667, https://doi.org/10.48550/arXiv.2412.18667.

155. Y. Zhang, D. Kong, Y. Shi, et al., "Recent Progress on Underwater Soft Robots: Adhesion, Grabbing, Actuating, and Sensing," *Frontiers in Bioengineering and Biotechnology* 11 (2023): 1196922, https://doi.org/10.3389/fbioe.2023.1196922.

156. Y. Zhou, X. Zhao, J. Xu, et al., "A Multimodal Magnetoelastic Artificial Skin for Underwater Haptic Sensing," *Science Advances* 10, no. 1 (2024): adj8567, https://doi.org/10.1126/sciadv.adj8567.

157. T. Wang, T. A. Kent, and S. Bergbreiter, "Design of Whisker-Inspired Sensors for Multi-Directional Hydrodynamic Sensing," (2023), https://doi.org/10.48550/arXiv.2307.09569.

158. X. Mu, B. He, S. Wu, X. Zhang, Y. Song, and T. Yan, "A Practical INS/GPS/DVL/PS Integrated Navigation Algorithm and Its Application on Autonomous Underwater Vehicle," *Applied Ocean Research* 106 (2021): 102441, https://doi.org/10.1016/j.apor.2020.102441.

159. F. Güder, A. Ainla, J. Redston, et al., "Paper-Based Electrical Respiration Sensor," *Angewandte Chemie International Edition* 55, no. 19 (2016): 5727–5732, https://doi.org/10.1002/anie.201511805.

160. K. J. Kim and S. Tadokoro, *Electroactive Polymers for Robotic Applications*, (Springer London, 2007), https://doi.org/10.1007/978-1-84628-372-7.

161. I. Spiga, S. Cheesman, A. Hawkins, et al., "Understanding the Scale and Impacts of Anthropogenic Noise Upon Fish and Invertebrates in the Marine Environment," in *SoundWaves Consortium Technical Report ME5205, Newcastle University, UK* (Department for Environment, Food and Rural Affairs (DEFRA), 2012), Accessed: August 5, 2025, https://www.researchgate.net/publication/312530792_Understanding_the_Scale_and_Impacts_of_Anthropogenic_Noise_upon_Fish_and_Invertebrates_in_the_Marine_Environment.

162. D. F. Quintero-Bernal, H. Kaschel-Cárcamo, and J. Kern-Molina, A Survey of Multimodal Data Fusion: Applications and Adverse Conditions una Revisión De Fusión De Datos Multimodal: Aplicaciones y Condiciones Adversas, 2025, https://revistascientificas.cuc.edu.co/ingecuc/article/download/5275/5658/56942.

163. H. Bleckmann, T. Breithaupt, R. Blickhan, and J. Tautz, "The Time Course and Frequency Content of Hydrodynamic Events Caused by Moving Fish, Frogs, and Crustaceans," *Journal of Comparative Physiology A* 168, no. 6 (1991), https://doi.org/10.1007/BF00224363.

164. J. Yu, M. Ai, C. Liu, et al., "Cilia-Inspired Bionic Tactile E-Skin: Structure, Fabrication and Applications," *Sensors* 25, no. 1 (2024): 76, https://doi.org/10.3390/s25010076.

165. R. Gao, M. Liang, H. Dong, X. Luo, and P. N. Suganthan, "Underwater Acoustic Signal Denoising Algorithms: A Survey of the State-of-the-Art," *IEEE Transactions on Instrumentation and Measurement* (2025), https://doi.org/10.1109/TIM.2025.3551006.

166. Z. Yang, Z. Zhu, Y. Zhao, et al., A Comprehensive Survey on Underwater Acoustic Target Positioning and Tracking: Progress, Challenges, and Perspectives, (2025), https://doi.org/10.48550/arXiv.2506.14165.

167. J. Zhao, P. Zhao, J. Sun, and Q. Yan, "Submarine Pile Foundation and Cable Monitoring Based on Sensor Fusion and Big Data Analysis,"

2365709x, 0, Downloaded from https://advanced.onlinelibrary.wiley.com/doi/10.1002/admt.202502446 by Tongji University, Wiley Online Library on [05/02/2026]. See the Terms and Conditions (https://onlinelibrary.wiley.com/terms-and-conditions) on Wiley Online Library for rules of use; OA articles are governed by the applicable Creative Commons License

International Journal of Reasoning-based Intelligent Systems 17, no. 7 (2025): 21–32, https://doi.org/10.1504/IJRIS.2025.146671.

168. H. Nasution, H. Harahap, N. F. Dalimunthe, et al., "Hydrogel and Effects of Crosslinking Agent on Cellulose-based Hydrogels: a Review," *Gels* 8, no. 9 (2022): 568, https://doi.org/10.3390/gels8090568.

169. A. W. Asohan, R. Hashim, K. M. Ku Ishak, Z. A. Abdul Hamid, N. Jasme, and Y. Bustami, "Preparation and Characterisation of Cellulose Nanocrystal/Alginate/Polyethylene Glycol Diacrylate (CNC/Alg/PEGDA) Hydrogel Using Double Network Crosslinking Technique for Bioprinting Application," *Applied Sciences* 12, no. 2 (2022): 771, https://doi.org/10.3390/app12020771.

170. Q. Wang, Z. Wang, W. Tian, et al., "TPU/MOFs Electrospun Composite Film for Underwater Tactile Sensing and Finger Joint Bending Monitoring," *Small* 21, no. 48 (2025): 10062, https://doi.org/10.1002/smll.202510062.

171. Y. Liu, J. Lin, J. Wei, T. Chen, and W. Wang, "Skin-like Heterogeneous and Self-Healing Conductive Hydrogel toward Ultrasensitive Marine Sensing," *ACS sensors* 10, no. 3 (2025): 2276–2286, https://doi.org/10.1021/acssensors.4c03619.

172. C. Richards, A. Slaimi, N. E. O'Connor, A. Barrett, S. Kwiatkowska, and F. Regan, "Bio-inspired Surface Texture Modification as a Viable Feature of Future Aquatic Antifouling Strategies: A Review," *International Journal of Molecular Sciences* 21, no. 14 (2020): 5063, https://doi.org/10.3390/ijms21145063.

173. G. Tian, D. Fan, X. Feng, and H. Zhou, "Thriving Artificial Underwater Drag-reduction Materials Inspired from Aquatic Animals: Progresses and Challenges," *RSC Advances* 11, no. 6 (2021): 3399–3428, https://doi.org/10.1039/D0RA08672J.

174. W. M. Elsayed, M. Alsabaan, M. I. Ibrahem, and E. El-Shafeiy, "The Potential of Deep Learning in Underwater Wireless Sensor Networks and Noise Canceling for the Effective Monitoring of Aquatic Life," *Sensors* 24, no. 18 (2024): 6102, https://doi.org/10.3390/s24186102.

175. F. Bruno, M. Muzzupappa, L. Barbieri, et al., "The CoMAS project: New Materials and Tools for Improving the in Situ Documentation, Restoration, and Conservation of Underwater Archaeological Remains," *Marine Technology Society Journal* 50, no. 4 (2016): 108–118, https://doi.org/10.4031/MTSJ.50.4.2.

176. R. Helim, A. Zazoua, and H. Korri-Youssoufi, "Sustainable Biopolymer-Based Electrochemical Sensors for Trace Heavy Metal Determination in Water: a Comprehensive Review," *Chemosensors* 12, no. 12 (2024): 267, https://doi.org/10.3390/chemosensors12120267.

2365709x, 0, Downloaded from https://advanced.onlinelibrary.wiley.com/doi/10.1002/admt.202502446 by Tongji University, Wiley Online Library on [05/02/2026]. See the Terms and Conditions (https://onlinelibrary.wiley.com/terms-and-conditions) on Wiley Online Library for rules of use; OA articles are governed by the applicable Creative Commons License